

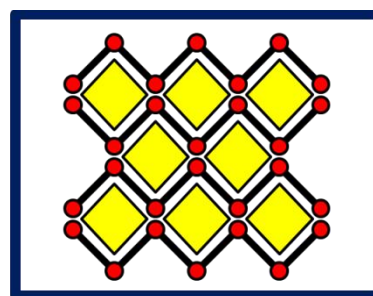
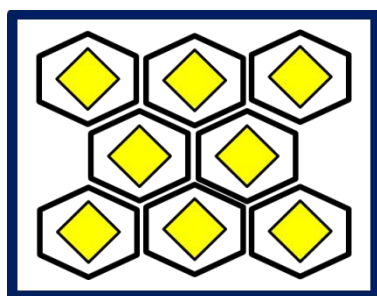
# SEPARATION OF ISOMERS BY ENCLATHRATION

Leena Desiree Patel

Thesis presented for the degree of Magister Technologiae:  
Chemistry

in the Faculty of Applied Sciences at the  
CAPE PENINSULA UNIVERSITY OF TECHNOLOGY

November 2014



Supervisor: Prof. Luigi R. Nassimbeni  
Co-supervisor: Dr Nikoletta B. Báthori

## **DECLARATION**

**I, Leena Desiree Patel, declare that the contents of this thesis represent my own unaided work, and that the thesis has not previously been submitted for academic examination towards any qualification. Furthermore, it represents my own opinions and not necessarily those of the Cape Peninsula University of Technology.**

**Signed .....**

**Date**

## **ACKNOWLEDGEMENTS**

**My special thanks to:**

- **Firstly Professor Luigi R. Nassimbeni for his excellent mentorship, kindness, encouragement and sharing his broad knowledge on the subject.**
- **Dr Nikoletta B. Báthori for the brilliant ideas, her willingness to help, inspiration and insistence on excellence.**
- **The staff of the Department of Chemistry, CPUT.**

## **DEDICATION**

**I dedicate my thesis to my father, Rolf Patel and the three most influential women in my life; my mother Rosita Patel, my sister Pushpa Patel and my dear friend Natasha Mudaliar-Patel.**

## PUBLICATIONS AND CONFERENCES

- Chapter 5 of this thesis has been published: Nassimbeni, L. R., Báthori, N. B., Patel, L.D., Su. H & Weber, E., Separation of xylenes by enclathration, *Chem. Comm.*, 2014, DOI: 10.1039/C4CC05329J.
- Chapter 5 of this thesis was presented as an oral presentation at the 2<sup>nd</sup> U6 Consortium international conference held at the Cape Peninsula University of Technology, Cape Town, South Africa, on the 10<sup>th</sup> of September 2014. The presentation title was 'Separation of xylenes by enclathration'.

## ABSTRACT

The separation of isomers with similar chemical structures is one of the most difficult procedures in chemistry. This is because their physical and chemical properties are generally so similar that most of the common techniques are not successful. In such situations one employs host-guest chemistry, as a tool of separation technology.

In this thesis three aromatic hydrocarbon host compounds 9,9'-bianthryl (**H1**), 9,9'-spirobifluorene (**H2**) and *trans*-2,3-dibenzoylspro(cyclopropane-1,9'-fluorene) (**H3**) were investigated in terms of their selectivity towards heterocyclic aromatic compounds (pyridine, **PYR**; piperidine, **PIP**; morpholine, **MOR** and 1,4-dioxane, **DIO**), cyclohexanone derivative compounds (cyclohexanone, **CYHA**; 2-methylcyclohexanone, **2-MCYHA**; 3-methylcyclohexanone, **3-MCYHA** and 4-methylcyclohexanone, **4-MCYHA**) and the xylene isomers (*ortho*-xylene, **ox**; *meta*-xylene, **mx** and *para*-xylene, **px**). The **H1**, **H2** and **H3** host compounds were combined with a series of the heterocyclic compounds and six inclusion compounds were formed: **H1•MOR**, **H2•2PYR**, **H2•PIP**, **H2•MOR**, **H2•DIO** and **H3•PYR**. In the second part the derivatives of cyclohexanone formed inclusion compounds with the hosts **H1** and **H2**. The **H1•2CYHA**, **H1•ANT**, **H1•0.5(2-MCYHA)** and **H3•CYHA** structures were obtained. In the third part the **H1** formed clathrates with **ox** and **px**; **H2** and **H3** only formed clathrates with **px** and **ox** respectively. The following four structures were obtained: **H1•0.5ox**, **H1•0.5px**, **H2•0.5px** and **H3•ox** and were analysed by single crystal X-ray diffraction (SCXD), powder X-ray diffraction (PXRD), proton nuclear magnetic resonance spectroscopy (<sup>1</sup>H-NMR), thermal gravimetry (TG) and differential scanning calorimetry (DSC).

It was concluded that **H2** discriminates between the four heterocyclic compounds as follows: **PIP > MOR ≈ DIO ≈ PYR** and this can be explained by the <sup>1</sup>H-NMR results and the packing features. In analysis of the xylene isomers, it was found that the three hydrocarbon host compounds **H1**, **H2** and **H3** efficiently discriminate between the isomers by forming inclusion compounds. **H1** enclathrates both **ox** and **px** but prefers the former. This can be explained in terms of the packing features and lattice energies. **H2** and **H3** only enclathrate **px** and **ox** respectively. It was concluded that host compounds with small conformational movements are potentially good in selective inclusion.

## ABBREVIATIONS AND SYMBOLS

<b>H</b>	Host
<b>G</b>	Guest
$\alpha_{\text{phase}}$	non-porous phase of the host compound (apohost)
$\beta_{\text{phase}}$	complexed host phase
$\pi$ - $\pi$	pi-pi
<b>H1</b>	9,9'-bianthryl
<b>H2</b>	9,9'-spirobifluorene
<b>H3</b>	<i>trans</i> -2,3-dibenzoylspiro(cyclopropane-1,9'-fluorene)
<b>ox</b>	<i>ortho</i> -xylene
<b>mx</b>	<i>meta</i> -xylene
<b>px</b>	<i>para</i> -xylene
<b>CYHA</b>	cyclohexanone
<b>2-MCYHA</b>	2-methylcyclohexanone
<b>3-MCYHA</b>	3-methylcyclohexanone
<b>4-MCYHA</b>	4-methylcyclohexanone
<b>ANT</b>	anthracene
<b>PIP</b>	piperidine
<b>PYR</b>	pyridine
<b>MOR</b>	morpholine
<b>DIO</b>	dioxane
<b>CSD</b>	Cambridge Structural Database
<b>DNA</b>	deoxyribonucleic acid
<b>PXRD</b>	Powder X-ray Diffraction
<b>SCXD</b>	Single Crystal X-ray Diffraction
<b>TG</b>	Thermogravimetry
<b>DSC</b>	Differential Scanning Calorimetry
<b>HSM</b>	Hot Stage Microscopy
$^1\text{H-NMR}$	Proton Nuclear Magnetic Resonance
<b>K</b>	selectivity co-efficient
$X_A$	mole fraction of guest A in the mother liquor
$X_B$	mole fraction of guest B in the mother liquor
$Z_A$	mole fraction of guest A in the crystal
$Z_B$	mole fraction of guest B in the crystal
$2\theta$	$\theta$ is the angle between the incident ray and the scattering planes
$T_{\text{on}}$	onset temperature
$T_{\text{peak}}$	peak temperature
<b>r</b>	distance
<b>pKa</b>	-log (acid ionisation constant)
<b>a, b, c</b>	unit cell axes
$\alpha$	angle between b and c unit cell axes
$\beta$	angle between a and c unit cell axes
$\gamma$	angle between a and b unit cell axes
<b>V</b>	unit cell volume
<b>Z</b>	number of formula units per unit cell
<b>au</b>	atomic unit

## ATOM COLOURS





## TABLE OF CONTENTS

Declaration .....	i
Acknowledgements .....	ii
Dedication .....	iii
Publications and Conferences.....	iv
Abstract .....	v
Abbreviations and symbols .....	vi
Atom colours .....	vii
<b>Chapter 1: Introduction.....</b>	<b>1</b>
1.1 Supramolecular chemistry .....	1
1.2 Host-guest compounds and their classification.....	4
1.3 Intermolecular interactions.....	5
1.4 Host compounds under study .....	6
1.5 Guest compounds under study .....	7
1.5.1 Heterocyclic aromatic compounds .....	8
1.5.2 Cyclohexanone derivative compounds .....	8
1.5.3 Xylene isomers .....	10
1.6 Potential host-guest intermolecular interactions in analysed systems	11
1.6.1 $\pi$ - $\pi$ interactions .....	11
1.6.2 Van der Waals forces.....	12
1.7 Crystal engineering.....	13
1.8 Separation by selective inclusion.....	14
1.9 Physical chemistry of inclusion compounds.....	15
1.10 Aims and objectives .....	16
References .....	17
<b>Chapter 2: Experimental .....</b>	<b>19</b>
2.1 Host and guest compounds .....	19
2.2 Crystal growth .....	22

2.3	Competition experiments .....	22
2.4	Thermal analysis.....	23
2.4.1	Hot-stage microscopy (HSM).....	23
2.4.2	Thermogravimetric analysis and differential scanning calorimetry .....	24
2.5	Proton NMR spectroscopy ( <sup>1</sup> H-NMR) .....	25
2.6	X-ray diffraction analysis.....	25
2.6.1	Powder X-ray diffraction (PXRD) .....	25
2.6.2	Single crystal X-ray Diffraction (SCXD).....	26
2.7	Computing components .....	28
	References .....	30
<b>Chapter 3: Selectivity experiments of heterocyclic guest compounds.....</b>		<b>31</b>
3.1	Introduction .....	31
3.2	Inclusion complex preparation .....	31
3.3	Inclusion complex analysis .....	32
3.4	Inclusion compound of <b>H1</b> with <b>MOR</b> .....	33
3.4.1	Thermal analysis of <b>H1•MOR</b> .....	33
3.4.2	Crystal structure analysis of <b>H1•MOR</b> .....	33
3.5	Inclusion compounds of <b>H2</b> with heterocyclic compounds.....	38
3.5.1	Thermal analysis of inclusion compounds of <b>H2</b> with heterocyclic compounds .....	38
3.5.2	Crystal structure analysis of inclusion compounds <b>H2</b> with heterocyclic compounds .....	40
3.5.2.1	Structure analysis of <b>H2•2PYR</b> .....	40
3.5.2.2	Structure analysis of <b>H2•PIP</b> .....	43
3.5.2.3	Structure analysis of <b>H2•MOR</b> .....	45
3.5.2.4	Structure analysis of <b>H2•DIO</b> .....	47
3.5.3	Competition experiments with <b>H2</b> and heterocyclic compounds .....	51
3.5.3.1	<sup>1</sup> H-NMR results of the selectivity experiments .....	51
3.5.3.2	Powder X-ray analysis .....	54
3.5.3.3	Hirshfeld surface analysis of <b>H2•2PYR</b> , <b>H2•PIP</b> , <b>H2•MOR</b> and <b>H2•DIO</b> .....	55
3.6	Inclusion compound of <b>H3</b> with <b>PYR</b> .....	57

3.6.1	Thermal analysis of <b>H3•PYR</b> .....	57
3.6.2	Crystal structure analysis of <b>H3•PYR</b> .....	58
	References .....	61
<b>Chapter 4: Selectivity experiments of cyclohexanone derivative guest compounds</b> .....		<b>62</b>
4.1	Introduction .....	62
4.2	Inclusion complex preparation .....	62
4.3	Inclusion complex analysis .....	63
4.4	Inclusion compounds of <b>H1</b> with <b>CYHA</b> and <b>2-MCYHA</b> .....	64
4.4.1	Crystal structure analysis of <b>H1•2CYHA</b> .....	64
4.4.2	Thermal analysis of <b>H1•2CHYA</b> .....	67
4.4.3	Crystal structure analysis of <b>H1•0.5(2-MCYHA)</b> .....	67
4.4.4	Decomposition of <b>H1</b> host compound .....	69
4.4.4.1	Photo-decomposition of <b>H1</b> host.....	69
4.4.4.2	Crystal structure analysis of <b>H1•ANT</b> .....	70
4.4.4.3	Thermal analysis of <b>H1•ANT</b> .....	73
4.4.4.4	Powder X-ray analysis of <b>H1•ANT</b> .....	74
4.5	Inclusion compound of <b>H3</b> with <b>CYHA</b> .....	75
4.5.1	Crystal structure analysis of <b>H3•CYHA</b> .....	75
4.5.2	Thermal analysis of <b>H3•CYHA</b> .....	78
	References .....	79
<b>Chapter 5: Separation of xylenes</b> .....		<b>80</b>
5.1	Introduction .....	80
5.2	Inclusion complex preparation .....	81
5.3	Inclusion complex analysis .....	81
5.4	<sup>1</sup> H-NMR of <b>H1</b> , <b>H2</b> and <b>H3</b> inclusion compounds .....	82
5.5	Inclusion compounds of <b>H1</b> with <b>ox</b> and <b>px</b> .....	86
5.5.1	Thermal analysis of <b>H1•0.5ox</b> and <b>H1•0.5px</b> .....	86
5.5.2	Crystal structure analysis <b>H1•0.5ox</b> and <b>H1•0.5px</b> .....	87
5.5.2.1	Structure analysis of <b>H1•0.5ox</b> .....	87

<b>5.5.2.2</b>	Structure analysis of <b>H1•0.5px</b> .....	90
<b>5.5.3</b>	Torsion angles in <b>H1</b> inclusion compound .....	92
<b>5.5.4</b>	Hirshfeld surface analysis of <b>H1•0.5ox</b> and <b>H1•0.5px</b> .....	93
<b>5.5.5</b>	Comparison of stabilities of <b>H1•05ox</b> and <b>H1•05px</b> .....	95
<b>5.6</b>	Inclusion compounds of <b>H2</b> with <b>px</b> and <b>H3</b> with <b>ox</b> .....	95
<b>5.6.1</b>	Thermal analysis of <b>H2•0.5px</b> and <b>H3•ox</b> .....	95
<b>5.6.2</b>	Crystal structure analysis of <b>H2•0.5px</b> and <b>H3•ox</b> .....	97
<b>5.6.2.1</b>	Structure analysis of <b>H2•0.5px</b> .....	97
<b>5.6.2.2</b>	Structure analysis of <b>H3•ox</b> .....	99
	References .....	102
<b>Chapter 6: Summary and conclusion</b> .....		<b>103</b>

## LIST OF FIGURES

<b>Figure.1.1</b>	The scope of Supramolecular Chemistry showing the phenomenon of selectivity .....	2
<b>Figure 1.2</b>	Schematic illustration of molecular and lattice inclusion .....	5
<b>Figure 1.3</b>	Structural diagram of hosts: 9,9'-bianthryl ( <b>H1</b> ), 9,9'-spirobifluorene ( <b>H2</b> ) and trans-2,3-dibenzoylspiro(cyclopropane-1,9'-fluorene) ( <b>H3</b> ) .....	7
<b>Figure 1.4</b>	Skeletal structures of pyridine ( <b>PYR</b> ), piperidine ( <b>PIP</b> ), morpholine ( <b>MOR</b> ) and 1,4-dioxane ( <b>DIO</b> ).....	8
<b>Figure 1.5</b>	Skeletal structures of cyclohexanone ( <b>CYHA</b> ), 2-methylcyclohexanone ( <b>2-MCYHA</b> ), 3-methylcyclohexanone ( <b>3-MCYHA</b> ) and 4-methylcyclohexanone ( <b>4-MCYHA</b> ).....	9
<b>Figure 1.6</b>	Skeletal structures of xylene isomers .....	10
<b>Figure 1.7</b>	Possible aromatic stacking arrangements <b>(a)</b> parallel face-centred, <b>(b)</b> parallel offset, <b>(c)</b> Perpendicular t-shaped, <b>(d)</b> perpendicular y-shaped and <b>(e)</b> parallel offset for toluene .....	12
<b>Figure 1.8</b>	Possible interactions between $\pi$ systems .....	12
<b>Figure 1.9</b>	Examples of supramolecular synthons .....	14
<b>Figure 2.1</b>	Schematic diagram of host and guest compounds applied in the study .	20
<b>Figure 3.1</b>	Schematic diagrams of heterocyclic guest compounds .....	31
<b>Figure 3.2</b>	TG and DSC traces for <b>H1•MOR</b> (endo down) .....	33
<b>Figure 3.3</b>	Intermolecular interactions in <b>H1•MOR</b> .....	36
<b>Figure 3.4</b>	Dolos and <b>H1</b> host compound.....	37
<b>Figure 3.5</b>	Packing diagram of <b>H1•MOR</b> down [100] .....	37
<b>Figure 3.6</b>	Packing diagram of <b>H1•MOR</b> down [010] .....	37
<b>Figure 3.7</b>	TG and DSC traces for <b>H2•2PYR</b> , <b>H2•PIP</b> , <b>H2•MOR</b> and <b>H2•DIO</b> (endo down).....	39
<b>Figure 3.8</b>	Intermolecular interactions in <b>H2•2PYR</b> .....	42
<b>Figure 3.9</b>	Packing diagram for <b>H2•2PYR</b> viewed along [100]. Guests are coloured green.....	42
<b>Figure 3.10</b>	Intermolecular interactions in <b>H2•PIP</b> .....	43
<b>Figure 3.11</b>	Packing diagram of <b>H2•PIP</b> viewed down [100]. Guests are coloured purple .....	44

<b>Figure 3.12</b>	Packing diagram of <b>H2•PIP</b> viewed down [010]. Guests are coloured purple.....	44
<b>Figure 3.13</b>	Intermolecular interactions in <b>H2•MOR</b> .....	45
<b>Figure 3.14</b>	Packing diagram of <b>H2•MOR</b> viewed down [100]. Guests coloured turquoise.....	46
<b>Figure 3.15</b>	Packing diagram of <b>H2•MOR</b> viewed down [010]. Guests coloured turquoise.....	46
<b>Figure 3.16</b>	Asymmetric unit of <b>H2•DIO</b> . Guest molecules 1 and 2 are ordered while 3 is disordered.....	47
<b>Figure 3.17</b>	Disordered <b>DIO</b> guest in <b>H2•DIO</b> . (Site occupancy factor 80% atoms coloured with red and 20% with blue).....	48
<b>Figure 3.18</b>	Intermolecular interactions in <b>H2•DIO</b> . Guest molecules 1 and 2 are ordered while 3 is disordered.....	48
<b>Figure 3.19</b>	Packing diagram for <b>H2•DIO</b> viewed along [100] Guest molecules 1 (blue) and 2 (green) are ordered while 3 (yellow) is disordered.....	49
<b>Figure 3.20</b>	Packing diagram of <b>H2•DIO</b> , single layer viewed down [010]. Guest molecule 1 and 2 are ordered while 3 is disordered.....	50
<b>Figure 3.21</b>	Selectivity curve for the <b>H2•(PYR)/(MOR)</b> system.....	53
<b>Figure 3.22</b>	PXRD patterns: <b>H2•MOR</b> (calculated-purple), <b>H2•2PYR</b> (calculated-red), <b>H2•PYR/MOR</b> (measured-green) and <b>H2</b> (measured-blue).....	54
<b>Figure 3.23</b>	PXRD patterns: <b>H2•PIP</b> (calculated-orange), <b>H2•2PYR</b> (calculated-red), <b>H2•PYR/MOR</b> (measured-green) and <b>H2</b> (measured-blue).....	55
<b>Figure 3.24</b>	Fingerprint plots of Hirshfeld surfaces generated for <b>H2•PIP</b> , <b>H2•MOR</b> , <b>H2•2PYR</b> and <b>H2•DIO</b> crystal structures.....	57
<b>Figure 3.25</b>	TG and DSC traces for <b>H3•PYR</b> (endo down).....	58
<b>Figure 3.26</b>	Intermolecular interactions in <b>H3•PYR</b> structure.....	60
<b>Figure 3.27</b>	Packing diagram for <b>H3•PYR</b> viewed along [100]. Guests are presented with space filling and coloured green.....	60
<b>Figure 4.1</b>	Schematic diagrams of cyclic ketone guest compounds.....	62
<b>Figure 4.2</b>	Asymmetric unit of <b>H1•2CYHA</b> . Guest molecules 1 is ordered and 2 is disordered.....	64
<b>Figure 4.3</b>	Intermolecular interactions in <b>H1•2CYHA</b> .....	66
<b>Figure 4.4</b>	Packing diagram of <b>H1•2CYHA</b> viewed along [100]. Guests are presented with space filling and coloured green.....	66
<b>Figure 4.5</b>	TG trace for <b>H1•2CYHA</b> .....	67
<b>Figure 4.6</b>	Asymmetric unit of <b>H1•0.5(2-MCYHA)</b> . Guest molecule is disordered ...	68

<b>Figure 4.7</b>	Intermolecular interactions in <b>H1•0.5(2-MCYHA)</b> .....	68
<b>Figure 4.8</b>	Packing diagram of <b>H1•0.5(2-MCYHA)</b> viewed along [100]. Guests are presented with space filling and coloured red and blue .....	69
<b>Figure 4.9</b>	Decomposition of <b>H1</b> host.....	69
<b>Figure 4.10</b>	Intermolecular interactions in <b>H1•ANT</b> .....	72
<b>Figure 4.11</b>	Packing diagram of <b>H1•ANT</b> viewed along [100]. <b>ANT</b> molecules are presented with space filling and coloured yellow .....	72
<b>Figure 4.12</b>	TG and DSC traces for <b>H1</b> (endo down) .....	73
<b>Figure 4.13</b>	PXRD patterns: impure <b>H1</b> (measured-green), <b>H1</b> apohost 1 (calculated-red) and <b>H1</b> apohost (calculated-blue) .....	74
<b>Figure 4.14</b>	Intermolecular interactions in <b>H1•ANT</b> .....	77
<b>Figure 4.15</b>	Packing diagram of <b>H3•CYHA</b> viewed along [100]. Host are coloured pink and guests are coloured grey .....	77
<b>Figure 4.16</b>	Packing diagram of <b>H3•CYHA</b> viewed along [010]. Host are coloured yellow and guests are coloured red .....	78
<b>Figure 4.17</b>	TG trace for <b>H3•CYHA</b> .....	78
<b>Figure 5.1</b>	Schematic diagram of xylene isomers .....	80
<b>Figure 5.2</b>	<sup>1</sup> H-NMR spectrum for <b>ox</b> .....	84
<b>Figure 5.3</b>	<sup>1</sup> H-NMR spectrum for <b>px</b> .....	84
<b>Figure 5.4</b>	<sup>1</sup> H-NMR spectrum for <b>H1</b> with <b>ox/mx/px</b> .....	85
<b>Figure 5.5</b>	TG and DSC traces for <b>H1•0.5ox</b> (endo down).....	86
<b>Figure 5.6</b>	TG and DSC traces for <b>H1•0.5px</b> (endo down).....	87
<b>Figure 5.7</b>	Packing diagram for <b>H1•0.5px</b> .....	89
<b>Figure 5.8</b>	Packing diagram for <b>H1•0.5ox</b> viewed along [1-10]. Guests are presented with space filling and coloured purple .....	90
<b>Figure 5.9</b>	$\pi$ -stacking in <b>H1•0.5px</b> .....	91
<b>Figure 5.10</b>	Packing diagram for <b>H1•0.5px</b> viewed along [010]. Guests are presented with space filling and coloured pink.....	92
<b>Figure 5.11</b>	Hirshfeld plots for <b>H1•0.5ox</b> ( <b>a</b> - molecule A, <b>b</b> - molecule B) and for <b>H1•0.5px</b> ( <b>c</b> ).....	94
<b>Figure 5.12</b>	TG and DSC traces for <b>H2•0.5px</b> (endo down).....	96
<b>Figure 5.13</b>	TGA and DSC traces for <b>H3•ox</b> (endo down) .....	96
<b>Figure 5.14</b>	$\pi$ -stacking in <b>H2•0.5px</b> .....	98

<b>Figure 5.15</b>	Packing diagram for <b>H2•0.5px</b> viewed along [010]. Guests are presented with space filling and coloured maroon .....	99
<b>Figure 5.16</b>	$\pi$ -stacking in <b>H3•ox</b> .....	100
<b>Figure 5.17</b>	Packing diagram for <b>H3•ox</b> viewed along [010]. Guests coloured blue .....	101



## LIST OF TABLES

<b>Table 1.1</b>	Timeline of supramolecular chemistry.....	3
<b>Table 1.2</b>	Summary of non-covalent interactions.....	6
<b>Table 1.3</b>	Normal boiling and melting points of cyclohexanone ( <b>CYHA</b> ), 2-methylcyclohexanone ( <b>2-MCYHA</b> ), 3-methylcyclohexanone ( <b>3-MCYHA</b> ) and 4-methylcyclohexanone ( <b>4-MCYHA</b> ) .....	9
<b>Table 1.4</b>	Normal boiling and melting points of xylenes.....	10
<b>Table 2.1</b>	Guests employed for the study .....	21
<b>Table 2.2</b>	Physical properties of guest compounds. ....	21
<b>Table 2.3</b>	Crystallographic data files.....	29
<b>Table 3.1</b>	Enclathration results of <b>H1</b> , <b>H2</b> and <b>H3</b> with <b>PYR</b> , <b>PIP</b> , <b>MOR</b> and <b>DIO</b> ...	32
<b>Table 3.2</b>	Crystal data for <b>H1•MOR</b> .....	35
<b>Table 3.3</b>	Intermolecular interactions in <b>H1•MOR</b> .....	36
<b>Table 3.4</b>	TG and DSC results for <b>H2•2PYR</b> , <b>H2•PIP</b> , <b>H2•MOR</b> and <b>H2•DIO</b> .....	40
<b>Table 3.5</b>	Crystal data for <b>H2•2PYR</b> , <b>H2•PIP</b> , <b>H2•MOR</b> and <b>H2•DIO</b> .....	41
<b>Table 3.6</b>	Intermolecular interactions in <b>H2•2PYR</b> .....	42
<b>Table 3.7</b>	Intermolecular interactions in <b>H2•PIP</b> .....	44
<b>Table 3.8</b>	Intermolecular interactions in <b>H2•MOR</b> .....	46
<b>Table 3.9</b>	Intermolecular interactions in <b>H2•DIO</b> .....	49
<b>Table 3.10</b>	<sup>1</sup> H-NMR data for <b>PYR</b> , <b>PIP</b> , <b>MOR</b> and <b>DIO</b> .....	51
<b>Table 3.11</b>	<sup>1</sup> H-NMR results and selectivity constants (K) of <b>H2</b> with binary equimolar mixtures of the guests. Preferred guest are in bold.....	52
<b>Table 3.12</b>	Selectivity values for <b>H2•(PYR)/(MOR)</b> .....	53
<b>Table 3.13</b>	Intermolecular interactions in inclusion compounds of <b>H2</b> .....	57
<b>Table 3.14</b>	Crystal data for <b>H3•PYR</b> .....	59
<b>Table 3.15</b>	Intermolecular interactions in <b>H3•PYR</b> .....	60
<b>Table 4.1</b>	Enclathration results of <b>H1</b> , <b>H2</b> and <b>H3</b> with <b>CYHA</b> and binary equimolar mixtures of <b>2-MCYHA</b> , <b>3-MCYHA</b> and <b>4-MCYHA</b> .....	63
<b>Table 4.2</b>	Crystal data for <b>H1•2CYHA</b> and <b>H1•0.5(2-MCYHA)</b> .....	65
<b>Table 4.3</b>	Intermolecular interactions in <b>H1•2CYHA</b> .....	66
<b>Table 4.4</b>	Intermolecular interactions in <b>H1•0.5(2-MCYHA)</b> .....	69
<b>Table 4.5</b>	Crystal data for <b>H1•ANT</b> .....	71

<b>Table 4.6</b>	Intermolecular interactions in <b>H1•ANT</b> .....	72
<b>Table 4.7</b>	Crystal data for <b>H3•CYHA</b> .....	76
<b>Table 4.8</b>	Intermolecular interactions in <b>H3•CYHA</b> .....	77
<b>Table 5.1</b>	Enclathration results of <b>H1</b> , <b>H2</b> and <b>H3</b> with xylene isomers .....	82
<b>Table 5.2</b>	<sup>1</sup> H-NMR data for <b>ox</b> , <b>mx</b> and <b>px</b> .....	83
<b>Table 5.3</b>	<sup>1</sup> H-NMR spectral data for <b>H1</b> , <b>H2</b> and <b>H3</b> with <b>ox/mx/px</b> .....	85
<b>Table 5.4</b>	Crystal data for <b>H1•0.5ox</b> and <b>H1•0.5px</b> .....	88
<b>Table 5.5</b>	C-H••• $\pi$ interactions in <b>H1•0.5ox</b> structure .....	90
<b>Table 5.6</b>	C-H••• $\pi$ interactions in <b>H1•0.5px</b> structure. ....	91
<b>Table 5.7</b>	Torsion angles for <b>H1</b> .....	93
<b>Table 5.8</b>	The intermolecular interactions in the <b>H1</b> crystal structures.....	94
<b>Table 5.9</b>	Lattice energies and density values for <b>H1•05ox</b> and <b>H1•05px</b> .....	95
<b>Table 5.10</b>	Crystal data for <b>H2•0.5px</b> and <b>H3•ox</b> .....	97
<b>Table 5.11</b>	C-H••• $\pi$ interactions in <b>H2•0.5px</b> structure .....	99
<b>Table 5.12</b>	C-H••• $\pi$ interactions in <b>H3•ox</b> structure .....	100

# Chapter 1: Introduction

---

## 1.1 Supramolecular chemistry

*“Supramolecular chemistry may be defined as “chemistry beyond the molecule”, bearing on the organized entities of higher complexity that result from the association of two or more chemical species held together by intermolecular forces.”*

Jean-Marie Lehn (1987), *Supramolecular chemistry*<sup>1,2</sup>

Supramolecular chemistry has received much attention in recent years due to its multidisciplinary nature. The field attracts a diversity of scientific disciplines such as chemistry, biochemistry, biology, environmental science, engineering, physics, mathematics and a number of other advanced research fields.<sup>3</sup> The concept can be visualised and applied to everyday theories at the molecular level.

Supramolecular chemistry, like many advances in science emerged by chance. The current definition is relatively young, dating back to the late 1960s and the early 1970s. However the concept and roots, and essentially many supramolecular chemical systems, may be traced back to the 18<sup>th</sup> century when modern chemistry itself was introduced; a descriptive timeline is given in **Table 1.1**.<sup>4</sup> In 1810, the first inclusion compound was discovered by Sir Humphrey Davy. In 1948, Herman Emil Fisher described enzyme-substrate interactions using a *lock and key* analogy, anticipating the principles for molecular recognition and host-guest chemistry. This was a fundamental step in establishing supramolecular chemistry as a field of study.<sup>5</sup> Jean-Marie Lehn introduced the term ‘supramolecular chemistry’ in 1987 which he defined as the ‘chemistry of molecular assemblies and of the intermolecular bond’ and won the Nobel Prize for his leading contribution. Other prominent expressions used are ‘the chemistry of the non-covalent bond’ and ‘non-molecular chemistry’, hence supramolecular chemistry may be described as the study of simple or complex systems (supramolecules) held together by non-covalent bonds such as electrostatic or dipole interactions, dispersive forces, hydrogen bonding and hydrophobic effect<sup>1</sup> (**Figure 1.1**). Supramolecular chemistry may be divided into two

subsets, namely host-guest chemistry and self-assembly.<sup>6</sup> The difference between the two areas concerns the size and shape of the molecules involved. In host-guest chemistry systems a large 'host' compound envelopes a smaller 'guest' molecule in the binding region. In contrast, in the case of self-assembly there is no significant difference in the size of the interacting species. Host-guest chemistry is an important area to the current study, namely 'selectivity by enclathration'.

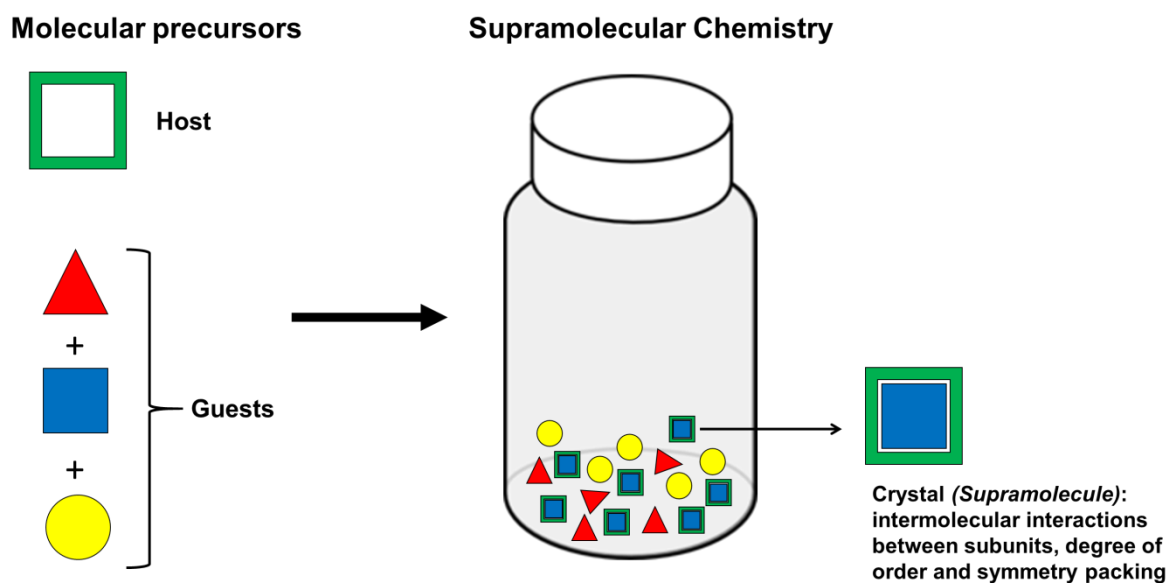


**Figure 1.1** The scope of Supramolecular Chemistry showing the phenomenon of selectivity.

**Table 1.1** Timeline of supramolecular chemistry<sup>4</sup>

Year	Event
1810	Sir H. Davy: discovery of chlorine hydrate
1823	M. Faraday: formula of chlorine hydrate
1841	C. Schafhäütl: study of graphite inclusion intercalates
1849	F. Wöhler: $\beta$ -quinol H <sub>2</sub> S clathrate
1891	A. Villiers and R. Hebd: cyclodextrin inclusion compounds
1893	A. Werner: co-ordination chemistry
1894	H.E. Fischer: 'lock and key' concept
1906	P. Ehrlich: introduction of the concept of a <i>receptor</i>
1937	K.L. Wolf: the term <i>Übermoleküle</i> is coined to describe organised entities arising from the association of co-ordinatively saturated species, e.g the acetic acid dimer
1939	L. Pauling: hydrogen bonds included in the ground-breaking book, <i>The Nature of the Chemical Bond</i>
1940	M.F. Bengen: urea channel inclusion compounds
1948	H.M. Powell: X-ray crystal structures of $\beta$ -quinol inclusion compounds; the word 'clathrate' is introduced to describe compounds where one component is enclosed within the framework of another
1949	C.J. Brown and A.C. Farthing: synthesis of [2.2]paracyclophane
1953	J.D. Watson and F. Crick: described the structure of DNA
1956	D.C. Hodgkin: X-ray crystal structure of vitamin B <sub>12</sub>
1959	D.J. Cram: attempted synthesis of cyclophane charge transfer complexes with (NC) <sub>2</sub> C=C(CN) <sub>2</sub>
1961	N.F. Curtis: first Schiff's base macrocycle from acetone and ethylenediamine
1964	D.H. Busch and E.G. Jäger": Schiff's base macrocycles
1967	C.J. Pedersen: crown ethers
1968	C.H. Park and H.E. Simmonds: <i>Katapinand</i> anion hosts
1969	J-M. Lehn: synthesis of the first cryptands
1969	J.L. Atwood: liquid clathrates from alkyl aluminium salts
1973	D.J. Cram: spherands hosts produced to test the importance of preorganization
1978	J-M. Lehn: introduction of the term 'supramolecular chemistry'
1979	G.W. Gokel and M. Okahara: development of the lariat ethers as a subclass of hosts
1981	F. Vögtle and E. Weber: podand hosts and development of nomenclature
1987	Award of the Nobel prize for chemistry to D.J. Cram, J-M Lehn and C.J. Pedersen for their work in supramolecular chemistry
1996	J.L. Atwood, J.E.D. Davis, D.D. MacNicol and F. Vögtle: publication of the <i>Comprehensive Supramolecular Chemistry</i> containing contributions from almost all the key groups and summarising the development and state of the art
1996	Award of the Nobel prize for Chemistry to H.W. Kroto, R.E. Smalley and R.F. Curl for their work on the chemistry of the fullerenes
1999	The Royal Society launches the journal CrystEngComm with D. Braga as the chairman of the editorial board
2012	J.W. Steed and P.A. Gale: Supramolecular chemistry: From molecules to Nanomaterials

## 1.2 Host-guest compounds and their classification

*“Mankind is divisible into two great classes: host and guest”*

Max Beerbohm (1872), Host and Guest<sup>4</sup>

One of the first formal definitions of a supramolecular cage-like host-guest structure was presented by H.M. Powell in 1948. He coined the term ‘clathrate’ which he introduced to describe a kind of inclusion, where ‘one component is enclosed within the framework of another’.<sup>4</sup> This ‘kind of inclusion’ may be described as a ‘molecular recognition’ defined as the specific binding of a host compound, whose shape is complementary to that of a given guest forming a host-guest complex according to the following equation:  $H_{\alpha\text{phase(s)}} + nG_{(l)} \rightarrow H \cdot G_{n\beta\text{phase(s)}}$ , whereby generally the host, **H** (non-porous  $\alpha$  phase) is a solid that dissolves in a liquid guest, **G**, yielding a host-guest compound ( $\beta$  phase) of given stoichiometry controlled by ‘**n**’. The majority of these host-guest compounds can be classified into two distinct groups depending on the type of the host compound and the topological relationship between the host and the guest (**Figure 1.2**):

- (1) The host (cavitand) is a single large molecule containing a central hole such as a cavity, which encapsulates a smaller guest molecule to form a ‘molecular inclusion’. Examples of host molecules that form this type of inclusion are crown ethers, cyclodextrins, cyclophanes and cryptands.<sup>3,7</sup>
- (2) Alternatively, large host compounds (clathrands) pack in such a way to form voids, where small guest molecules can be placed and resulting in inclusion compounds referred to as a ‘crystal lattice inclusion’. Familiar hosts of this type are water, urea, helical tabuland diols and MacNicol’s hexahosts.<sup>3,4</sup>

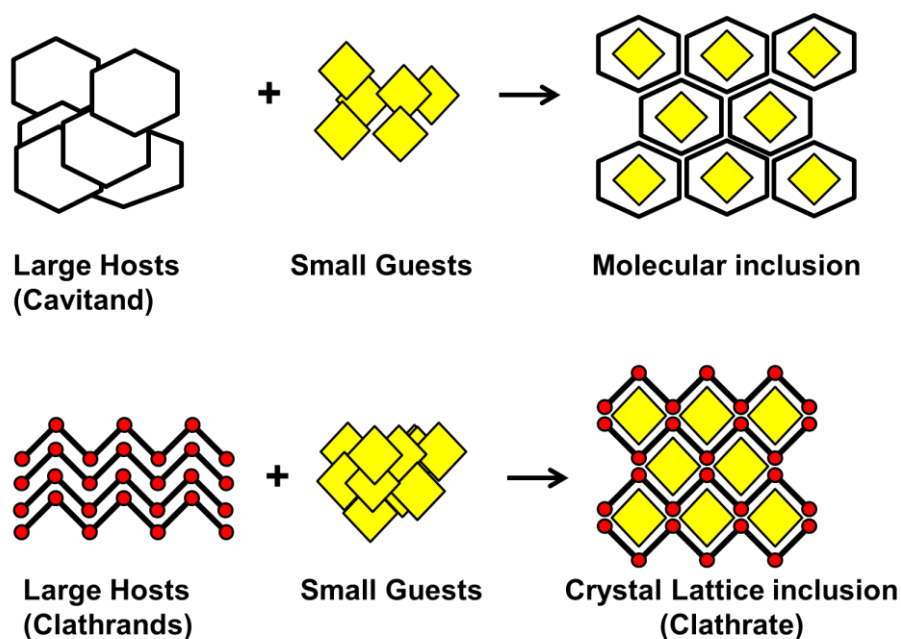


Figure 1.2 Schematic illustration of molecular and lattice inclusion.

### 1.3 Intermolecular interactions

The non-covalent interactions that hold hosts and guests together include a wide range of attractive and repulsive forces. These forces control the packing of the systems and can be classified according to their strength, directional influence and distance dependence. The most common intermolecular interactions are ion-ion, ion-dipole, dipole-dipole interactions, hydrogen bonding, cation- $\pi$ ,  $\pi$ - $\pi$  interactions, van der Waals forces and hydrophobic effects which are summarised in **Table 1.2**<sup>6</sup> along with their approximate energies. Ion-ion (ionic bonding) is the strongest interaction; its strength is comparable to that of a covalent bond. It is non-directional, meaning it can occur in any orientation. Ion-dipole and dipole-dipole interactions, unlike ion-ion, are directionally dependent and therefore only arise when the geometry is optimal. Ion-dipole interactions are strong compared to dipole-dipole interactions, but are weaker than ion-ion interactions. Hydrogen bonding can also be defined as a type of dipole-dipole interaction; its strength varies from strong to weak. Hydrogen bonding is one of the most useful interactions in supramolecular chemistry<sup>8</sup> due to its complex range of lengths, strengths and geometries. Hydrogen bonds hold many organic crystals together and are responsible for the overall shape of many proteins, the recognition of substrates by various enzymes and for the double helix of DNA.<sup>4</sup> The cation- $\pi$  interaction is relatively weak similar to the  $\pi$ - $\pi$  interactions. Van der

Waals forces (London dispersion forces and exchange –repulsion interaction) arise from the polarisation of an electron cloud between two nuclei in close proximity. Hence the strength is dependent on the polarisability of the nuclei and the distance separating the nuclei from one another. Hydrophobic effect arises from the non-polar groups and solvent-solvent interaction energy. Hydrophobic effects are crucially important in macromolecular biological assemblies.<sup>4</sup>

**Table 1.2** Summary of non-covalent interactions<sup>7</sup>

Interaction	Strength bond energy (kJ mol <sup>-1</sup> )	Example
Ion-ion	100-350	Sodium-chloride (NaCl)
Ion-dipole	50-200	Crown ethers and alkaline metal ions
Dipole-dipole	5-50	Acetone
Hydrogen bonding	4-120	Amino acids
Cation- $\pi$	5-80	K <sup>+</sup> in benzene
$\pi$ - $\pi$ interaction	0-50	Benzene and graphite
Van der Waals	<5 kJ mol <sup>-1</sup> but variable depending on surface area	Argon; molecular crystals
hydrophobic effect	Related to solvent-solvent interaction	Cyclodextrin inclusion compounds

## 1.4 Host compounds under study

Most host compounds operate via strong non-bonded interactions with their guest. Typically the host has functional groups with hydrogen bond donor possibilities such as –OH, –NH<sub>2</sub> or –COOH, which interact with acceptor moieties in the guest, such as oxygen or nitrogen atoms. These compounds have been named coordinato-clathrates.<sup>9</sup> However, the host compounds under investigation contain no strong hydrogen bonding possibilities. The 9,9'-bianthryl (C<sub>28</sub>H<sub>18</sub>, **H1**), 9,9'-spirobifluorene (C<sub>25</sub>H<sub>16</sub>, **H2**) and *trans*-2,3-dibenzoylspiro(cyclopropane-1,9'-fluorene) (C<sub>29</sub>H<sub>20</sub>O<sub>2</sub>, **H3**) have scissor-like molecular shapes with the absence of a functional group of the coordinato-clathrate-forming molecules (**Figure 1.3**). These host compounds were synthesised by Professor Edwin Weber at the Institut für Organische Chemie, Freiberg, Germany.<sup>10,11,12,13</sup> The enclathration capabilities of these host compounds with a variety of hydrocarbons and simple heterocyclic guests have been studied by Weber, Ahrendt, Czugler and Csöreg, <sup>10,14</sup> who showed that the **H1** and **H2**



compounds have a molecular shape that renders them efficient host molecules. The above authors list a number of guest molecules that are entrapped by these two host compounds. The guest molecules include cyclic hydrocarbons, the isomers of xylene, cyclic ketones and various amines. **H1** exhibits two polymorphic structures,<sup>15,16</sup> and crystal structures with the **H1** apohost and benzene,  $\alpha$ -ionone<sup>17</sup> and chlorocyclohexane<sup>18</sup> have been elucidated. The bifluorene host, **H2**, also manifests two different solid forms of the apohost,<sup>19,20</sup> and its clathrates with benzene and biphenyl have been characterised. Only one crystal structure of the host **H3** has been published, which is that of its inclusion compound with toluene.<sup>21</sup> The lack of hydrogen bond donor moieties on the host compounds means the hosts will operate on the principle of enclathration by virtue of the topology of the inclusion compound formed. In other words, the guest molecules enclosed in the crystal lattice with the host will occur by 'lattice imprisonment' (clathrate formation).<sup>13</sup>

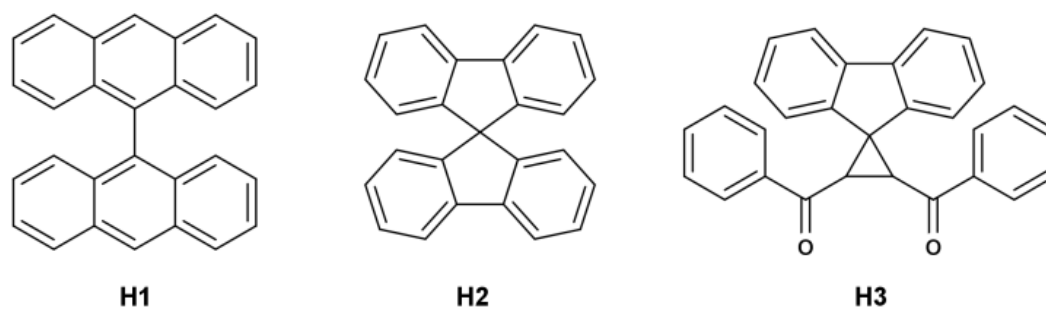


**Figure 1.3** Structural diagram of hosts: 9,9'-bianthryl (**H1**), 9,9'-spirobifluorene (**H2**) and *trans*-2,3-dibenzoylspiro(cyclopropane-1,9'-fluorene) (**H3**).

## 1.5 Guest compounds under study

The application and production of important industrial isomeric compounds in the current study will be outlined in this section. The guest isomers under investigation were chosen according to compatibility with the host compounds; therefore small guest molecules with similar aromatic groups and cyclohexanone derivatives were selected, rendering to possible  $\pi$ - $\pi$  interactions. The guest molecules include structurally similar heterocyclic aromatic compounds, derivatives of cyclohexanone and xylene isomers.

### 1.5.1 Heterocyclic aromatic compounds

The selectivity of host compounds **H1**, **H2** and **H3** towards pyridine (**PYR**), piperidine (**PIP**), morpholine (**MOR**) and 1,4-dioxane (**DIO**) was studied. The structurally similar heterocyclic compounds (**Figure 1.4**) are used in a wide range of applications. Pyridine, piperidine, and morpholine are used in manufacturing of many bioactive substances like drugs, insecticides, herbicides, food preservatives and food additives.<sup>22</sup> Dioxane is used in the productions of inks and adhesives.<sup>23</sup> Numerous structures with these guest compounds have been reported in the Cambridge Structural Database (CSD)<sup>24</sup> highlighting the importance of these guests.

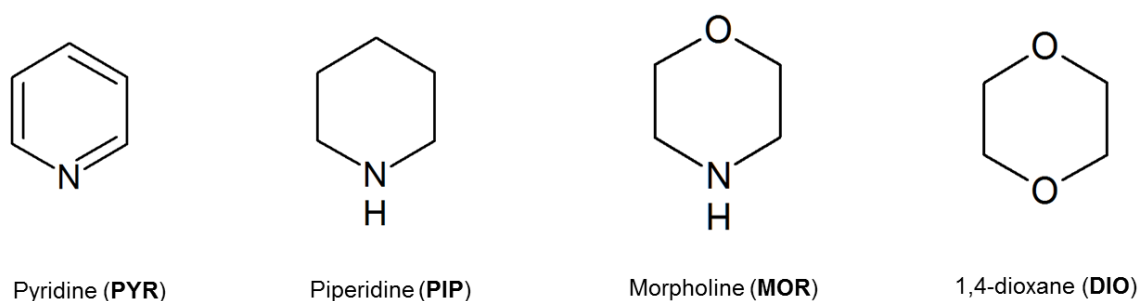


**Figure 1.4** Skeletal structures of pyridine (**PYR**), piperidine (**PIP**), morpholine (**MOR**) and 1,4-dioxane (**DIO**).

### 1.5.2 Cyclohexanone derivative compounds

This research attempts to separate cyclohexanone (**CYHA**), 2-methylcyclohexanone (**2-MCYHA**), 3-methylcyclohexanone (**3-MCYHA**) and 4-methylcyclohexanone (**4-MCYHA**) from their mixtures by employing the principle of host-guest chemistry. The skeletal structures of these cyclic ketone guests are displayed in **Figure 1.5**. The **CYHA** guest is an important material in the nylon industry; it is used for the manufacture of caprolactam, a raw material used in the production of nylon and other synthetic fibres. The purity of **CYHA** directly affects the quality of the final product and thus separating of **CYHA** with a high percentage yield is important. Studies show that generally distillation is used in separation of organic compounds such as **CYHA**, however the separation of **CYHA** requires a three step distillation process and from an energy saving point of view this is relatively inefficient.<sup>25,26</sup> Shimidzu and Oskushita used a poly-(N-vinylpyrrolidone-co-acrylonitrile) membrane that selectively separates cyclohexanone and cyclohexanol from a cyclohexane-

cyclohexanone-cyclohexanol mixture by pervaporation.<sup>27</sup> The methylcyclohexanone (**MCYHA**) isomers are used in flavour and fragrance agents and, similarly to the xylenes, display similar chemical and physical properties. The boiling points are close, differing only by 8°C. Therefore they cannot easily be separated by distillation columns (**Table 1.3**). **2-MCYHA** and **3-MCYHA** are chiral compounds while **4-MCYHA** is achiral. Previous studies mainly focus on enantioseparation of these isomers. Toda and Tanaka employed the chiral host compound (*R,R*)-(-)-1,6-bis(*o*-chlorophenyl)-1,6-diphenylhexa-2,4-diyne-1,6-diol to resolve 3-methylcyclohexanone by dissolving the two enantiomers in petroleum ether at room temperature and harvesting the crystals.<sup>28,29</sup> The current thesis is concerned with separating the **MCYHA** racemates from one another. Chromatographic methods are commonly used in separating the three **MCYHA** isomers, but this technique is limited to a small amount of sample. Industrial amounts would render this technique inefficient.<sup>30</sup>

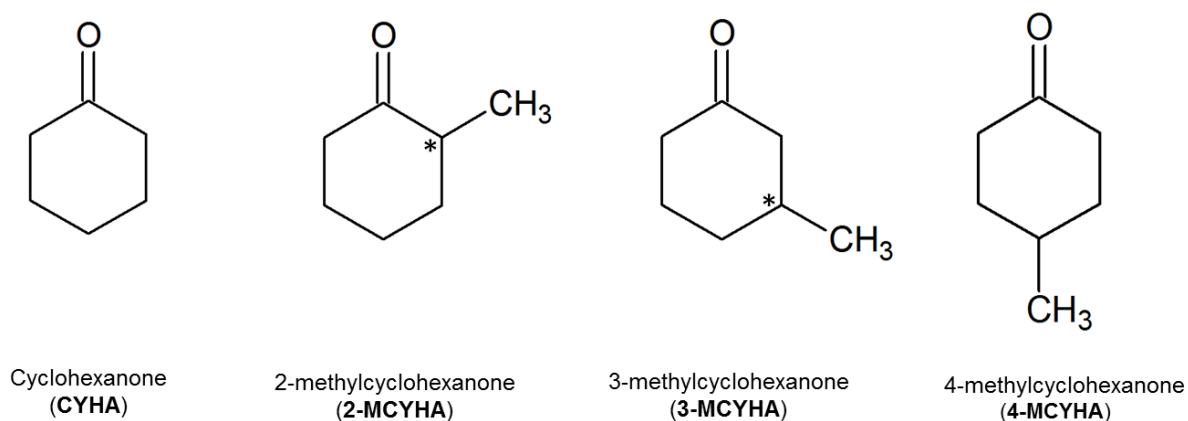


**Figure 1.5** Skeletal structures of cyclohexanone (**CYHA**), 2-methylcyclohexanone (**2-MCYHA**), 3-methylcyclohexanone (**3-MCYHA**) and 4-methylcyclohexanone (**4-MCYHA**).

**Table 1.3** Normal boiling and melting points of cyclohexanone (**CYHA**), 2-methylcyclohexanone (**2-MCYHA**), 3-methylcyclohexanone (**3-MCYHA**) and 4-methylcyclohexanone (**4-MCYHA**)<sup>31</sup>

	<b>CYHA</b>	<b>2-MCYHA</b>	<b>3-MCYHA</b>	<b>4-MCYHA</b>
<b>Boiling point/ °C</b>	144.4	162-163	169-170	156
<b>Melting point/ °C</b>	-47	-14	-73	-41

### 1.5.3 Xylene isomers

The three isomers of xylene; *ortho*-xylene (**ox**), *meta*-xylene (**mx**) and *para*-xylene (**px**) are obtained by the catalytic process of naphtha reforming<sup>32,33</sup> (**Figure 1.6**). The isomers are important raw materials for the manufacture of a variety of products.<sup>34</sup> *Para*-xylene is converted into terephthalic acid and dimethylterephthalate and subsequently to poly(ethyleneterephthalate). *Ortho*-xylene is converted to phthalic anhydride, used in plasticisers and *meta*-xylene is used to obtain isophthalic acid and isophthalic nitrite. The xylene isomers have similar boiling points but different melting points (**Table 1.4**), thus the separation of the isomers by distillation is difficult. Fractional crystallisation has been employed to separate *para*-xylene from the other two isomers because of its higher melting point. The process is however rendered inefficient by the formation of an eutectic mixture of components. Most industrial separations currently use selective adsorption on zeolites and these processes have been reviewed.<sup>35,36</sup> The separation of xylene isomers by metal organic frameworks and by host-guest chemistry techniques have been studied.<sup>37,38</sup> Lusi and Barbour<sup>39</sup> utilized the Werner-host  $[\text{Ni}(\text{NCS})_2(\textit{para}\text{-phenylpyridine})_4]$  to selectively enclathrate **ox** over **mx** and **px** from an equimolar ternary mixture and **mx** over **px** from a binary mixture of the xylene vapours. The following study applies host-guest chemistry as a tool of separation technology.

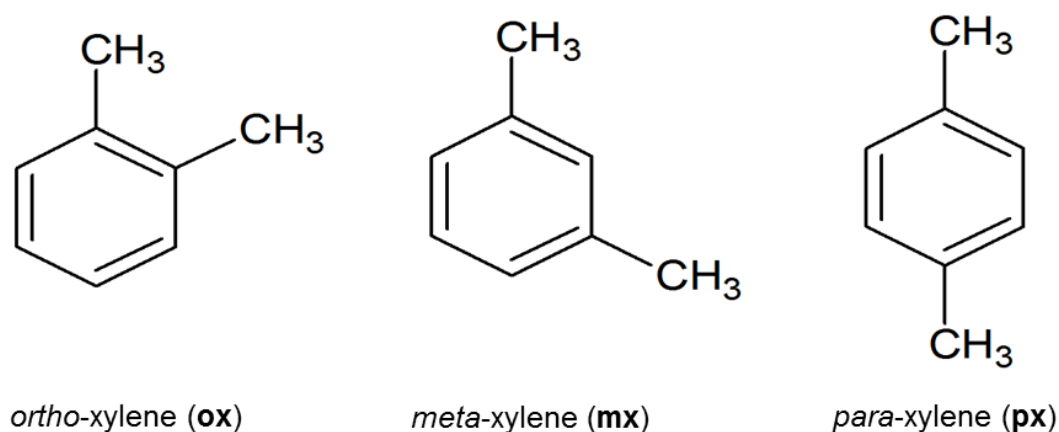


**Figure 1.6** Skeletal structures of xylene isomers.

**Table 1.4** Normal boiling and melting points of xylenes<sup>32</sup>

	<b>ortho-xylene</b>	<b>meta-xylene</b>	<b>para-xylene</b>
<b>Boiling point/ °C</b>	144.4	139.1	138.3
<b>Melting point/ °C</b>	-25.2	-47.9	+13.4

## 1.6 Potential host-guest intermolecular interactions in analysed systems

### 1.6.1 $\pi$ - $\pi$ interactions

According to previous studies organic crystalline materials composed of aromatic hydrocarbons and heteroaromatic molecules exhibit  $\pi$ - $\pi$  interactions, hence the importance of  $\pi$ - $\pi$  interactions to the present study.  $\pi$ - $\pi$  interactions are weak electrostatic attractions that occur between neighbouring aromatic rings, whereby one is moderately electron rich and one is electron poor. These interactions display a wide variety of geometric arrangements illustrated in **Figure 1.7**.<sup>3,40,41</sup> Parallel face-centred and parallel offset  $\pi$ -stacking is responsible for the 'slippery texture' of graphite. The covalently bonded lattice sheets in the graphite structure are arranged in layers held together by  $\pi$ - $\pi$  interactions that easily slide over each other. This explains graphite's useful lubricant properties. Similarly the  $\pi$ -interactions between the aryl ring of the nucleobase pairs help stabilise the DNA double helix. Perpendicular t-shaped and y-shaped geometries are responsible for the typical herringbone packing of small aromatic hydrocarbons in crystal structures. Hunter and Sanders<sup>42</sup> have provided a good qualitative understanding of these interactions. They proposed a simple model that considers the competing electrostatic and van der Waals influences which are related to polarised  $\pi$ -systems. The model explains the different geometries observed in  $\pi$ -interactions and quantitatively predicts the interaction energies. Their model is centred on an overall attractive van der Waals interaction, which is relative to the contact surface area of two  $\pi$ -systems. This attractive interaction signifies the overall energy of the  $\pi$ - $\pi$  interaction and may be observed as the attraction between a negatively charged  $\pi$ -electron cloud of one molecule and positively charged  $\sigma$ -framework of an adjacent molecule. The electrostatic repulsions between two negatively charged  $\pi$ -systems predict the orientation of the interacting molecules<sup>3</sup> (**Figure 1.8**). The above authors stress the significance of interacting atom pairs rather than whole molecules and their approach has been relatively successful, however there is still a great deal of ambiguity over the nature of  $\pi$ - $\pi$  interactions.

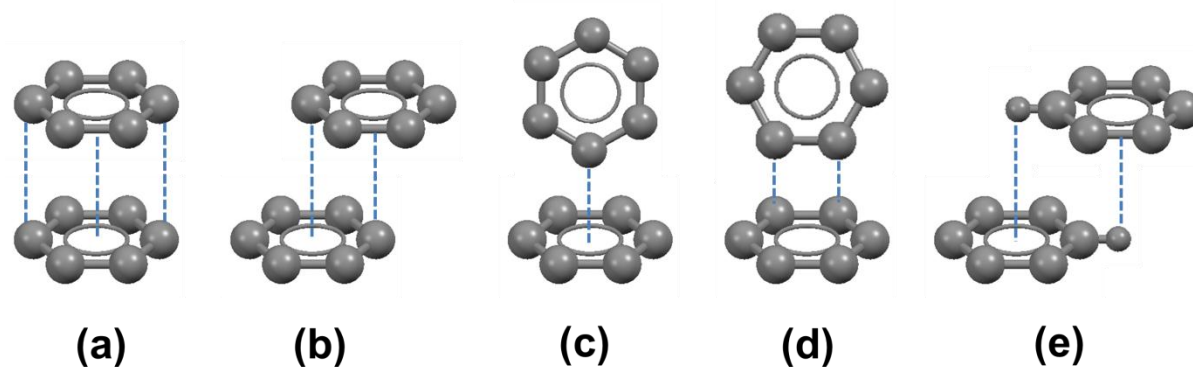


**Figure 1.7** Possible aromatic stacking arrangements **(a)** parallel face-centred, **(b)** parallel offset, **(c)** Perpendicular t-shaped, **(d)** perpendicular y-shaped and **(e)** parallel offset for toluene.<sup>41</sup>

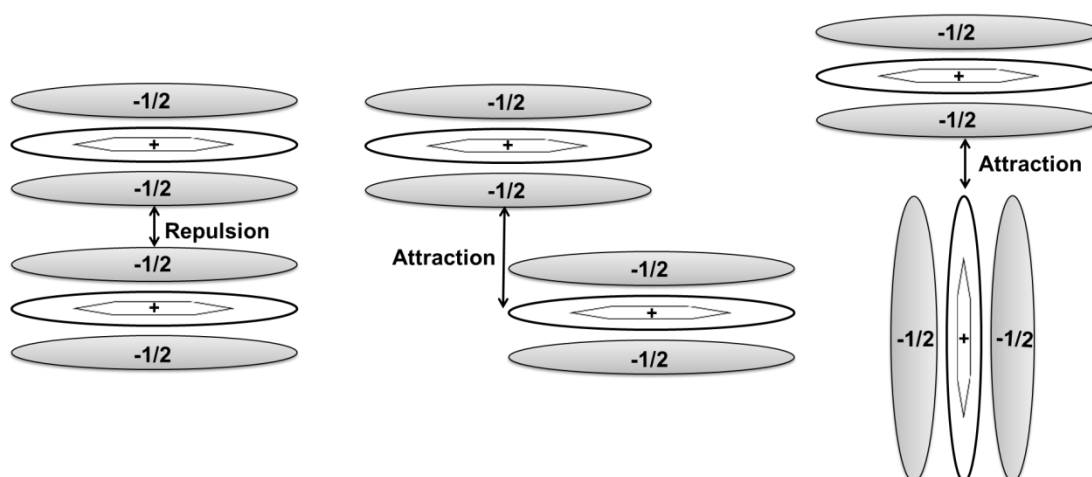


**Figure 1.8** Possible interactions between  $\pi$  systems.

### 1.6.2 Van der Waals forces

Van der Waals forces arise from polarisation of an electron cloud of two neighbouring nuclei in close proximity producing a weak electrostatic attraction. They are non-directional and therefore have a limited effect on the supramolecular design. Van der Waals forces typically provide a general attractive interaction for most polarisable species. Van der Waals forces are responsible for the interactions between noble gases. In supramolecular chemistry they are essential for the formation of inclusion compounds where small organic guests are loosely packed within crystal lattices or molecular cavities. An example is the inclusion of toluene with *p*-*tert*-butylcalix[4]arene where the toluene guest is held in molecular cavities of

the *p*-*tert*-butylphenol-based host.<sup>4</sup> Van der Waals interactions can be split into London dispersion forces and exchange–repulsion<sup>4</sup>. Attractive dispersion forces are caused by fluctuating electron clouds in neighbouring species. The attraction is proportional to the size of interacting molecules and inversely proportional to their distance ( $r^{-6}$  dependence) contributing to the overall energy. Exchange-repulsion stabilises the dispersion forces and defines the molecular shape; it plays a significant role in crystal packing.

## 1.7 Crystal engineering

*“Crystallisation of organic ions with metal-containing complex ions of suitable sizes, charges and solubilities results in structures with cell and symmetries determined chiefly by the packing of complex ions.”*

Ray Pepinsky (1955)

Ray Pepinsky first used the term ‘crystal engineering’ at the meeting of the American Physical Society in Mexico City in 1955.<sup>43</sup> His definition incorporated the scope of engineering as it is being practised today because it contains the three important aspects of engineering, namely function, design and analysis. Crystal engineering may be defined as the understanding of intermolecular interactions and molecular architecture to design new solids with desirable physical and chemical properties.<sup>44</sup> Crystal engineering emerged from the field of supramolecular chemistry; its final recognition stage was in 1991 when Jack Dunitz described an organic crystal as a ‘*supramolecule par excellence*’ where he based his hypothesis on supramolecular chemistry.<sup>45</sup> From Dunitz’ concept of ‘*a crystal as supramolecular entity*’ Gautam Desiraju suggested that crystal engineering, the design and construction of crystalline materials, is a form of solid state supramolecular synthesis. The term ‘synthon’ is used by supramolecular chemists to describe structural units within a crystal that can be designed by acknowledged and possible synthetic operations. **Figure 1.9** displays some examples of supramolecular synthons that can be used to produce predictable patterns.<sup>44,46</sup>

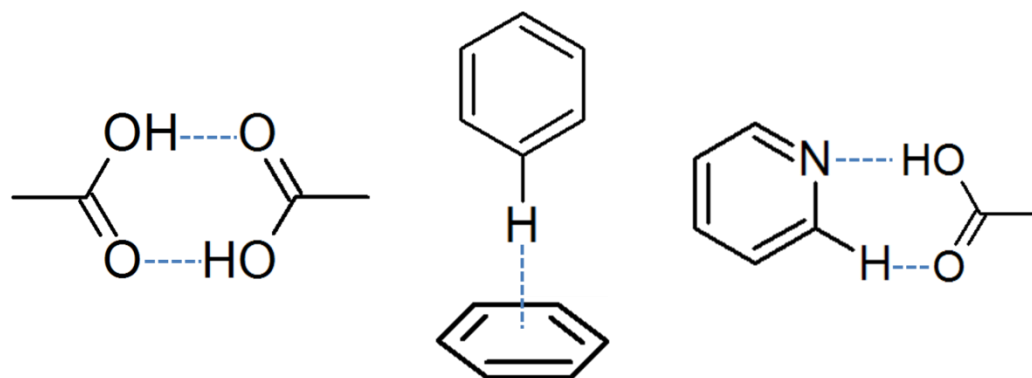


**Figure 1.9** Examples of supramolecular synthons.

## 1.8 Separation by selective inclusion

One of the most difficult procedures in chemistry is the separation of isomers with similar chemical structures. This is because their physical and chemical properties are generally so similar that most of the common separation techniques do not work. The typical separation techniques used in chemistry are distillation, filtration and chromatography. The specific reasons why some of the methods are ineffective are because isomers have similar boiling point and therefore cannot easily be separated by distillation. Filtration is only good for separating heterogeneous mixtures and chromatography is effective with small scale samples only. Well-established separation techniques used in industry that result in high purity products are distillation, precipitation, solvent extraction and reverse osmosis. A common disadvantage with these conventional methods is that most of them rely on the chemical properties and behaviour of the compounds being separated; they are not species specific. Selective inclusion is a useful separation tool and has been applied in the separation of constitutional isomers, stereoisomers and regioisomers. Selective inclusion when using a chiral host compound has successfully resolved several racemates and thus plays a significant role in the pharmaceutical industry. The reason for this is that although enantiomers have identical physico-chemical properties (except their interaction with polarised light), they react differently towards other chiral compounds. The resolution of racemic ibuprofen is one of the many studies carried out, whereby selective inclusion was used to resolve this pharmaceutical product.<sup>47</sup> A tragic example was the use of thalidomide in 1958 to treat morning sickness in pregnant women. The ingestion of the racemic mixture



resulted in severe limb deformities of the newly born children.<sup>48</sup> In recent years, most synthesised optically active drugs have been resolved as single isomers by using selective inclusion methods or by direct asymmetric synthesis.

Urea in the petroleum industry has been used to separate linear and branched hydrocarbons from one another.<sup>49</sup> Union oil company uses Ni(4-methylpyridine)<sub>4</sub>(SCN)<sub>2</sub> for separating *meta*- and *para*-xylene.<sup>50</sup> The importance of separation processes by enclathration to industry has been outlined in a book called separation technology in petroleum and chemical industries in the USA.<sup>51</sup> There is need for new separation methods that would be more cost effective, environmentally friendly and more energy efficient. The importance of research on alternative methods for industry is evident.

## 1.9 Physical chemistry of inclusion compounds

The discovery of X-rays in 1895 enabled scientists to investigate crystalline materials at an atomic level. X-ray diffraction is the main physical technique used in solid state supramolecular chemistry. X-rays are used in powder X-ray diffraction (PXRD) for the characterisation of crystalline materials and single crystal X-ray diffraction (SCXD) for the determination of crystal structures. The SCXD method allows important information of a crystal structure to be easily obtained such as the geometries and interatomic distances, giving rise to the type of non-covalent interactions and furthermore the packing of the system can be determined, revealing whether the guest is located in channels, cavities or layers within the host framework. The PXRD method produces X-ray powder patterns, unique to each crystalline substance and is used as a “fingerprint” for identification. X-ray diffraction is not a “stand alone” technique. This method does not quantify the relative percentages of host and guest. This is because inclusion compounds are often non-stoichiometric therefore other techniques such as gas chromatography, mass spectroscopy, infrared spectroscopy and nuclear magnetic resonance spectroscopy must be employed.

Thermal analysis is another very important technique used in the characterisation of inclusion compounds. Thermal analysis measures change in the physical properties

of a substance as a function of temperature. The two main methods are thermogravimetry (TG) and differential scanning calorimetry (DSC). TG is used for the determination of the host-guest ratios of inclusion compounds and DSC estimates the onset temperatures of decomposition as well as the enthalpy changes accompanied by the departure of a volatile guest from the host-guest inclusion compound. These changes can be due to desolvation, phase transformation, melting and other thermal events.

## 1.10 Aims and objectives

This study attempts to separate isomers and structurally similar guest compounds with similar physical and chemical properties by employing host-guest chemistry.

The three host compounds: 9,9'-bianthryl ( $C_{28}H_{18}$ , **H1**), 9,9'-spirobifluorene ( $C_{25}H_{16}$ , **H2**) and *trans*-2,3-dibenzoylspiro(cyclopropane-1,9'-fluorene) ( $C_{29}H_{20}O_2$ , **H3**) were employed to separate the following three target isomeric mixtures;

- (1) Pyridine (**PYR**), piperidine (**PIP**), morpholine (**MOR**) and 1,4-dioxane (**DIO**)
- (2) Cyclohexanone (**CYHA**), 2-methylcyclohexanone (**2-MCYHA**),  
3-methylcyclohexanone (**3-MCYHA**) and 4-methylcyclohexanone (**4-MCYHA**)
- (1) *Ortho*-xylene (**ox**), *meta*-xylene (**mx**) and *para*-xylene (**px**).

The aim was to achieve a high level of separation and if the given separation is successful and the host compounds can be recycled, then we have the possibility of a patent application.

The study inclusively attempts to obtain important information from analysis, which will be beneficial to design more efficient host compounds for the separation experiments.

## References

---

- <sup>1</sup> Lehn, J.-M. *Supramolecular Chemistry: Concepts and Perspectives.*, 1995, VCH: New York.
- <sup>2</sup> Lehn, J.-M. *Comprehensive Supramolecular Chemistry (Volume 6)*, edn., 1996, United Kingdom.
- <sup>3</sup> Desiraju, G.R. *J. Am. Chem. Soc.*, 2013, 135: 9952.
- <sup>4</sup> Steed, J.W. & Atwood, J.L. *Supramolecular Chemistry*, 2<sup>nd</sup> edn., 2009, Wiley, United Kingdom.
- <sup>5</sup> Nagendrappa, G., *Resonance*, 2011, 606.
- <sup>6</sup> Steed, J.W., Turner, D.R. & Wallace, K.J. *Core Concepts in Supramolecular chemistry and Nanochemistry*, 2007, John Wiley & Sons.
- <sup>7</sup> Matsumoto, K. & Hayashi, N. *Heterocyclic Supramolecules II*, 2009, Springer, London, New York.
- <sup>8</sup> Taylor, R., *CrystEngComm*, 2014, 16: 6852.
- <sup>9</sup> Báthori, N.B. & Nassimbeni, L.R. *Cryst. Growth. Des.*, 2010, 10: 1782.
- <sup>10</sup> Weber, E., Adrendt, J., Czugler, M. & Csöreg, I. *Angew. Chem. Int. Ed.*, 1986, 25, 746.
- <sup>11</sup> Synthesis of **H1**: Bell, F. & Waring, D.H. *J. Chem. Soc.*, 1949, 267:1579.
- <sup>12</sup> Synthesis of **H2**: Clarkson, R.G. & Gomberg, M. *Ibid.*, 1930, 52: 2881; Haas, G. & Prelog, V. *Helv. Chim. Acta.*, 1969, 52: 1202.
- <sup>13</sup> Institut für Organische Chemie, TU Bergakademie Freiberg, Leipziger Str. 29, Sachs, D-09596 Freiberg, Germany.
- <sup>14</sup> Csöreg, I., Gallardo, O., Weber, E., Hecker, M. & Wierig, A. *Supramol. Chem.*, 1994, 3: 319.
- <sup>15</sup> Langer, V., Seiler, J. & Becker, H.D. *Z. Kristallogr.*, 1992, 199: 300.
- <sup>16</sup> Kyziol, J.B. and Zaleski, J. *Acta Crystallogr., Sect. E*, 2007, 63: 1235.
- <sup>17</sup> Toda, F., Tanaka, K. and Fujiwara, T. *Angew. Chem. Int. Ed.*, 1990, 29: 662.
- <sup>18</sup> Hirano, S., Toyota, S., Kato, M. & Toda, F. *Chem. Commun.*, 2005: 3646.
- <sup>19</sup> Schenk, H. *Acta Crystallogr., Sect. B*, 1972, 28: 625.
- <sup>20</sup> Douhwaite, R.E., Taylor A. & Whitwood, A.C. *Acta Crystallogr., Sect. C*, 2005, 61: 328.
- <sup>21</sup> Csöreg, I., Gallardo, O., Weber, E., Hecker M. & Wierig, A. *Supramol. Chem.*, 1994, 3: 319.
- <sup>22</sup> Báthori, N.B. & Nassimbeni, L.R. *Cryst. Growth. Des.*, 2010, 10: 1783.
- <sup>23</sup> Felix-Navarro, R. A., Wai Lin, S., Zizumbo-López, A., Pérez-Sicairos, S., Reynoso-Soto, E. A. & Espinoza-Gómez, J.H. *J. Mex. Chem. Soc.*, 2013, 51: 2.
- <sup>24</sup> Groom, C.R. & Allen, F.H. *Angew. Chem. Int. Ed.*, 2014, 53: 662.
- <sup>25</sup> Aucejo, A., Burguet, M.C., Muñoz, R. & Vazquez, M.I. *J. Chem. Eng. Data*, 1993, 38: 379.
- <sup>26</sup> Burguet, M.C., Montón, J.B., Sanchotello, M. & Vazquez, M.I. *J. Chem. Eng. Data*, 1993, 38: 328.
- <sup>27</sup> Shimidizu, T & Okushita, H. *J. Membr. Sci.*, 1988, 39: 113.
- <sup>28</sup> Nassimbeni, L. R., Su. H. & Curtin T-L. *Chem. Commun.*, 2012, 48: 8526.
- <sup>29</sup> Toda, F., Tanaka, K., Omata, T., Nakamura, K. & Oshima, T.J. *J. Am. Chem. Soc.*, 1983, 105: 5151.
- <sup>30</sup> Cirilli, R., Ferretti, R., La Torre, F., Secci, D., Bolasco, A., Carradori, S. & Pierini M., *J. Chromatogr., A*. 2007, 1172: 160.
- <sup>31</sup> Windholz, M. Ed. *The Merck Index: An Encyclopaedia for chemicals and drugs*, Merck & Co. Inc., 1976, New Jersey.
- <sup>32</sup> Turaga, U.T. & Ramanathan, R. *J. Sci. Ind. Res.*, 2003, 62: 963.
- <sup>33</sup> Rahimpour, M.R., Jafari, M. & Iranshahi, D. *Appl. Energy*, 2013, 109: 79.
- <sup>34</sup> Arpe, H.J. *Industrielle Organische Chemie.*, 6th Ed., 2007, Wiley-VCH, Weinheim.
- <sup>35</sup> Santos, K.A.O., Dantas Neto, A.A., Moura M.C.P.A. & Casto Dantas, T.N. *Braz. J. Petrol. Gas.*, 2011, 5: 25.

- 
- <sup>36</sup> Cannella, W.J. *Kirk-Othmer Encyclopaedia of Chemical Technology*, 2007, Wiley, New York.
- <sup>37</sup> Finsy, V., Kirshhock, C.E.A., Vedts, G., Maoes, M. Alaerts, L., DeVos, D.E. Barou, G.V. & Denayer, J.F.M. *Chem. Eur. J.*, 2009, 15: 7724.
- <sup>38</sup> Gu, Z.Y., Jiang, D.Q., Wang, H.F., Cui, X.Y. & Yan, X.P. *J. Phys. Chem. Solids*, 2010, 114: 311.
- <sup>39</sup> Lusi, M. & Barbour, L.J. *Angew. Chem. Int. Ed.*, 2012, 51: 3931.
- <sup>40</sup> McGaughey, G.B., Gagne, M. & Rappe, A. K. *J. Biol. Chem.*, 1998, 273:15458.
- <sup>41</sup> Martinez, C.R. & Iverson, B. L. *J. Chem. Sci.*, 2012, 3: 2191.
- <sup>42</sup> Hunter, C.A. & Sanders, J.K.M. *J. Am. Chem. Soc.*, 1990, 112: 5525.
- <sup>43</sup> Desiraju, G.R., Vittal, J.J. & Ramanan, A. *Crystal Engineering A Text Book*, 2011, World Scientific, India.
- <sup>44</sup> Desiraju, G.J. *Chem.Sci.*, 2010, 22: 667.
- <sup>45</sup> Dunitz, J.D. *Pure Appl. Chem. Ed.*, 1991, 63: 177.
- <sup>46</sup> Desiraju, G.R. and Vittal, J.J. (eds). *Crystal engineering. Structure and Function. Perspectives in supramolecular chemistry*, 2003, Wiley, Chichester.
- <sup>47</sup> Molnár, P., Bombicz, P., Varaga, C., Bereczky, L., Székely, E., Pokol, G., Fogassy, E. & Simándi, B. *Chirality*, 2009, 21: 628.
- <sup>48</sup> Smithells, R.W. & Newman, C.G.H. *J. Med. Genet.*, 1992, 29: 716.
- <sup>49</sup> Arousseau, B. & Bauchart, D.J. *Am. Oil Chem. Soc.*, 1980, 7: 125.
- <sup>50</sup> Davis, J.E.D., Kemula, W., Powel, H.M. & Smith, N. O. *J. Incl. Phenomen.* 1983, 1: 3.
- <sup>51</sup> Panel on Separation Technology for industrial Reuse and Recycling, Committee on Industrial Technology Assessments, National Research Council, *Separation technologies for the Industries on the Future*, National Academy Press, 1999, Chapter 3, Washington.
- <sup>51</sup> Vögte, F., 1991, *Supramolecular Chemistry*, Wiley, England.
- <sup>52</sup> Atwood, J.L. & Steed, J.W. *Encyclopaedia of Supramolecular Chemistry*, 2004, Marcel Dekker, New York.
- <sup>54</sup> Schneider, H. & Yatsimirsky, A. *Principle and Methods in Supramolecular Chemistry*, 2000, Wiley, England

## Chapter 2: Experimental

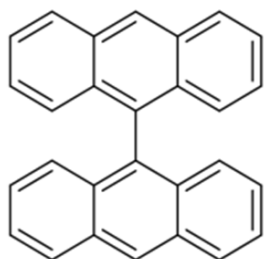
---

### 2.1 Host and guest compounds

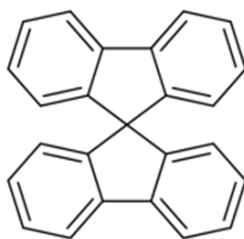
The host compounds 9,9'-bianthryl ( $C_{28}H_{18}$ , **H1**), 9,9'-spirobifluorene ( $C_{25}H_{16}$ , **H2**) and trans-2,3-dibenzoylspiro(cyclopropane-1,9'-fluorene) ( $C_{29}H_{20}O_2$ , **H3**) were synthesised by Professor Edwin Weber from the Institute for Organic chemistry, Freiberg, Germany.<sup>1,2,3,4</sup> These scissor-like molecular hosts lack hydrogen bond donor moieties such as  $-OH$ ,  $-NH_2$  or  $-COOH$  (**Figure 2.1**). The absence of the hydrogen bonding functional groups means no strong hydrogen bonding can occur and the possible non-bonding interactions between host and guest are  $C-H\cdots\pi$  interactions,  $\pi\cdots\pi$  interactions and van der Waals forces, all of which are weak.

Guest compounds under investigation are presented in **Table 2.1**. They are categorised into three target mixtures; (i) heterocyclic aromatic compounds, (ii) cyclohexanone derivatives and (iii) xylene isomers (**Figure 2.1**). Due to similarity of shape and chemical structure, these target mixtures tend to have similar physical and chemical properties (**Table 2.2**) which make them very difficult to separate. Common separation techniques are not efficient and thus the current study employs host-guest chemistry to try and separate them.

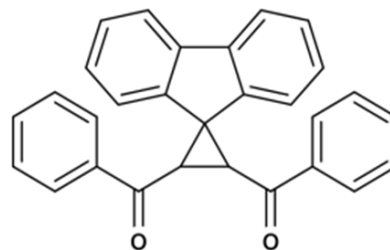
## Hosts compounds



H1

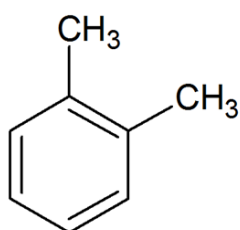
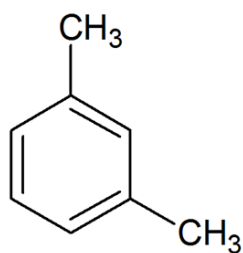
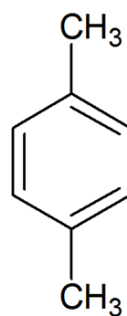
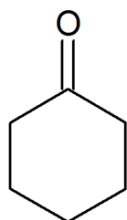


H2

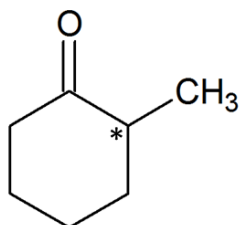


H3

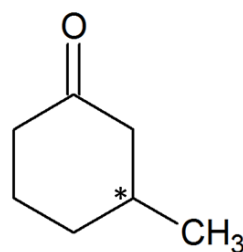
## Guest molecules

*ortho*-xylene*meta*-xylene*para*-xylene

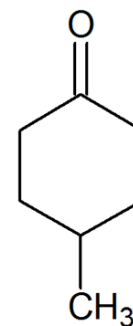
cyclohexanone



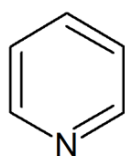
2-methylcyclohexanone



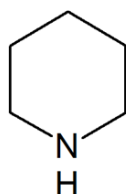
3-methylcyclohexanone



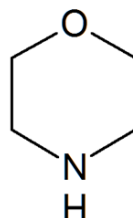
4-methylcyclohexanone



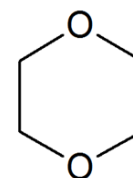
pyridine



piperidine



morpholine



1,4-dioxane

**Figure 2.1** Schematic diagram of host and guest compounds applied in the study.

**Table 2.1** Guests employed for the study

	Target mixtures	Guests employed	Abbreviation
<b>i</b>	Heterocyclic aromatic compounds	Pyridine	<b>PYR</b>
		Piperidine	<b>PIP</b>
		Morpholine	<b>MOR</b>
		1,4-dioxane	<b>DIO</b>
<b>ii</b>	Cyclohexanone derivatives	Cyclohexanone	<b>CYHA</b>
		2-methylcyclohexanone	<b>2-MCYHA</b>
		3-methylcyclohexanone	<b>3-MCYHA</b>
		4-methylcyclohexanone	<b>4-MCYHA</b>
<b>iii</b>	Xylene isomers	<i>Ortho</i> -xylene	<b>ox</b>
		<i>Meta</i> -xylene	<b>mx</b>
		<i>Para</i> -xylene	<b>px</b>

**Table 2.2** Physical properties of guest compounds<sup>5</sup>

Guest	Molecular formula	Molecular mass (g/mol)	Density (g/ml)	Melting point (°C)	Boiling point (°C)	pKa
<b>PYR</b>	C <sub>5</sub> H <sub>5</sub> N	79.10	0.98	-42	115	5.25
<b>PIP</b>	C <sub>5</sub> H <sub>11</sub> N	85.15	0.86	-7	106	11.22
<b>MOR</b>	C <sub>4</sub> H <sub>9</sub> NO	87.12	1.00	-5	129	8.36
<b>DIO</b>	C <sub>4</sub> H <sub>8</sub> O <sub>2</sub>	88.11	1.03	+12	101	-
<b>CYHA</b>	C <sub>6</sub> H <sub>10</sub> O	98.15	0.95	-47	156	-
<b>2-MCYHA</b>	C <sub>7</sub> H <sub>12</sub> O	112.17	0.92	-14	162-163	-
<b>3-MCYHA</b>	C <sub>7</sub> H <sub>12</sub> O	112.17	0.91	-73	169-170	-
<b>4-MCYHA</b>	C <sub>7</sub> H <sub>12</sub> O	112.17	0.91	-41	169-170	-
<b>ox</b>	C <sub>8</sub> H <sub>10</sub>	106.16	0.88	-25	144	-
<b>mx</b>	C <sub>8</sub> H <sub>10</sub>	106.16	0.86	-48	139	-
<b>px</b>	C <sub>8</sub> H <sub>10</sub>	106.16	0.86	+13	138	-

## 2.2 Crystal growth

The inclusion compounds were prepared using the slow evaporation technique. This method involves the crystals being synthesised by slowly dissolving a specific host compound in a given guest until the resultant solution is completely saturated and clear. The solution was then left open at room temperature to evaporate and crystallise. For slower evaporation the solution was sealed with a pierced cover; this was carried out when tiny crystals formed too quickly. The host-guest complex was then subjected to the relevant analysis.

## 2.3 Competition experiments

Competition experiments were set up to determine the selectivity of a host towards a particular mixture of guests. A known mass of single host (**H1**, **H2** or **H3**) was dissolved separately into each pure guest (see **Table 2.1**), the binary equimolar mixture of the two guests and the tertiary equimolar mixture of all three guests in a set of target mixtures. The slow evaporation method was used for crystal growth. The crystals formed were harvested and analysed.

The selectivity of a given host towards the guests is dependent on the level of recognition between the two. A convenient measure for selectivity is the determination of the selectivity co-efficient. The selectivity co-efficient is defined by:

$$K_{A:B} = (K_{B:A})^{-1} = Z_A/Z_B \times X_B/X_A \quad (X_A + X_B = 1)$$

Where by  $X_A$  and  $X_B$  are the mole fractions of the two guests A and B in the mother liquor and  $Z_A$  and  $Z_B$  are the mole fractions of the guests entrapped in the resultant crystals. The study employed two guest mixtures where one of the given guest's mole fraction varied from 0 to 1 in steps of 0.1.<sup>6</sup> For example, an equimolar mixture was made of the guests A and B (mole fraction  $X_A$ ,  $X_B = 0.5$ ), and then added to the host compound and then their mole fractions in the crystals obtained were determined by a suitable analytical technique. For example, the results showed that



the host preferentially captured A over B in the crystal to give  $Z_A = 0.8$  and  $Z_B = 0.2$ , then  $K_{A:B} = 0.8/0.2 \times 0.5/0.5 = 4$ . A selectivity curve was then plotted for the mole fraction 0 to 1 in the crystal and mother liquor according to the chosen guests evaluated.

## 2.4 Thermal analysis

Thermal analysis is a group of techniques whereby the property changes of a substance are measured as a function of the temperature. The thermal methods employed in this study were hot-stage microscopy (HSM), thermogravimetric analysis (TGA) and differential scanning calorimetry (DSC).

### 2.4.1 Hot-stage microscopy (HSM)

Hot-stage microscopy (HSM) apparatus incorporates microscopy and thermal analysis to enable the study of materials as a function of temperature and time. This technique gives a unique opportunity to visually record the thermal degradation of inclusion compounds obtaining valuable information such as the melting point and any other thermal changes that occur during heating. In this study the thermal events of interest were guest release (vapour leaving the crystals), melting and decomposition. The data in the form of still images were analysed and correlated with TG and DSC.

Experimentally the crystal samples were submerged in silicone oil for the purpose of even heat distribution and for easy observation of any vapour being released. The samples were then placed in between two glass coverslips on a Linkam THMS600 hot stage apparatus connected to a Linkam TP92 manual temperature controller. The samples were then monitored and captured using a Sony Digital Hyper HAD colour camera positioned at the top of a Nikon stereomicroscope. The thermal changes were observed and recorded using the computer program *analySIS*.<sup>7</sup> All the experiments were carried at the heating rate of 10 °C/ min.

## 2.4.2 Thermogravimetric analysis and differential scanning calorimetry

The analysis of the change in mass of a sample on heating under a controlled atmosphere is known as thermogravimetry (TG). This method utilises a thermobalance that measures accurate mass changes of a substance as a function of temperature according to a controlled temperature programme. The method shows the mass loss of a sample as a result of volatile guest loss and decomposition. A TG (mass loss) curve is plotted as the temperature is varied and can be used to calculate the stoichiometry of the inclusion compound being analysed.<sup>8</sup>

Differential scanning calorimetry (DSC) is a technique that demonstrates the energy events produced during heating or cooling of a substance. DSC can be used to determine the onset temperatures of decomposition and the enthalpy change accompanied by the release of a volatile guest from an inclusion compound. These changes can be due to desolvation, phase transformation, melting and other thermal events. A heat flow against temperature is plotted, presenting peaks at the occurrence of endothermic and exothermic thermal events.<sup>9</sup>

TG and DSC samples were prepared similarly. The samples were removed from the mother liquor and lightly crushed and blotted dry using filter paper to dry off any surface solvent. The mass of the samples varied from 3 to 7 mg for the TG analysis and the DSC sample masses were ranging from 1 to 3 mg. TG samples were heated in an open platinum pan, whereas the DSC utilises two identical, crimped and vented aluminium closed pans. A sample pan and a reference pan both were subjected to a controlled temperature programme.

The experimental conditions of the TG and DSC are crucial and thus the following parameters have influenced the results of each measurement: sample size, heating rate, the flow rate of the purge gas and the geometry of the sample holder.

A TA-Q500 thermogravimetric analyser and differential scanning calorimeter instrumentation using Universal Analysis 2000 software (v4.5A, TA Instrument—

Waters LLC) operating at a nitrogen purge gas flow rate of  $50 \text{ cm}^3 \cdot \text{min}^{-1}$  was employed. The heating rate of  $20 \text{ K} \cdot \text{min}^{-1}$  was used for most analysis and the temperature range for each experiment was selected according to the nature of the host molecule in the crystalline compound.

## 2.5 Proton NMR spectroscopy ( $^1\text{H-NMR}$ )

Proton nuclear magnetic resonance ( $^1\text{H-NMR}$ ) spectroscopy chemical shift, spin coupling and relaxation time parameters are sensitive to short-range intermolecular interactions, which makes it an ideal technique for qualitative and quantitative analysis.  $^1\text{H-NMR}$  was used to determine the stoichiometry (mole percentage) of the guests and host in the inclusion complexes. The host and guest components were simultaneously observed, but difficulties were encountered when host and guest signals were overlapping.

All samples were thoroughly dried with filter paper and dissolved in deuterated solvent,  $\text{CDCl}_3$ . The experiments were carried out with Bruker Ultrashield 400 plus (400 MHz) spectrometer.<sup>9</sup> The data were analysed using the program ACD/NMR processor Academic Edition.<sup>10</sup>

## 2.6 X-ray diffraction analysis

X-ray diffraction is a fundamental tool extensively used in this study for the determination of new single crystal structures and the identification of inclusion compounds.

### 2.6.1 Powder X-ray diffraction (PXRD)

PXRD is a quick analytical method that monitors the characteristic phase changes for a solid crystalline compound and thus predominately used for the identification of crystalline materials.

Samples were ground into a fine powder and placed on a zero background silicon sample holder and then loaded onto a reflection transmission spinner of the D8 Advanced Bruker Phaser diffractometer with graphite-monochromated Cu K $\alpha$  radiation ( $\lambda = 1.5418 \text{ \AA}$ ) at room temperature.

A PXRD produces data as a plot of total diffracted intensity against the  $2\theta$  diffracted angle. All data were collected at room temperature, therefore in certain cases when the experimental data was compared to the single crystal X-ray data which is collected at low temperatures, the peaks would appear shifted slightly to the right, to higher  $2\theta$  values.<sup>11</sup>

### 2.6.2 Single crystal X-ray diffraction (SCXD)

SCXD is a non-destructive technique that utilises diffraction of X-rays from a suitable single crystal providing accurate data of cell parameters and diffraction intensities. This data undergoes a Fourier transform, whereby intensive calculations yield the exact positions of individual atoms in a unit cell of a crystal. Once the appropriate refinement is done one can accurately interpret important information, such as bond lengths and bond angles of the molecules in the unit cell, including the secondary intermolecular interactions.

Single crystals of a suitable size and quality were selected (generally between 0.1 to 0.5 mm in all dimensions) under a polarising microscope. The selected crystal was then mounted on a loop while coated with paratone oil, to prevent decomposition and provide a rigid mount during low-temperature data collections. In some cases, X-ray intensity data were collected on the Nonius Kappa CCD diffractometer with a graphite-monochromated MoK $\alpha$  radiation ( $\lambda = 0.71703 \text{ \AA}$ ) at 173K using and Oxford Cryostream 600. The strategy for data collection was evaluated using COLLECT<sup>12</sup> software. The structures intensity data was collected by standard phi-omega scan technique and the integration and scaling was done using the program DENZO-SMN.<sup>13</sup> Some X-ray intensity data were collected on a Bruker KAPPA APEX II DUO single crystal X-ray diffractometer.<sup>14</sup> This instrumentation employed a graphite monochromated MoK $\alpha$  radiation ( $\lambda = 0.71703 \text{ \AA}$ ) generated by a Bruker K780 generator (50 kV, 30 mA) at 173 K using an Oxford Cryostream 700. The data

reduction and cell refinement was performed using the program SAINT-Plus.<sup>15</sup> The space group was determined from the systematic absences using the program XPREP<sup>16</sup> and further verified by the refinement results. This program also prepared the input file of SHELXS-97 and SHELXL-97<sup>17</sup> which are programs for structure solution and refinement. The graphical interface X-Seed<sup>18</sup> was employed in the structure solution and refinement. All non-hydrogen atoms were refined anisotropically (exceptions are discussed in the appropriate chapters). The hydrogen atoms bound to carbon atoms were placed at idealized positions and refined as riding atoms.

### SHELXS-97

The SHELXS-97 software involves minimising the value of the function  $\sum w (F_o^2 - F_c^2)^2$  by employing the full-matrix least number of squares method. The agreement between the observed ( $F_o$ ) and calculated ( $F_c$ ) intensities of reflections is expressed by the residual indices  $R_1$  and  $wR_2$  – equations (1) and (2) based on the structure factors  $F$  and  $F^2$ , respectively. The collective residual index  $R$  is an indirect measure of the structural accuracy and is used to monitor the refinement by achieving the lowest possible value giving a satisfactory model.

$$R_1 = \frac{\sum |F_o| - |F_c|}{\sum |F_o|} \quad (1)$$

$$wR_2 = \left( \frac{\sum w (F_o^2 - F_c^2)^2}{\sum w (F_o^2)^2} \right)^{\frac{1}{2}} \quad (2)$$

The default weighting  $w$  scheme employed including parameters  $a$  and  $b$  was refined for each structure and is shown in equation (3) where  $P$  is defined in equation (4).

$$w = [\sigma^2(F_o^2) + (aP)^2 + bP]^{-1} \quad (3)$$

$$P = \frac{\max(0, F_o^2) + 2F_o^2}{3} \quad (4)$$

The ‘Goodness of Fit’  $S$  is also based on  $F^2$  (equation 5) and was determined for each structure, where  $n$  is the number of reflections and  $p$  is the number of refined

parameters. For well-behaved structures  $S$  is expected to be close to unity and the over-determination ratios ( $n/p$ ) should be around about 10.

$$S = \left( \frac{\sum w(F_o^2 - F_c^2)^2}{n-p} \right)^{\frac{1}{2}} \quad (5)$$

## 2.7 Computing components

The following computer packages were used for the analysis and evaluation of crystal structures;

- The Cambridge Structural Data Base (CSD) was used to access all published structures that were relevant to the hosts to obtain important information and to ensure that the experimentation being done is not just a repetition.<sup>19,20</sup>
- LAYER<sup>21,22</sup> displays the intensity data as a stimulated precision photograph at all reciprocal lattice levels. It was used for determining space group symmetry and systematic absences.
- LAZY PULVERIX<sup>23</sup> was used to generate calculated PXRD patterns from the crystal structure based on atomic fractional coordinates, thermal parameters and space group data. The theoretical PXRD patterns were compared to experimental patterns to identify phase changes and check for any similarities.
- POV-RAY<sup>24</sup> is a raytracer program used to create images of all the molecular and packing diagrams.
- X-seed<sup>14</sup> served as a graphical interface for SHELXS-97, LAYER, POV-RAY and LAZY PULVERIX.
- PLATON<sup>25</sup> was used to calculate molecular structure parameters such as bond angles, torsion angles, bond lengths and parameters defining non-covalent interactions (e.g  $\pi$ - $\pi$  stacking). Standard deviations were given to all calculated parameters.
- Crystal Explorer was used to create Hirshfeld surface plots which explore the packing modes and intermolecular interactions of a crystal structure.<sup>26,27</sup>

The final crystallographic data files are given in the formats presented in **Table 2.3**.

**Table 2.3** Crystallographic data files

<b>Files extensions</b>	<b>Details</b>
<b>.HKL</b>	Reflection data
<b>.RES</b>	SHELX co-ordinate data
<b>.CIF</b>	Crystallographic information
<b>.FCF</b>	Structure factors
<b>.XL</b>	SHELX output
<b>.LIS</b>	PLATON output
<b>.INS</b>	SHELX input

## References

- <sup>1</sup> Weber, E., Adrendt, J., Czugler, M. & Csöreg, I. *Angew. Chem. Int. Ed.*, 1986, 25, 746.
- <sup>2</sup> Synthesis of **H1**: Bell, F. & Waring, D.H. *J. Chem. Soc.*, 1949, 267:1579.
- <sup>3</sup> Synthesis of **H2**: Clarkson, R.G. & Gomberg, M. *Ibid.*, 1930, 52: 2881; Haas, G. & Prelog, V. *Helv. Chem. Acta.*, 1969, 52: 1202.
- <sup>4</sup> Institut für Organische Chemie, TU Bergakademie Freiberg, Leipziger Str. 29, Sachs, D-09596 Freiberg, Germany.
- <sup>5</sup> Windholz, M. Ed. *The Merck Index: An Encyclopaedia for chemicals and drugs*, Merck & Co. Inc., 1976, New Jersey.
- <sup>6</sup> Nassimbeni, L.R. & Báthori, N.B. *CrystEngComm.*, 2011, 13: 3156.
- <sup>7</sup> Soft Imaging System GmbH: Digital Solutions for imaging and Microscopy, *Version 3.1* windows.
- <sup>8</sup> Haines, P.J. *Thermal Methods of Analysis*. 1995, Blackie Academic & Professional, London.
- <sup>9</sup> Bruker, APEX2, *Version 1.0-27*, Bruker, AXS Inc., 2005, Madison, Wisconsin, USA.
- <sup>10</sup> Moser, A., Sasaki, R. & Hachery, M. *ACD/2D NMR, Version 12.01, Advanced chemical development Inc.*, 2010, Toronto, Canada.
- <sup>11</sup> Karki, S., Fábrián, L., Frišćić, T. & Jones, W. *Org. Lett.*, 2007, 9: 3133.
- <sup>12</sup> COLLECT, data collection software: Nonius BV Delft, The Netherlands, 2000.
- <sup>13</sup> Otwinowski Z, Minor W (1997) *Methods Enzymol* 276:30.
- <sup>14</sup> Bruker 2005, APEX2, *Version 1.0-27*, Bruker AXS Inc., Madison, Wisconsin, USA.
- <sup>15</sup> SAINT-plus (including XPREP), *Version 7.12*, Bruker AXS Inc., 2004, Madison, Wisconsin, USA.
- <sup>16</sup> Bruker, XPREP, *Version 6.14*, Bruker AXS inc., 2005, Madison, Wisconsin, USA.
- <sup>17</sup> Sheldrick, G. M. *SHELXS-97 and SHELXL-97, Program for Crystal Structures, Determination and Refinement*, 1997, University of Göttingen: Göttingen, Germany.
- <sup>18</sup> Barbour, L.J. X-Seed: A Software Tool for Supramolecular Crystallography, *J. Supramol. Chem.*, 2001, 1:189.
- <sup>19</sup> Groom, C.R. & Allen, F.H. *Angew. Chem. Int. Ed.*, 2014, 53: 662.
- <sup>20</sup> ConQuest, A program for the search of the CSD, *Version 1.16*, 2013, United Kingdom.
- <sup>21</sup> Barbour, L.J. LAYER, A computer program for the graphic display of intensity data as simulated precession photographs. *Appl. Crystallogr.*, 1999, 32: 351.
- <sup>22</sup> Barbour, L.J. LAYER, A computer program for the graphic display of cross sections through a unit cell. *Appl. Crystallogr.*, 1999, 32: 353.
- <sup>23</sup> Yvon, K., Jeitschko, W & Parthe, E.J. LAZY PULVERIX, A computer program, for calculating X-ray and neutron diffraction powder patterns. *J. Appl. Cryst.*, 10: 73.
- <sup>24</sup> PoV-Ray for Windows: *Version 3.1e.watcom.win32*, The persistence of Vision Development Team: © 1991-1999.
- <sup>25</sup> Spek, A.L. PLATON, A multipurpose crystallographic tool, *Version 10500: e*, 1980-2000.
- <sup>26</sup> McKinnon, J., Spackman, M.A. & Mitchell, A.S. *Acta crystallogr.*, 2004, B40: 327.
- <sup>27</sup> Spackman, M. A. & McKinnon, J.J. *CrystEngComm*, 2002, 4: 378.



# Chapter 3: Selectivity experiments of heterocyclic guest compounds

## 3.1 Introduction

Pyridine (C<sub>5</sub>H<sub>5</sub>N, **PYR**), piperidine (C<sub>5</sub>H<sub>11</sub>N, **PIP**), morpholine (C<sub>4</sub>H<sub>9</sub>NO, **MOR**) and dioxane (C<sub>4</sub>H<sub>8</sub>O<sub>2</sub>, **DIO**) are structurally similar heterocyclic compounds (**Figure 3.1**) that have a wide range of applications. Pyridine, piperidine and morpholine are used in manufacturing of many bioactive substances like drugs, insecticides, herbicides, food preservatives and food additives.<sup>1</sup> Dioxane is used in the production of inks and adhesives.<sup>2</sup> The enclathration experiments of the three different host compounds, 9,9'-bianthryl (**H1**), 9,9'-spirobifluorene (**H2**) and *trans*-2,3-dibenzoylspiro(cyclopropane-1,9'-fluorene) (**H3**) with the heterocyclic guests were investigated and analysed in terms of their crystal structures, thermal behaviour, <sup>1</sup>H-NMR spectra and Hirshfeld surfaces.

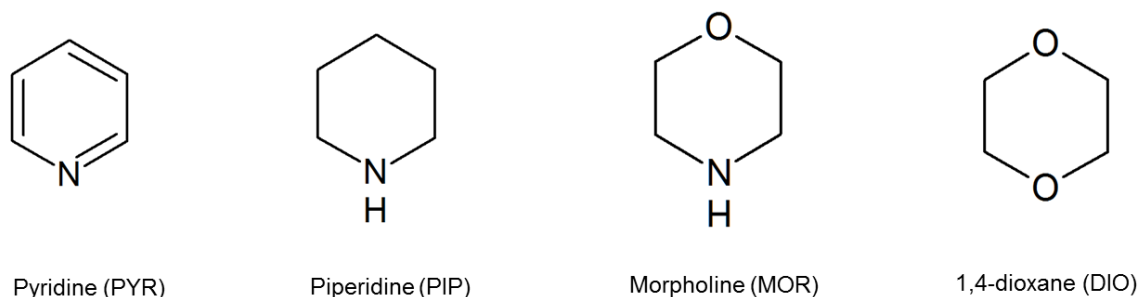


**Figure 3.1** Schematic diagrams of heterocyclic guest compounds.

## 3.2 Inclusion complex preparation

Single crystals of the hosts **H1**, **H2** and **H3** with **PYR**, **PIP**, **MOR** and **DIO** solvents were grown using the slow evaporation technique. Approximately 2 ml of the **PYR** guest was added to 40-60 mg of each host (**H1**, **H2** or **H3**) separately. The resulting solutions were filtered and then sealed into a closed vial with a pierced parafilm.

Colourless crystalline material appeared after a day. The procedure was then repeated with the other pure solvents and all the possible binary combinations of guest mixtures in 1:1 ratios.

### 3.3 Inclusion complex analysis

The ensuing crystalline products were analysed by single crystal X-ray diffraction (SCXD), powder X-ray diffraction (PXRD), proton nuclear magnetic resonance spectroscopy ( $^1\text{H-NMR}$ ), thermal gravimetry (TG) and differential scanning calorimetry (DSC). The enclathration results with their respective TG results are summarised in **Table 3.1**. The experimentally determined TG percentage mass loss of the inclusion compounds correlates well with all the calculated values confirming the host:guest ratios for all the structures. From the experiments set up with **H1**, only **H1•MOR** inclusion compound was prepared because of the unexpected decomposition of **H1**. Thus preparations of the inclusion compounds were not completed. This will be explained in detail in Chapter 4. For host **H2** all inclusion compounds with **PYR**, **PIP**, **MOR** and **DIO** were formed, while host **H3** formed an inclusion compound exclusively with the **PYR** guest.

**Table 3.1** Enclathration results of **H1**, **H2** and **H3** with **PYR**, **PIP**, **MOR** and **DIO**

Host	Solvent	Resulting Crystal	TG % mass loss found (calc)
<b>H1</b>	PYR	Not done	-
	PIP	Not done	-
	MOR	H1•MOR	20.1 (19.7)
	DIO	Not done	-
<b>H2</b>	PYR	H2•2PYR	25.8 (33.3)*
	PIP	H2•PIP	21.1 (21.2)
	MOR	H2•MOR	20.9 (21.6)
	DIO	H2•DIO	20.9 (21.8)
<b>H3</b>	PYR	H3•PYR	16.6 (16.5)
	PIP	H3 apohost	-
	MOR	gel	-
	DIO	H3 apohost	-

\*See explanation on page 38

## 3.4 Inclusion compound of H1 with MOR

### 3.4.1 Thermal analysis of H1•MOR

The TG and DSC trace of **H1•MOR** is presented in **Figure 3.2**. The TG trace exhibits a mass loss of 20.1% associated with a volatile guest release within the temperature range of 70°C to 122°C. This measured mass loss implies a host-guest ratio of 1:1 (calculated value 19.7%), confirming the **H1•MOR** crystal structure stoichiometry. The DSC trace for the **H1•MOR** inclusion compound has two endotherms, the first endotherm ( $T_{\text{on}} = 85.8^\circ\text{C}$ ,  $T_{\text{peak}} = 122.7^\circ\text{C}$ ) describes the loss of the **MOR** guest in a single step and the second endotherm describes the melting of the host **H1** ( $T_{\text{on}} = 308.4^\circ\text{C}$ ,  $T_{\text{peak}} = 311.6^\circ\text{C}$ ). There is a small endotherm at about 251°C which relates to the decomposition of the host and this will be discussed on page 72 (Chapter 4).

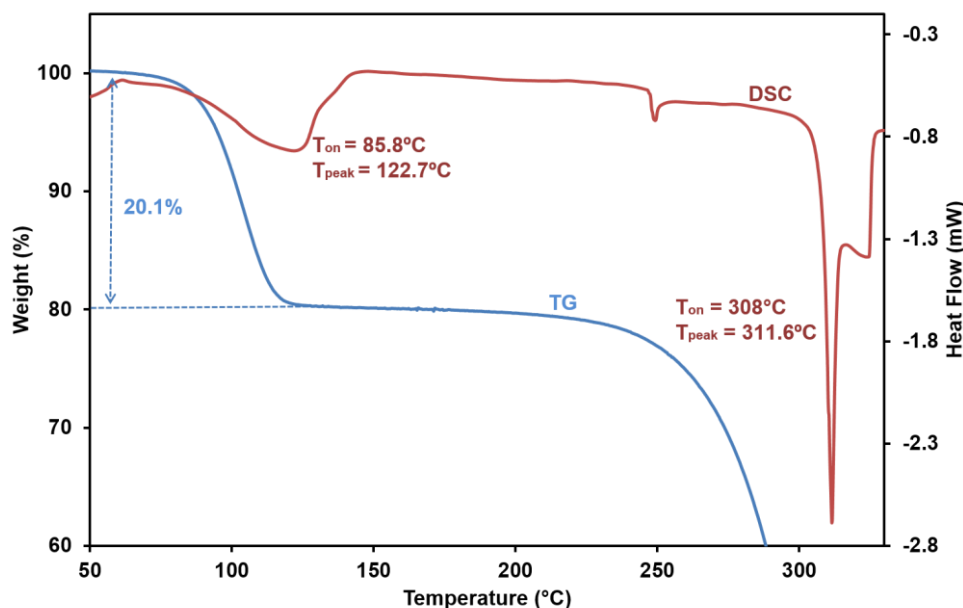


**Figure 3.2** TG and DSC traces for **H1•MOR** (endo down).

### 3.4.2 Crystal structure analysis of H1•MOR

A colourless **H1•MOR** crystal with the dimensions of  $0.04 \times 0.10 \times 0.30$  mm was selected for single crystal X-ray diffraction analysis. The data was collected on a Bruker APEX II DUO diffractometer. The **H1•MOR** compound crystallises in the triclinic crystal system, in the space group  $P\bar{1}$  (No.2). The structure was refined to

$R_1 = 0.0585$  and  $wR_2 = 0.1817$ . The asymmetric unit contains one **H1** molecule and one **MOR** guest with the molecular formula of  $C_{32}H_{27}NO$  and  $Z = 2$ . The crystal was modelled with a 1:1 host-guest ratio based on the TG results. It is noticeable that the thermal motions of the atoms of the guest are high and some remaining electron density was localised around the guest. An attempt was made to model possible disorder of the guest but this was unsuccessful. The crystal data and refinement details are summarised in **Table 3.2**. The **H1•MOR** crystal structure is stabilised by various types of weak interactions, such as C-H... $\pi$  interactions, H...H and H...O close contacts presented in **Figure 3.3** and labelled A-F. The C-H... $\pi$  interactions (A, C4-H4... $c_g(C23-C28)$ , 2.82 Å) occurs between two host molecules located in the perpendicular y-shaped geometry<sup>3</sup> (**Table 3.3**). The C-H... $\pi$  interactions labelled B also occur between two host molecules in a similar manner, the perpendicular y-shaped geometry. These C-H... $\pi$  interactions have the contact distance of 3.10 and 3.24 Å between C18-H18 and C19-H19 of one host to the centroid  $c_g(C2-C7)$  of another respectively. The H...H close contacts C, take place between two host molecules (C11-H11...H22-C22, 2.27 Å). This contact is shorter than the sum of the van der Waals radii for two hydrogens.<sup>4</sup> The weaker interactions such as D (C17-H17...H1-N1, 2.57 Å) and E (C8-H8...O1, 2.77 Å) are due to close contacts between the guest and host molecules. The contact F results from a C-H... $\pi$  interaction between the guest and the host (C32-H32A... $c_g(C9-C14)$ , 3.11 Å).

Table 3.2 Crystal data for H1•MOR

Compounds	H1•MOR
Molecular formula	C <sub>32</sub> H <sub>27</sub> NO
Formula weight (g. mol <sup>-1</sup> )	441.55
Crystal system	triclinic
Space group	<i>P</i> -1 (No.2)
a (Å)	10.684(2)
b (Å)	11.1551(11)
c (Å)	11.3645(12)
α (°)	117.812(2)
β (°)	93.136(3)
γ (°)	100.195(3)
V (Å <sup>3</sup> )	1164.28
Z	2
ρ calc (g.cm <sup>-3</sup> )	1.260
μ (MoKα) (mm <sup>-1</sup> )	0.075
F (000)	468
Crystal size (mm)	0.04 x 0.10 x 0.30
Temperature (K)	173(2)
Radiation (Å)	0.71073
Theta min-max (°)	2.0, 27.9
Dataset (±h, ±k, ±l)	-11:14; -14:14; -14:12
Final R indices [I>2.0 (I)]	R <sub>1</sub> =0.0585, wR <sub>2</sub> =0.1474
R indices (all data)	R <sub>1</sub> =0.1293, wR <sub>2</sub> =0.1817
Tot., uniq. data, R(int)	11862, 5465, 0.026
N <sub>ref</sub> , N <sub>par</sub>	5465, 309
S	1.01
Max. and Av. Shift/Error	0.00, 0.00
Min. and Max. Resd. Electron Dens. (e/Å <sup>3</sup> )	-0.22, 0.41

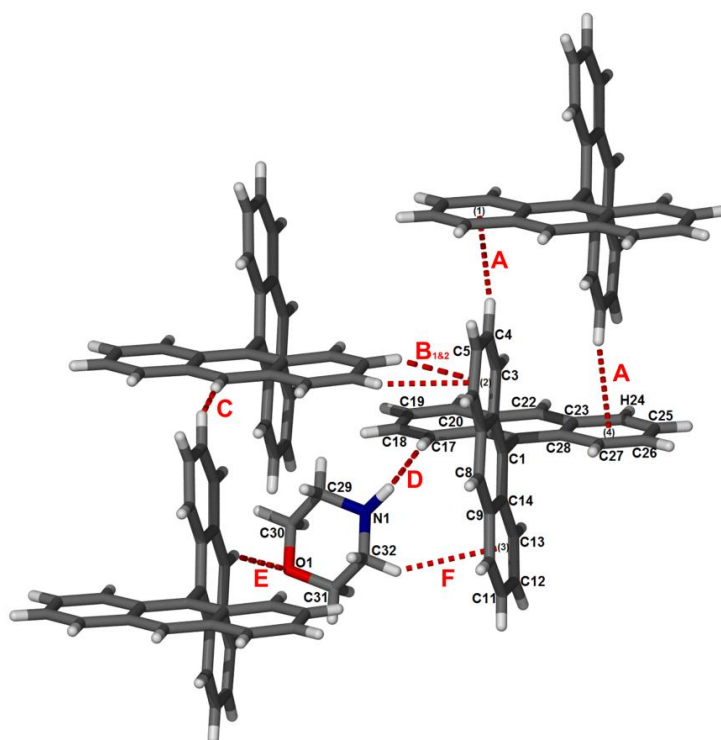


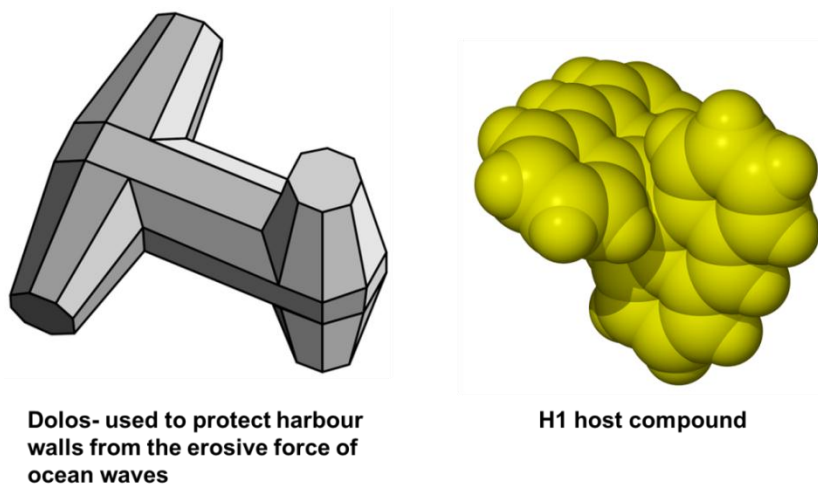
Figure 3.3 Intermolecular interactions in **H1•MOR**.

Table 3.3 Intermolecular interactions in **H1•MOR**

	D-H...A	d(D-H) (Å)	d(D-H...A) (Å)	(H...A) (Å)	∠ DHA (°)
<b>A</b>	C4-H4...c <sub>g</sub> (C23-C28)	0.95	3.63	2.82	143
<b>B<sub>1</sub></b>	C18-H18...c <sub>g</sub> (C2-C7)	0.95	3.79	3.10	132
<b>B<sub>2</sub></b>	C19-H19...c <sub>g</sub> (C2-C7)	0.95	3.87	3.24	125
<b>C</b>	C22-H22...H11-C11 <sup>a</sup>	0.95	2.92	2.27	174
<b>D</b>	C17-H17...H1-N1	0.95	3.49	2.57	164
<b>E</b>	C8-H8...O1 <sup>b</sup>	0.95	3.63	2.77	150
<b>F</b>	C32-H32B...c <sub>g</sub> (C9-C14)	0.99	3.96	3.11	138

**Symmetry operator:** <sup>a</sup>x,1+y,z; <sup>b</sup>1-x,-y,-z

The conformation of the **H1** molecule is similar to the shape of a dolos (**Figure 3.4**) with the torsion angle of C2-C1-C15-C16 = 85.9°. In the crystal lattice of **H1•MOR** the **H1** hosts are held together by numerous C-H... $\pi$  interactions and H...H close contacts. The C-H... $\pi$  interactions (**Figure 3.3**: A and B) connect the host molecules into layers (**Figure 3.5 H1**- grey and yellow) in a jig-saw puzzle pattern and the guest molecules are located in pockets between the surfaces of these layers (**Figure 3.6**). The H...H close contacts (C22-H22...H11-C11, 2.27 Å) are observed between these parallel layers.



**Figure 3.4** Dolos and H1 host compound.

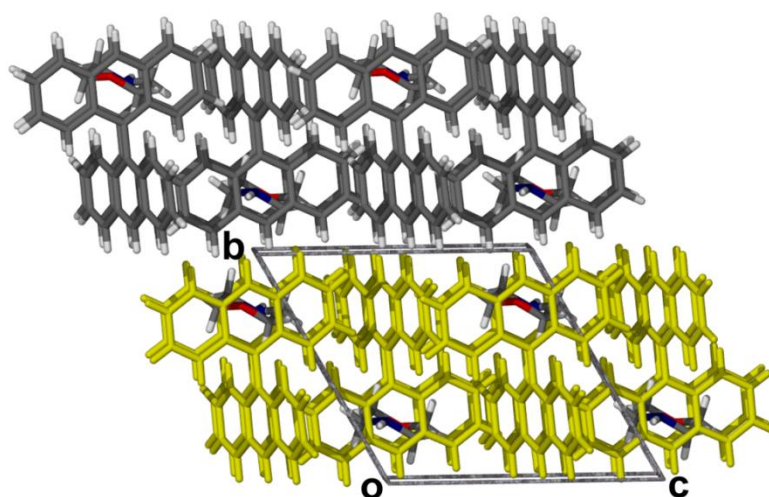


**Figure 3.5** Packing diagram of H1•MOR viewed down [100].

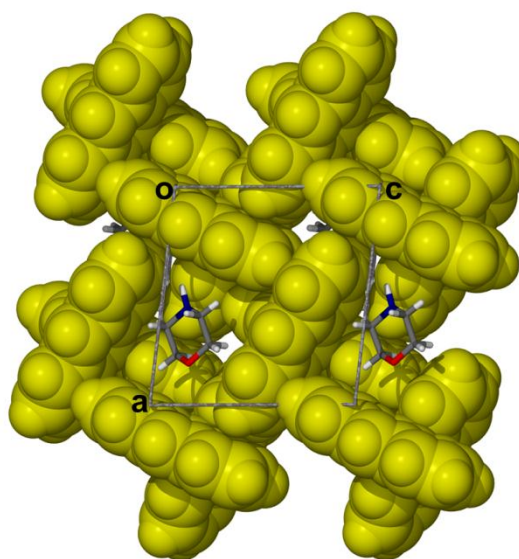


**Figure 3.6** Packing diagram of H1•MOR viewed down [010].

## 3.5 Inclusion compounds of H<sub>2</sub> with heterocyclic compounds

### 3.5.1 Thermal analysis of inclusion compounds of H<sub>2</sub> with heterocyclic compounds

The TG and DSC traces for the **H<sub>2</sub>•2PYR**, **H<sub>2</sub>•PIP**, **H<sub>2</sub>•MOR** and **H<sub>2</sub>•DIO** inclusion compounds are shown in **Figure 3.7** and the results are summarized in **Table 3.4**. The TG and DSC traces of the **H<sub>2</sub>** inclusion compounds show evidence of the guest loss before the host **H<sub>2</sub>** melts.

The **H<sub>2</sub>•2PYR** crystal structure contains one host and two crystallographically independent guests in the asymmetric unit. The TG trace of the **H<sub>2</sub>•2PYR** inclusion complex depicts a 25.8% mass loss in a two-step overlapping process (temperature range 31-133°C). The **H<sub>2</sub>•2PYR** crystals start to release the first **PYR** guests at a very low temperature of 31°C. The crystals of **H<sub>2</sub>•2PYR** start to decompose immediately after being removed from the mother liquor. The continuously decreasing mass can be seen on the TG trace and this explains the 7.5% difference between the calculated mass loss (33.3%) and the measured one (25.8%). A great effort was made to obtain better experimental values but all attempts were unsuccessful. The low stability of the **H<sub>2</sub>•2PYR** crystals can be explained by the loose packing of the structure. The corresponding DSC trace displays three endotherms where the first two reflect the two-step guest loss ( $T_{\text{on}} = 49.6^{\circ}\text{C}$ ,  $T_{\text{peak}} = 56.4^{\circ}\text{C}$  and  $T_{\text{on}} = 84.6^{\circ}\text{C}$ ,  $T_{\text{peak}} = 104.3^{\circ}\text{C}$ ). This confirms the 1:2 host:guest ratio of the crystals. The third endotherm is due to the melting of **H<sub>2</sub>** ( $T_{\text{on}} = 201.1^{\circ}\text{C}$ ,  $T_{\text{peak}} = 202.6^{\circ}\text{C}$ ).

The other **H<sub>2</sub>** inclusion compounds (**H<sub>2</sub>•PIP**, **H<sub>2</sub>•MOR** and **H<sub>2</sub>•DIO**) lose their guests in a single step. The **H<sub>2</sub>•PIP** TG trace shows a 21.1% mass loss between the temperature range of 49-95°C. The experimentally determined % mass loss corresponds with the calculated value (21.2%) and suggests a host to guest ratio of 1:1. The corresponding DSC trace has an endotherm related to the **PIP** guest loss with the  $T_{\text{on}} = 76.2^{\circ}\text{C}$  and  $T_{\text{peak}} = 99.4^{\circ}\text{C}$ . The **H<sub>2</sub>•PIP** DSC graph exhibits two melting points. There is a small endotherm at  $T_{\text{on}} = 194.1^{\circ}\text{C}$  and  $T_{\text{peak}} = 194.3^{\circ}\text{C}$ , followed by the main endotherm at  $T_{\text{on}} = 202.0^{\circ}\text{C}$ ,  $T_{\text{peak}} = 202.5^{\circ}\text{C}$ . The smaller



endotherm is associated with the occurrence of a possible polymorph of the apohost. The **H2•MOR** and **H2•DIO** TG traces show similar thermal behaviour. The **H2•MOR** trace depicts a 20.9% mass loss which agrees well with the calculated 21.6% and confirms the host:guest ratio of the crystal as 1:1. The TG trace of **H2•DIO** also shows a 20.9% mass loss (calculated 21.6%) corresponding to a host:guest ratio of 1:1. The **H2•MOR** and **H2•DIO** DSC traces have two endotherms. The first endotherm portraying a volatile guest loss with the  $T_{on} = 49.6^{\circ}\text{C}$  and  $T_{peak} = 56.4^{\circ}\text{C}$  for **H2•MOR** and  $T_{on} = 49.6^{\circ}\text{C}$  and  $T_{peak} = 56.4^{\circ}\text{C}$  for **H2•DIO** and the second endotherm on both traces fit the melting of **H2** (**H2•MOR**:  $T_{on} = 202.0^{\circ}\text{C}$ ,  $T_{peak} = 202.6^{\circ}\text{C}$  and **H2•DIO**:  $T_{on} = 202.0^{\circ}\text{C}$ ,  $T_{peak} = 202.5^{\circ}\text{C}$ ).

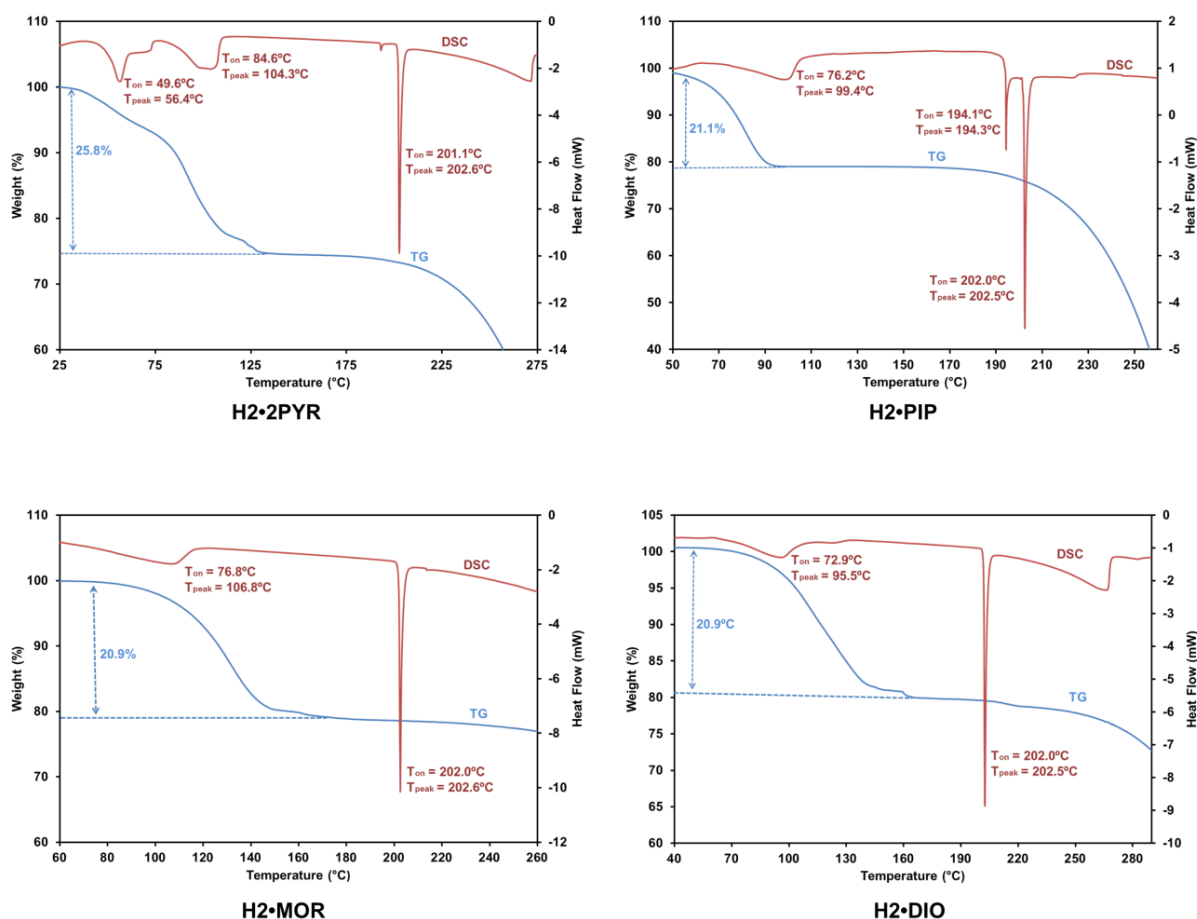


**Figure 3.7** TG and DSC traces for **H2•2PYR**, **H2•PIP**, **H2•MOR** and **H2•DIO** (endo down).

**Table 3.4** TG and DSC results for **H2•2PYR**, **H2•PIP**, **H2•MOR** and **H2•DIO**

Inclusion compound	Temperature range Guest loss (°C)	$\Delta$ Weight loss (%) (experimental)	Endotherms-Guest loss $T_{on}$ , $T_{peak}$ (°C)	Endotherm-Host melting $T_{on}$ , $T_{peak}$ (°C)
<b>H2•2PYR</b>	31-133	25.8	49.6, 56.4 (endo 1) 84.6, 104.3 (endo 2)	201.1, 202.6
<b>H2•PIP</b>	49-95	21.1	76.2, 99.4	201.0, 202.5
<b>H2•MOR</b>	82-166	20.9	76.8, 106.8	202.0, 202.6
<b>H2•DIO</b>	64-163	20.9	72.9, 95.5	202.2, 202.5

## 3.5.2 Crystal structure analysis of inclusion compounds of H2 with heterocyclic compounds

### 3.5.2.1 Structure analysis of H2•2PYR

A block-like crystal of **H2•2PYR** with the dimensions of 0.10 x 0.10 x 0.10 mm was selected for data collection. The structure crystallised in the non-centrosymmetric orthorhombic  $P2_12_12_1$  (No.19) space group and refined to  $R_1 = 0.0361$  and  $wR_2 = 0.0845$ . The asymmetric unit contains one host molecule and two guest molecules. **Table 3.5** lists the crystal data and the refinement parameters for the **H2•2PYR** crystal structure. It is interesting to note that although the host is an achiral compound it crystallised in a chiral space group. The handedness of the structure was chosen to minimize the Flack parameter<sup>5</sup> ( $F = 0.1306$  (2.7328)). The non-bonding interactions that hold the **H2•2PYR** crystal structure together are illustrated in **Figure 3.8** as red dotted lines and summarised in **Table 3.6**. The intermolecular interactions that occur in the **H2•2PYR** structure are a combination of C-H $\cdots\pi$  interactions, H $\cdots$ H and H $\cdots$ C close contacts. The C-H $\cdots\pi$  interactions (A) occur between a **PYR** and the centroid of a neighbouring host in the perpendicular y-shaped geometry (C27-H27 $\cdots$ c<sub>g</sub>(C20-C25), 3.00 Å). The other defined C-H $\cdots\pi$  interaction (B) in the structure results in the same orientation between the C32-H32 of the **PYR** to the centroid c<sub>g</sub>(C14-C19) of the nearest host (3.02 Å). The close contacts, C (C6-H6 $\cdots$ N1) and D (C22-H22 $\cdots$ N2) have the distance 2.68 Å and 2.59 Å, respectively. These contacts are shorter than the sum of van der Waals radii for nitrogen and hydrogen (2.75 Å).<sup>4</sup> The close contact E (C17-H17 $\cdots$ C24) occurs between two adjacent hosts (2.88 Å), and the distance is less than the sum of van der Waals radii for hydrogen and carbon.<sup>4</sup> The two crystallographic independent

PYR guests are located in separate channels running in the crystallographic direction [100] (Figure 3.9).

**Table 3.5** Crystal data for **H2•2PYR**, **H2•PIP**, **H2•MOR** and **H2•DIO**

Compounds	H2•2PYR	H2•PIP	H2•MOR	H2•DIO
Molecular formula	C <sub>35</sub> H <sub>26</sub> N <sub>2</sub>	C <sub>30</sub> H <sub>27</sub> N	C <sub>29</sub> H <sub>25</sub> NO	C <sub>29</sub> H <sub>24</sub> O <sub>2</sub>
Formula weight (g. mol <sup>-1</sup> )	474.58	401.53	403.50	1213.53
Crystal system	orthorhombic	monoclinic	monoclinic	monoclinic
Space group	<i>P</i> 2 <sub>1</sub> 2 <sub>1</sub> 2 <sub>1</sub> (No.19)	<i>P</i> 2 <sub>1</sub> / <i>n</i> (No.14)	<i>P</i> 2 <sub>1</sub> / <i>n</i> (No.14)	<i>P</i> 2 <sub>1</sub> / <i>n</i> (No.14)
a (Å)	8.6073(17)	10.712(2)	10.698(2)	10.611(2)
b (Å)	17.159(3)	18.451(4)	18.120(4)	18.653(4)
c (Å)	17.359(4)	11.056(2)	11.119(2)	32.703(7)
α (°)	90	90	90	90
β (°)	90	91.17(3)	90.60(3)	90.46(3)
γ (°)	90	90	90	90
V (Å <sup>3</sup> )	2563.8(9)	2184.7(7)	2155.3(7)	6473(2)
Z	4	4	4	12
ρ calc (g.cm <sup>-3</sup> )	1.230	1.221	1.243	1.245
μ (MoKα) (mm <sup>-1</sup> )	0.071	0.070	0.074	0.077
F (000)	1000	856	856	2568
Crystal size (mm)	0.10 x 0.10 x 0.10	0.13 x 0.28 x 0.38	0.09 x 0.20 x 0.28	0.20 x 0.24 x 0.30
Temperature (K)	173(2)	173(2)	173(2)	173(2)
Radiation (Å)	0.71073	0.71073	0.71073	0.71073
Theta min-max (°)	3.35, 27.5	2.2, 28.4	2.2, 27.5	2.2, 26.5
Dataset (±h, ±k, ±l)	-11:11 -22:22 -22:22	-14:14 -24:24 -14:14	-13:13 -23:23 -14:13	-13:50 -23:23 -38:40
Final R indices [I>2.0 (I)]	R <sub>1</sub> =0.0361, wR <sub>2</sub> = 0.0800	R <sub>1</sub> = 0.0489, wR <sub>2</sub> = 0.1133	R <sub>1</sub> = 0.0459 wR <sub>2</sub> = 0.1072	R <sub>1</sub> = 0.1025 wR <sub>2</sub> = 0.2726
R indices (all data)	R <sub>1</sub> = 0.0445, wR <sub>2</sub> = 0.0845	R <sub>1</sub> = 0.0825, wR <sub>2</sub> = 0.1320	R <sub>1</sub> = 0.0679 wR <sub>2</sub> = 0.1191	R <sub>1</sub> = 0.1974 wR <sub>2</sub> = 0.3470
Tot., uniq. data, R(int)	5835, 5835, 0.036	20720, 5470, 0.052	16241, 4959, 0.041	49415, 13292, 0.103
N <sub>ref</sub> , N <sub>paF</sub>	5835, 334	5470, 282	4959, 284	13292, 818
S	1.04	1.04	1.04	1.03
Max. and Av. Shift/Error	0.00, 0.00	0.00, 0.00	0.00, 0.00	1.16, 0.00
Min. and Max. Resd. Electron Dens. (e/Å <sup>3</sup> )	-0.14, 0.14	-0.22, 0.27	-0.25, 0.23	-0.56, 0.86

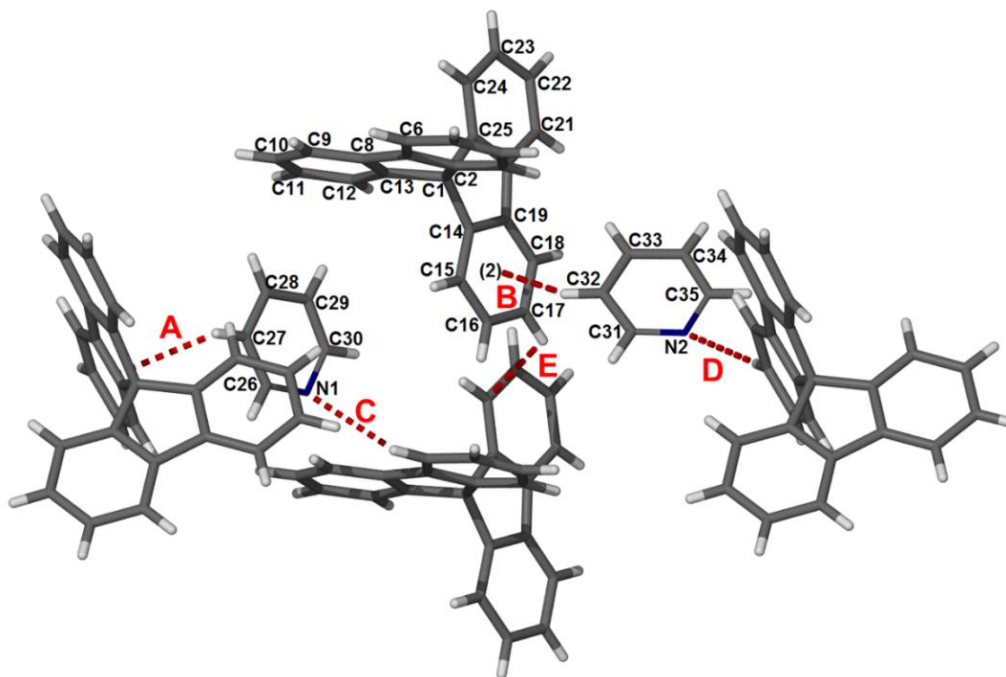


Figure 3.8 Intermolecular interactions in H2•2PYR.

Table 3.6 Intermolecular interactions in H2•2PYR

	D-H...A	d(D-H) (Å)	d(D-H...A) (Å)	(H...A) (Å)	∠ DHA (°)
A	C27-H27...C <sub>g</sub> (C20-C25)	0.95	3.76	3.00	138
B	C32-H32...C <sub>g</sub> (C14-C19)	0.95	3.63	3.02	123
C	C6-H6...N1 <sup>a</sup>	0.95	3.56	2.68	155
D	C22-H22...N2 <sup>b</sup>	0.95	3.44	2.59	148
E	C17-H17...C24 <sup>c</sup>	0.95	3.40	2.88	116
<b>Symmetry operator:</b> <sup>a</sup> x,-1,y,z <sup>b</sup> 3/2-x,1-y,1/2+z <sup>c</sup> x-1,y,z					

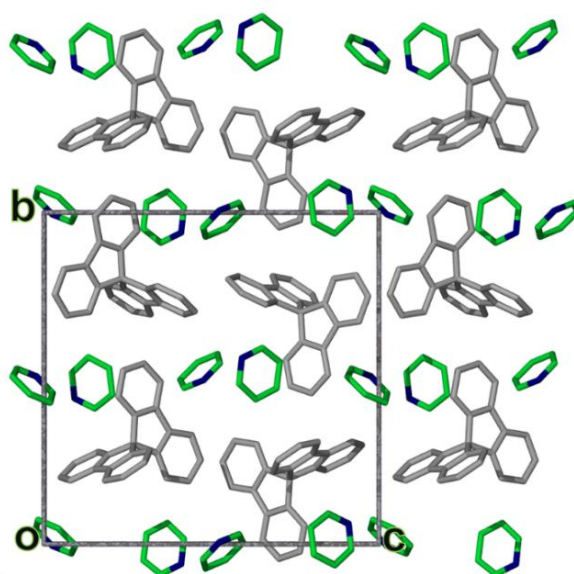
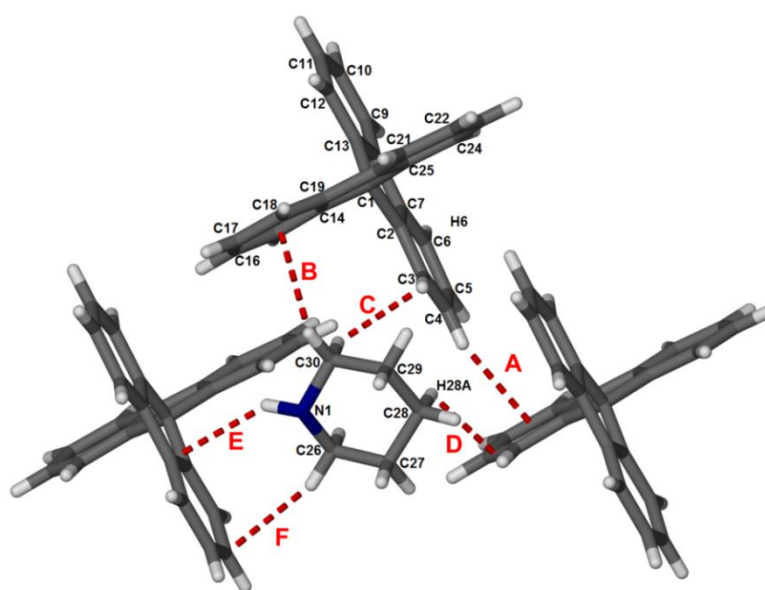


Figure 3.9 Packing diagram for H2•2PYR viewed along [100]. Guests are coloured green.

### 3.5.2.2 Structure analysis of H2•PIP

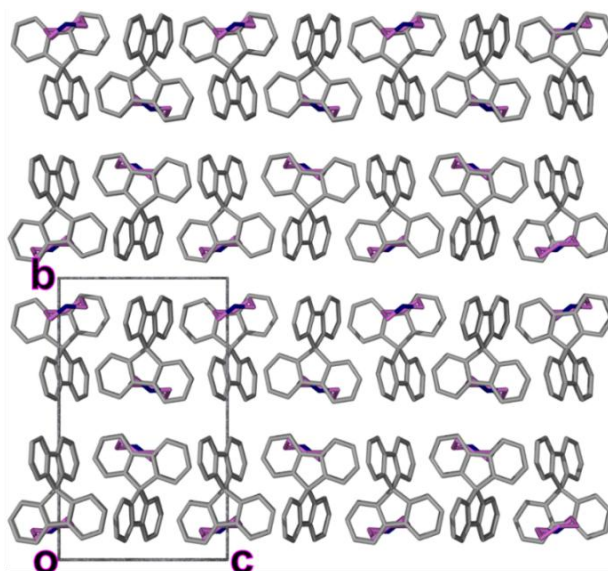
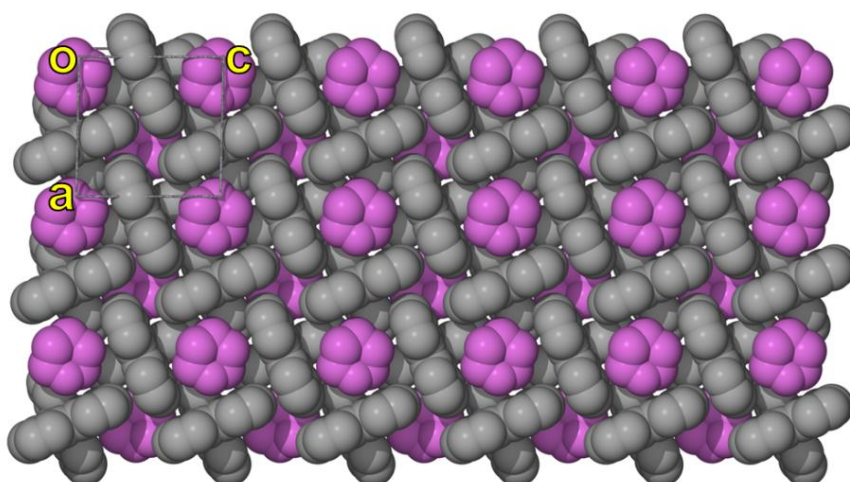
A colourless plate-like crystal with the dimensions of  $0.13 \times 0.28 \times 0.38$  mm was subjected to X-ray diffraction analysis. The unit cell dimensions specified a monoclinic crystal system and the space group  $P2_1/n$  (No.14) was chosen. The structure was successfully refined to  $R_1 = 0.0489$  and  $wR_2 = 0.1320$ . The unit cell consists of four host and four guest molecules ( $Z=4$ ). The crystallographic data is summarised in **Table 3.5**. The non-bonding interactions in the **H2•PIP** structure are displayed in Figure 3.10 and labelled A to F. The main intermolecular interaction between the host molecules is the C-H $\cdots\pi$  stacking (A and B). Interaction A occurs between C4-H4 and the centroid  $c_g(C14-C19)$  of a neighbouring host in a perpendicular y-shaped geometry (2.83 Å). Interaction B arises between the guest (C30-H30A) and an aromatic ring of a neighbouring host ( $c_g(C14-C19)$ , perpendicular t-shaped geometry, 2.99 Å). The H $\cdots$ H contacts are depicted as C, (C3-H3 $\cdots$ H30B-C30) and D, (C28-H28A $\cdots$ H15-C15) and have the distances 2.60 to 2.63 Å, respectively. The guests and hosts N-H $\cdots$ C and C-H $\cdots$ C interactions labelled E (N1-H1 $\cdots$ C7) and F (C26-H26A $\cdots$ C4) are relatively weak and have the intermolecular distance of 2.81 Å and 2.86 Å, respectively. The details of the interactions are summarised in **Table 3.7**. The C-H $\cdots\pi$  interactions between the **H2** molecules arranges them into layers (**Figure 3.11**). The **PIP** guests are located in cavities on the surface of each layer; this is demonstrated in **Figure 3.12** (single layer is viewed along the  $b$ -axis).



**Figure 3.10** Intermolecular interactions in **H2•PIP**.

**Table 3.7** Intermolecular interactions in **H2•PIP**

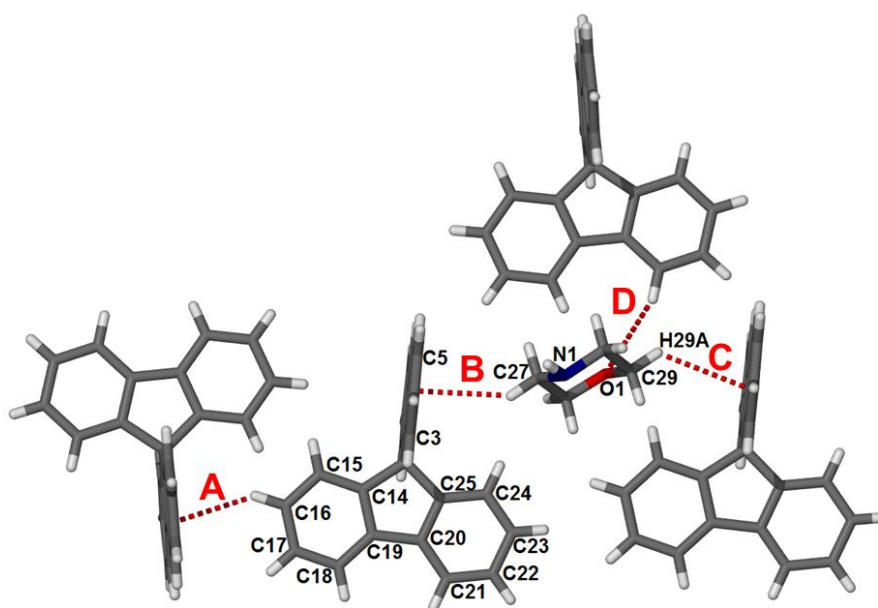
	D-H...A	d(D-H) (Å)	d(D-H...A) (Å)	(H...A) (Å)	∠ DHA (°)
<b>A</b>	C4-H4...c <sub>g</sub> (C14-C19)	0.95	3.65	2.83	146
<b>B</b>	C30-H30A...c <sub>g</sub> (C14-C19)	0.99	3.58	2.99	119
<b>C</b>	C3-H3...H30B-C30	0.95	3.17	2.60	129
<b>D</b>	C28-H28A...H15-C15 <sup>a</sup>	0.95	3.12	2.63	112
<b>E</b>	N1-H1...C7 <sup>b</sup>	0.94	3.59	2.81	141
<b>F</b>	C26-H26A...C4 <sup>b</sup>	0.99	3.79	2.86	156
<b>Symmetry operator:</b> <sup>a</sup> x-1/2, 1/2-y, 1/2+z <sup>b</sup> 1/2+x, 1/2-y, 1/2+z					

**Figure 3.11** Packing diagram of **H2•PIP** viewed down [100]. Guests are coloured purple.**Figure 3.12** Packing diagram of **H2•PIP** viewed down [010]. Guests are coloured purple.



### 3.5.2.3 Structure analysis of H2•MOR

A suitable crystal with dimensions of 0.09 × 0.20 × 0.28 mm was selected for X-ray analysis. The **H2•MOR** inclusion compound crystallises in the monoclinic space group  $P2_1/n$  (No.14). The asymmetric unit consists of one host and one guest molecule with the molecular formula of  $C_{29}H_{25}NO$ . The structure was refined successfully to the low residual indices of  $R_1 = 0.0459$  and  $wR_2 = 0.1191$ . **Table 3.5** contains the summary of the data collection and refinement details for **H2•MOR**. The main building motif of the **H2•MOR** structure is presented in **Figure 3.13**. The C-H... $\pi$  interaction A (C16-H16... $c_g$ (C8-C13), 2.85 Å) occurs between two host compounds in the perpendicular y-shaped position.<sup>4</sup> The C-H... $\pi$  interaction (B) bonds a guest and host via C27-H27A... $c_g$ (C2-C7) in the perpendicular t-shaped position<sup>4</sup> (2.94 Å). The C-H... $\pi$  interaction (C) is also due to a contact formed between a host and guest (C29-H29A... $c_g$ (C8-C13), 2.98Å) in the perpendicular t-shaped geometry. The C-H...O contact D (C18-H18...O1) arises between a guest and host with the distance of 2.96 Å. The **H2•MOR** interaction parameters are summarised in **Table 3.8**. The packing of the **H2•MOR** structure is similar to that of **H2•PIP**, and is demonstrated in **Figures 3.14** and **3.15**. The neighbouring hosts are kept in layers by C-H... $\pi$  stacking interactions in the crystallographic direction [100] illustrated in **Figure 3.14**. The **MOR** guests are situated in the cavities on the surface of the layers (**Figure 3.15**).

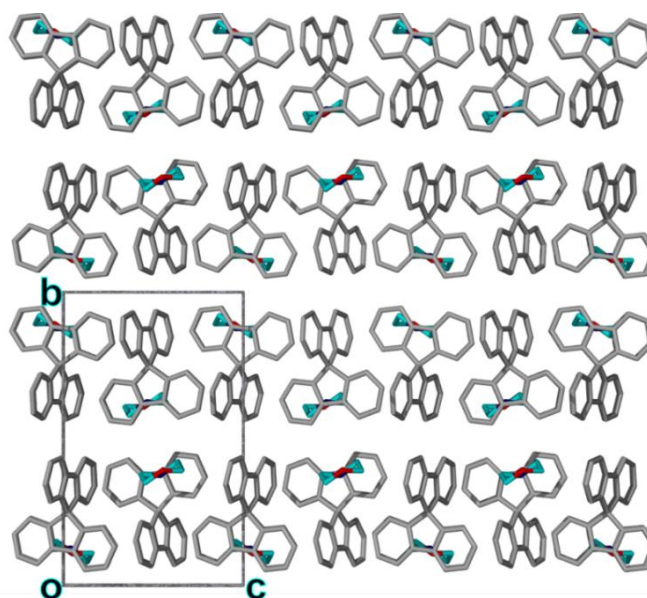
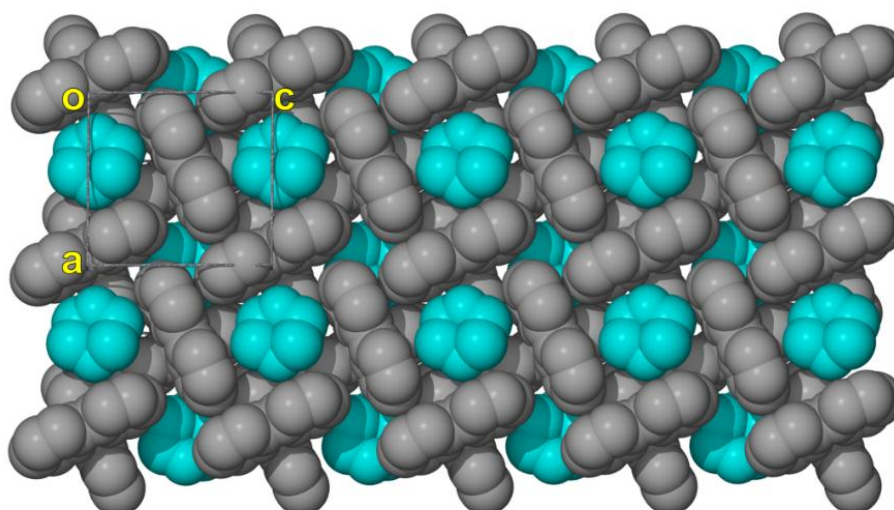


**Figure 3.13** Intermolecular interactions in **H2•MOR**.

**Table 3.8** Intermolecular interactions in H2•MOR

	D-H...A	d(D-H) (Å)	d(D-H...A) (Å)	(H...A) (Å)	∠ DHA (°)
<b>A</b>	C16-H16...C <sub>g</sub> (C8-C13)	0.95	3.65	2.85	142
<b>B</b>	C27-H27A...C <sub>g</sub> (C2-C7)	0.99	3.77	2.94	141
<b>C</b>	C29-H29A...C <sub>g</sub> (C8-C13)	0.99	3.61	2.98	122
<b>D</b>	C18-H18...O1 <sup>a</sup>	0.95	3.85	2.96	154

**Symmetry operator:** <sup>a</sup>1/2-x,y-1/2,3/2-z

**Figure 3.14** Packing diagram of H2•MOR viewed down [100]. Guests coloured turquoise.**Figure 3.15** Packing diagram of H2•MOR viewed down [010]. Guests coloured turquoise.



### 3.5.2.4 Structure analysis of H2•DIO

Single crystal X-ray analysis was conducted on a suitable crystal of **H2•DIO** with the dimensions of 0.20 × 0.24 × 0.30 mm. The inclusion compound crystallises in the monoclinic  $P2_1/n$  (No. 14) space group. The crystal structure was refined to  $R_1=0.1025$  and  $wR_2=0.3298$  (See **Table 3.5** for data collection and refinement parameters). These R values are high but this can be explained by the high Z value (12) and large number of included solvent molecules. The asymmetric unit consists of three **H2** host molecules and three **DIO** guests whereby two **DIO** molecules are ordered (**Figure 3.16** molecule 1 and 2) and one is disordered (**Figure 3.16** molecule 3).

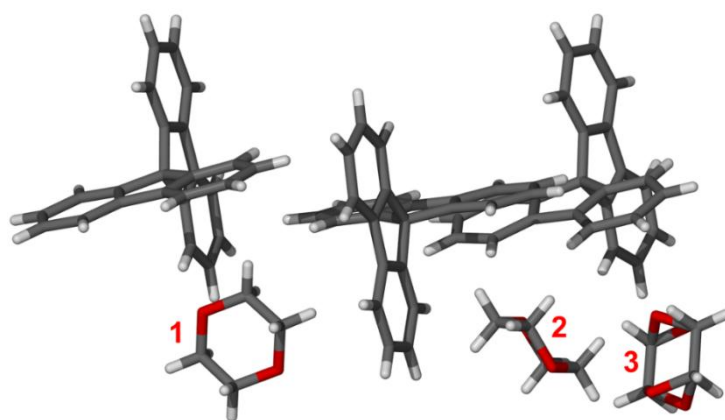


**Figure 3.16** Asymmetric unit of **H2•DIO**. Guest molecules 1 and 2 are ordered while 3 is disordered.

When a molecule adopting several orientations which can be associated with different and undistinguished local potential minima, in other words appears as a disordered entity, it generally presents weak intermolecular interactions towards the surrounding crystal field.<sup>6</sup> The nature of the disorder of **DIO** molecule 3 is pseudorotational and can be described as two chair conformations which are overlapping with each other.<sup>5</sup> The disordered **DIO** ring occupies one or the other chair confirmation in the crystal with site occupancy factors of 80% (**Figure 3.17** Red) and 20% (**Figure 3.17** Blue). Because of the significant site occupancy factor difference, the hydrogen atoms were placed onto the major orientation and this major component of the disordered **DIO** was used in the further analysis.

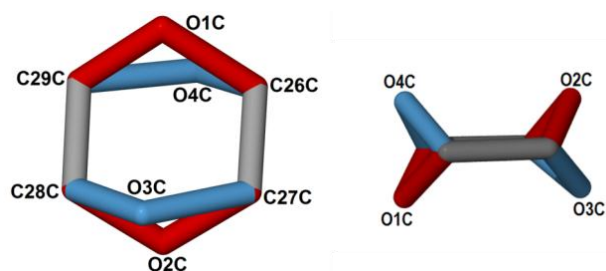


**Figure 3.17** Disordered **DIO** guest in **H<sub>2</sub>•DIO**. (Site occupancy factor 80% atoms coloured with red and 20% with blue).

The close contacts in the asymmetric unit of **H<sub>2</sub>•DIO** is presented in **Figure 3.18** labelled A to D and their details are summarised in **Table 3.9**. The C-H... $\pi$  interaction A involves two host molecules situated in the perpendicular y-shaped geometry (C11A-H11A... $c_g$ (C8B-C13B), 2.85 Å). The close contacts B, C and D occur between the guests and hosts in the structure. The interactions B (C24B-H24B...C28A, 2.89 Å) and C (C3B-H3B...C27B, 2.86 Å) are formed between C and H atoms. The O...H contact (D) has the distance 2.66 Å, which is below the sum of the van der Waals radius for an oxygen and a hydrogen.<sup>4</sup> The disordered **DIO** molecule does not have any close contacts with the surrounding crystal space.

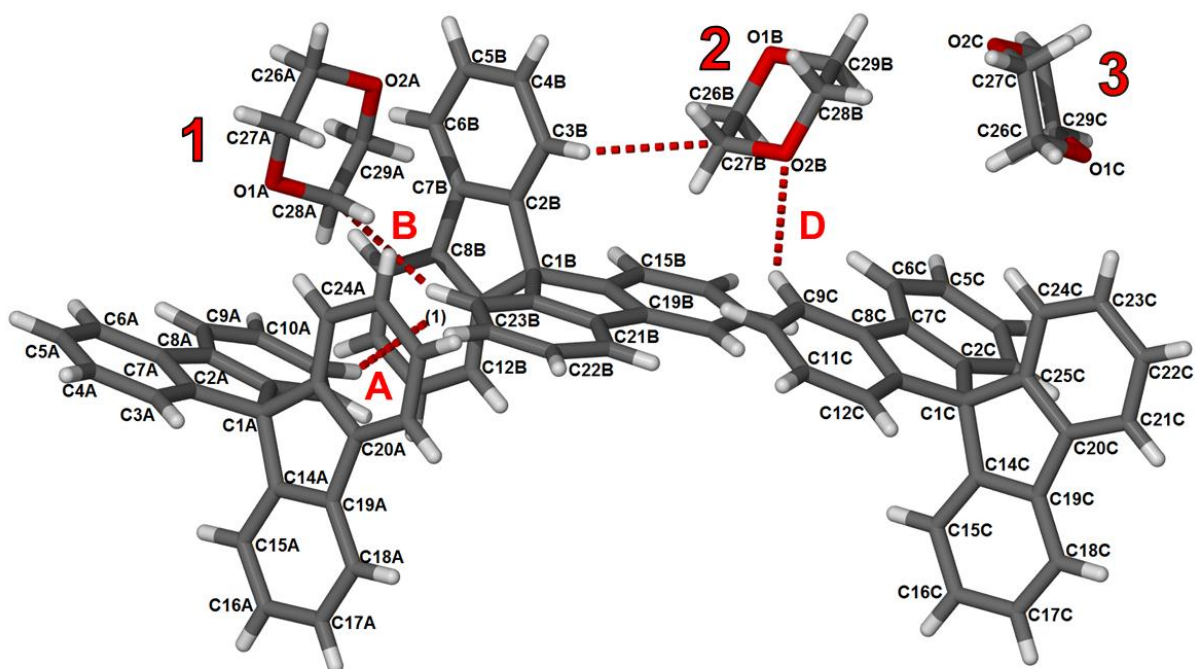


**Figure 3.18** Intermolecular interactions in **H<sub>2</sub>•DIO**. Guest molecules 1 and 2 are ordered while 3 is disordered.

**Table 3.9** Intermolecular interactions in **H2•DIO**

	D-H...A	d(D-H) (Å)	d(D-H...A) (Å)	(H...A) (Å)	∠ DHA (°)
<b>A</b>	C11A-H11A...cg(C8B-C13B)	0.95	3.65	2.85	142
<b>B</b>	C24B-H24B...C28A	0.95	3.62	2.89	135
<b>C</b>	C3B-H3B...C27B	0.95	3.74	2.86	153
<b>D</b>	C9C-H9C...O2B	0.95	3.44	2.66	141

The packing of **H2•DIO** is similar to that of **H2•PIP** and **H2•MOR**, whereby the **H2** molecules are held together in layers by C-H... $\pi$  interactions (**Figure 3.19**). It is observed that the ordered **DIO** molecules (1) face each other between the layers while the other ordered **DIO** molecules (2) and disordered **DIO** molecules (3) are opposite to one another. The **DIO** guests located in the cavities on the surface layer alternate along the crystallographic direction [001] (**Figure 3.20**).

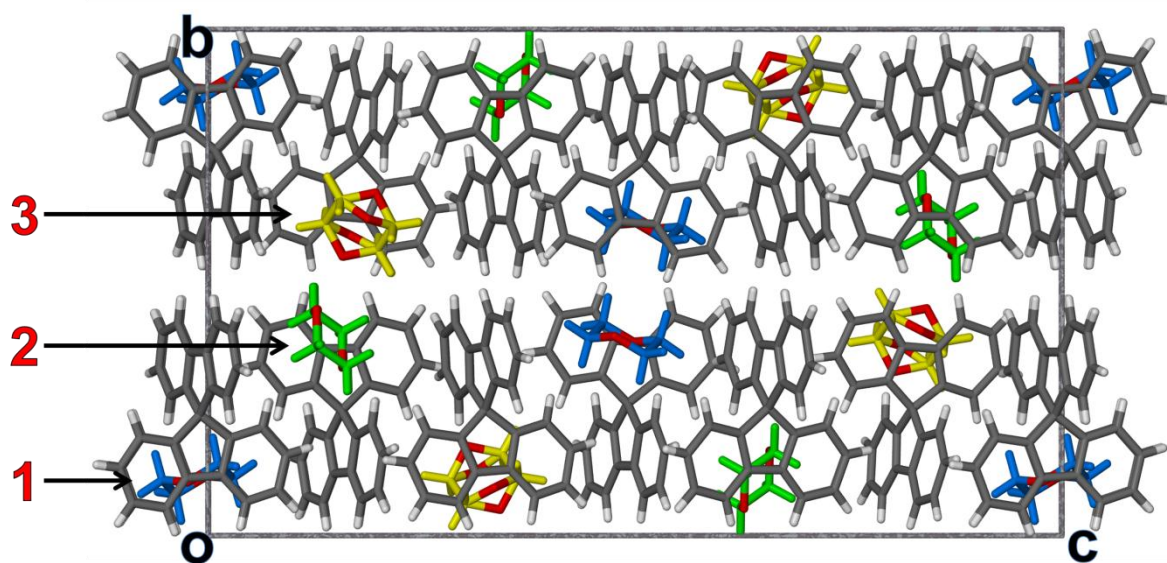


**Figure 3.19** Packing diagram for **H2•DIO** viewed along [100]. Guest molecules 1 (blue) and 2 (green) are ordered while 3 (yellow) is disordered.

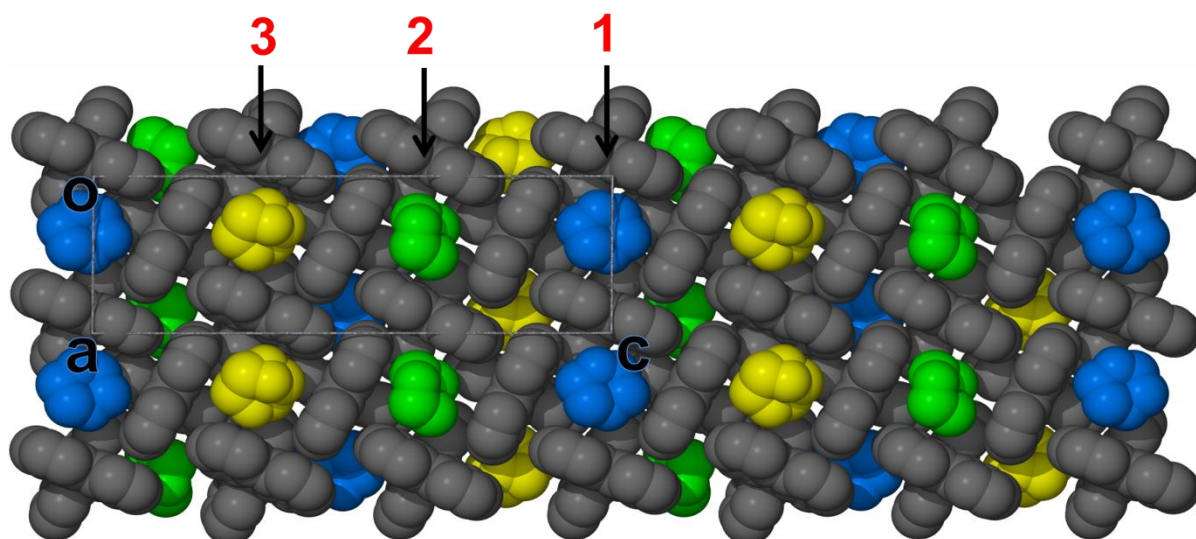


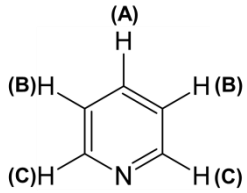
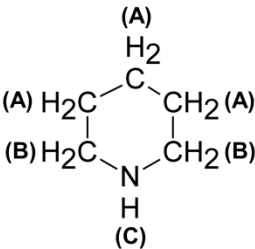
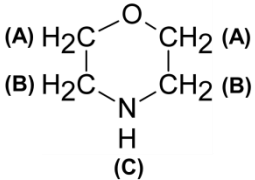
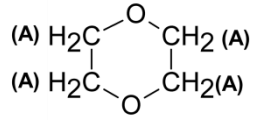
**Figure 3.20** Packing diagram of **H<sub>2</sub>•DIO**, single layer viewed down [010]. Guest molecule 1 and 2 are ordered while 3 is disordered.

### 3.5.3 Competition experiments with H2 and heterocyclic compounds

#### 3.5.3.1 <sup>1</sup>H-NMR results of the selectivity experiments

The competition experiments were carried out with host **H2** and the four guest compounds **PYR**, **PIP**, **MOR** and **DIO**. **H2** was exposed to six binary equimolar guest mixtures (**H2**/ 0.5**MOR**/ 0.5**PYR**, **H2**/ 0.5**PYR**/ 0.5**DIO**, **H2**/ 0.5**DIO**/ 0.5**MOR**, **H2**/ 0.5**PIP**/ 0.5**PYR**, **H2**/ 0.5**PIP**/ 0.5**DIO** and **H2**/ 0.5**PIP**/ 0.5**MOR**). Crystals were harvested and subjected to <sup>1</sup>H-NMR spectroscopy. The relative proportions of the guests were determined by integrating the signals from the –NH, –CH and –CH<sub>2</sub> protons. **Table 3.10** gives a summary of the spectra of the pure heterocyclic guest compounds.

**Table 3.10** <sup>1</sup>H-NMR data for **PYR**, **PIP**, **MOR** and **DIO**

							
PYR		PIP		MOR		DIO	
Assignment	δ (ppm)	Assignment	δ (ppm)	Assignment	δ (ppm)	Assignment	δ (ppm)
(A) H	7.68	(A) H <sub>2</sub>	1.53	(A) H <sub>2</sub>	3.67	(A) H <sub>2</sub>	3.71
(B) H	7.29	(B) H <sub>2</sub>	2.78	(B) H <sub>2</sub>	2.86		
(C) H	8.62	(C) H	2.18	(C) H	2.59		

The relative percentages of the two solvents captured in the crystals are shown in **Table 3.11**. The selectivity shows that **H2** does not exhibit exclusive preference towards any of the guests. The results indicate that **H2** has poor selectivity towards the three guests **PYR**, **MOR** and **DIO** (pairs 1, 2 and 3). The poorest selectivity is between **PYR** (47.8%) and **MOR** (52.5%) which has a low 4.7% difference in proportion. The second lowest difference is between the **PYR** (54.5%) and **DIO** (45.5%) pair, where **PYR** is 9% more favoured. From the mixture of **DIO** and **MOR**, **DIO** is preferred by 12%. From these results it is evident that there is no particular order of selectivity between the three guests, therefore **H2** does not discriminate between **PYR**, **MOR** and **DIO**. However, in the case of the other three competing pairs (4, 5 and 6), **H2** significantly favours **PIP** over **PYR**, **MOR** and **DIO**. The



greatest selectivity difference is between **PIP** and **PYR** which resulted in the enclathration of **PIP** in 75.9%. The guest pair 5 (66.4% **PIP** and 33.6% **DIO**) and 6 (63.2% **PIP** and 36.8% **MOR**) have a 32.8% and 26.4% lower enclathration compared to **PIP**, respectively and it may be concluded **H2** discriminates between the four as follows:



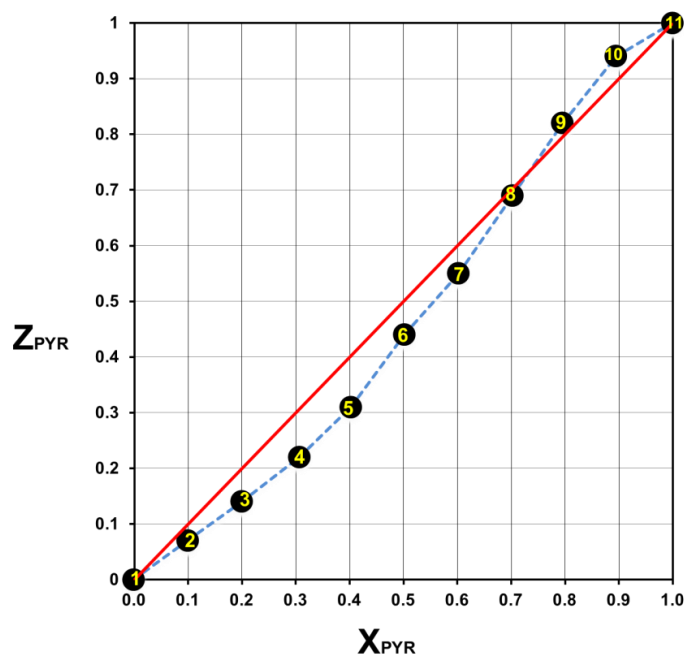
**Table 3.11**  $^1\text{H-NMR}$  results and selectivity constants ( $K$ ) of **H2** with binary equimolar mixtures of the guests. Preferred guest are in bold

Pair	Binary equimolar mixtures	Enclathration results	Selectivity constants ( $K$ )
1	MOR/PYR	52.2% ( <b>MOR</b> ) and 47.8% (PYR)	1.1
2	PYR/DIO	54.5% ( <b>PYR</b> ) and 45.5% (DIO)	1.2
3	DIO/MOR	56.0% ( <b>DIO</b> ) and 44.0% (MOR)	1.3
4	PIP/PYR	75.9% ( <b>PIP</b> ) and 24.1% (PYR)	3.1
5	PIP/DIO	66.4% ( <b>PIP</b> ) and 33.6% (DIO)	2.0
6	PIP/MOR	63.2% ( <b>PIP</b> ) and 36.8% (MOR)	1.7

Pair 1 (**PYR/MOR**) was chosen to conduct a full selectivity experiment to obtain selectivity co-efficient values for **H2** towards **PYR** and **MOR**. The competition experiment was carried out between the **PYR** and **MOR** guest pairs by dissolving **H2** into a series of solutions where the two guest mixtures' mole fraction was varied from 0 to 1. According to the equation (see chapter 2, page 22),  $X_A:X_B$  and  $Z_A:Z_B$  are the mole fractions of **PYR** (A) and **MOR** (B) in the liquid mixture and crystalline compound, respectively. The ensuing crystals were analysed by  $^1\text{H-NMR}$  spectroscopy. The resultant values are expressed in **Table 3.12**. The selectivity profile of **H2** in the mixtures of **PYR** and **MOR** is shown in **Figure 3.21**, where the red line is the reference line representing no selectivity ( $K_{A:B} = 1$ ) and the blue line is the experimental data. The results show that the host preferentially enclathrates **MOR** over **PYR** for most of the selectivity range ( $X_{\text{PYR}} < 0.8$ ) with a low selectivity co-efficient  $K_{\text{PYR:MOR}} = 0.8$ , thus overall **H2** virtually does not discriminate between **MOR** and **PYR** but **MOR** drives the packing of the system.

**Table 3.12** Selectivity values for H2•(PYR)/(MOR)

	Mole fraction of PYR in liquid ( $X_{\text{PYR}}$ )	Mole fraction of PYR in crystal ( $Z_{\text{PYR}}$ )
1	0.00	0.00
2	0.10	0.07
3	0.20	0.14
4	0.31	0.22
5	0.40	0.31
6	0.50	0.44
7	0.60	0.55
8	0.70	0.69
9	0.80	0.82
10	0.90	0.94
11	1.00	1.00

**Figure 3.21** Selectivity curve for the H2•(PYR)/(MOR) system.

The scarcity of the material H2 prevented further competition experiments of the remaining five guest pairs. The competition experiments were limited to only the equimolar guest mixtures. **Table 3.10** presents the selectivity constants for the six pairs given as  $K_{A:B} = (K_{B:A})^{-1} = Z_A/Z_B \times X_B/X_A$  where  $X_B = X_A = 0.5$ . The selectivity constants,  $K_{\text{MOR:PYR}} = 1.1$  ( $K_{\text{PYR:MOR}} = 0.9$ ),  $K_{\text{PYR:DIO}} = 1.2$  and  $K_{\text{DIO:MOR}} = 1.3$  are very close to the value 1, which defines no selectivity, therefore H2 does not discriminate between the three guests. The selectivity constants,  $K_{\text{PIP/PYR}} = 3.1$ ,  $K_{\text{PIP:DIO}} = 2.0$  and  $K_{\text{PIP:MOR}} = 1.7$  are significantly higher than 1 and this supports the results obtained from the previous competition experiments.

### 3.5.3.2 Powder X-ray analysis

The unit cell parameters of **H2•MOR**, **H2•PYR**, **H2•PIP** and **H2•PYR** differ sufficiently. A powder X-ray analysis (PXRD) was conducted on the crystals obtained from the equimolar mixture of **MOR/PYR** (Figure 3.22) and **PIP/PYR** (Figure 3.23). Comparisons of the relevant measured and calculated PXRD patterns were done to determine which structure is represented in the bulk. The green graph representing the inclusion compound of **H2** with the equimolar mixtures of **MOR/PYR** and **PIP/PYR** in both cases, is sufficiently different for the sum of **H2•MOR/ H2•PYR** and **H2•MOR/ H2•PYR** and suggests that new compounds were obtained. However, the quality of the single crystals in both cases was poor and further structure solution was not attempted.

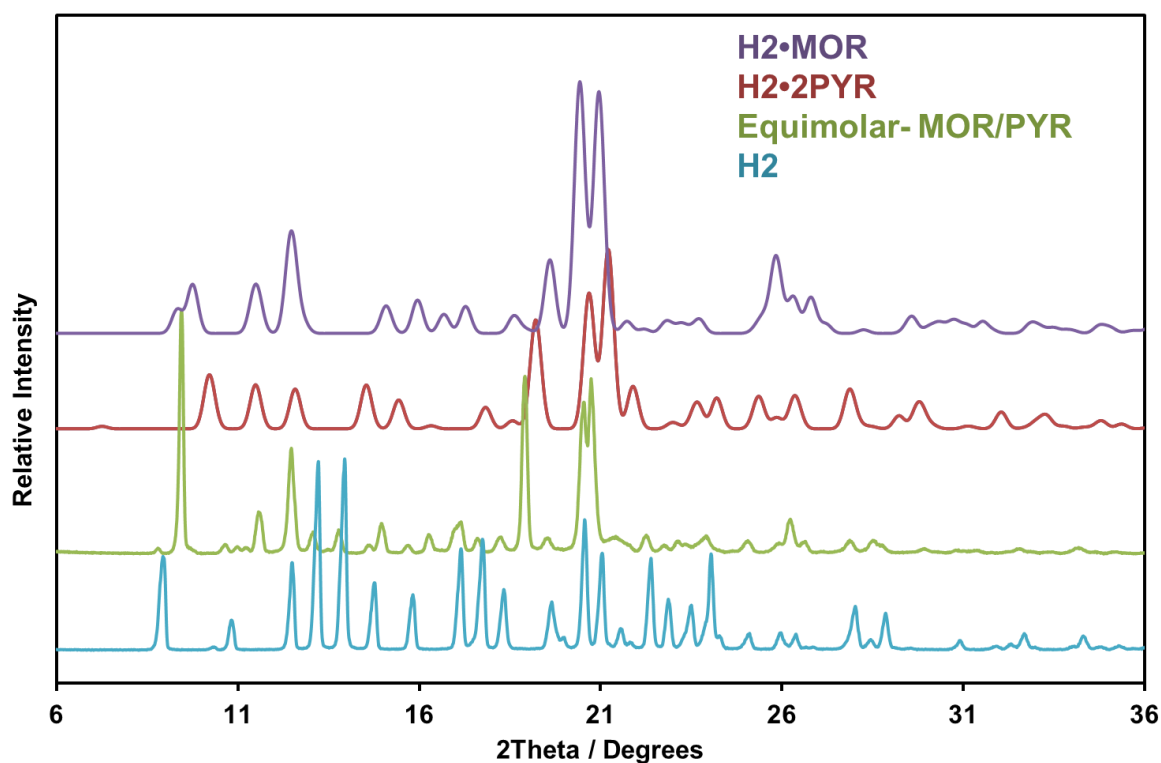


**Figure 3.22** PXRD patterns: **H2•MOR** (calculated-purple), **H2•2PYR** (calculated-red), **H2•PYR/MOR** (measured-green) and **H2** (measured-blue).



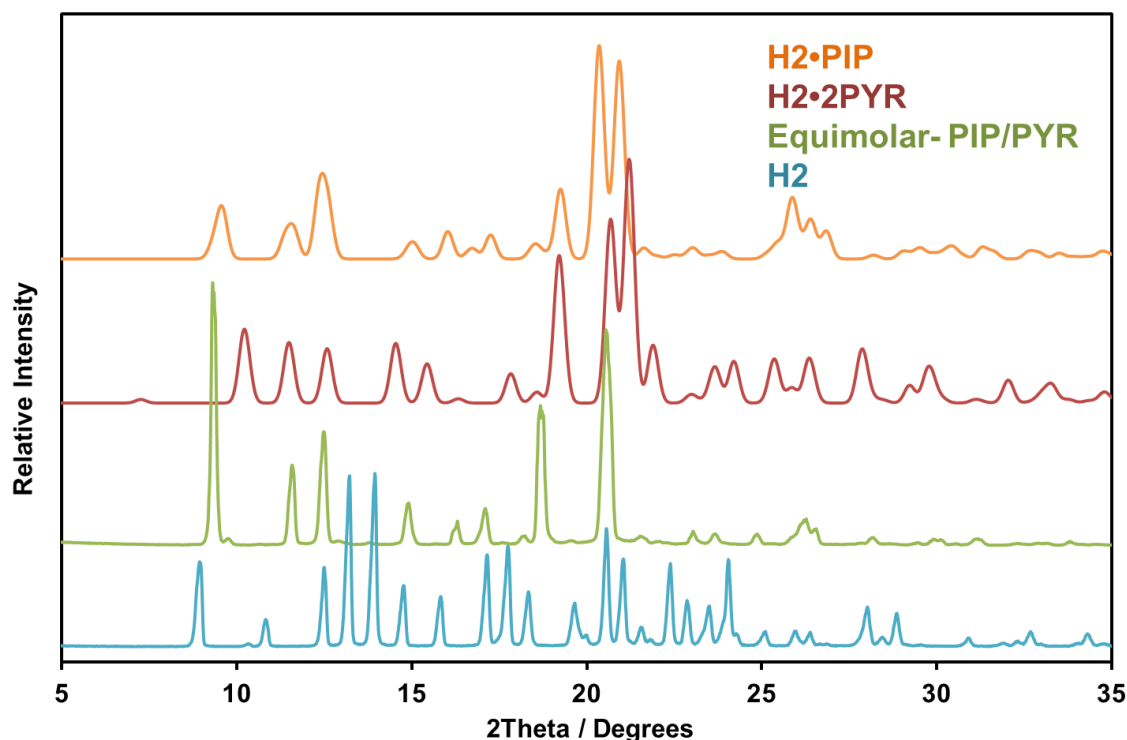


**Figure 3.23** PXRD patterns: **H2•PIP** (calculated-orange), **H2•2PYR** (calculated-red), **H2•PYR/MOR** (measured-green) and **H2** (measured-blue).

### 3.5.3.3 Hirshfeld surface analysis of H2•2PYR, H2•PIP, H2•MOR and H2•DIO

The software Crystal Explorer<sup>7</sup> is a versatile tool to explore the packing modes and intermolecular interactions in molecular crystals via analysing the Hirshfeld surface of a given component of a crystal. The Hirshfeld surface of a molecule reflects the relationship between the selective molecule and its direct environment in the crystal by mapping the intermolecular interactions in a novel graphical manner. The nature of interactions can be quickly identified and interpreted which may not be clear when examining traditional crystal packing diagrams.<sup>8,9,10</sup> Hirshfeld surface analysis was conducted on the guests of the **H2•PIP**, **H2•MOR**, **H2•2PYR** and **H2•DIO** structures and these three dimensional features were translated into two dimensional 'fingerprint plots' for easier interpretation. **Figure 3.24** presents 2D fingerprint plots where the points on the Hirshfeld surface, for the distances to the nearest atom outside ( $d_e$ ) and inside ( $d_i$ ), are readily defined. There are two unique Hirshfeld plots for the **H2•2PYR** due to the two crystallographically independent **PYR** guests. The plots show no significant differences. There are three unique fingerprint plots for

**H2•DIO** because of the three guest molecules in the asymmetric unit, of which two **DIO** guests are ordered (molecules 1 and 2) and one **DIO** is disordered (molecule 3). The Hirshfeld surface generated for molecule 3 has to be treated with care due to the fact that this does not represent fully the positioning of the guest. The ‘spike’ (1) and ‘wing’ (2) on the plots depict H•••H and C•••H contacts, respectively. The majority of the interactions in each structure are due to the H•••H close contacts (**Table 3.13**). The highest percentage of H•••H contacts is in the **H2•PIP** structure, which supports the results obtained from the competition experiments, when **H2** was selective towards **PIP** amongst all the other solvents. The shortest sum of  $d_e$  and  $d_f$  H•••H contacts (Peak 1) in all the structures is in **H2•PIP** (2.33 Å) confirming the close packing of the structure and again corresponding the superior selectivity of **H2** towards **PIP**. The **H2•PIP**, **H2•MOR**, **H2•2PYR** and **H2•DIO** structures are also stabilised by C•••H contacts, which are typically C-H••• $\pi$  interactions. It is interesting to note that **H2•2PYR** has the highest percentage of C•••H contacts but the lowest percentage (41%) of H•••H contacts (44%). The second highest C•••H contacts was observed in **H2•PIP** structure (23%). The rest of the close contacts (O•••H, N•••H and C•••O) do not appear in all the structures and if so have very low percentage values with no particular trend. This may be the reason why **H2** is not selective towards the **MOR**, **PYR** and **DIO** guests in any particular order. The **H2•PIP** structure appears to be the most closely packed structure and this correlates to the competition experiments where **H2** overall prefers the **PIP** guest.

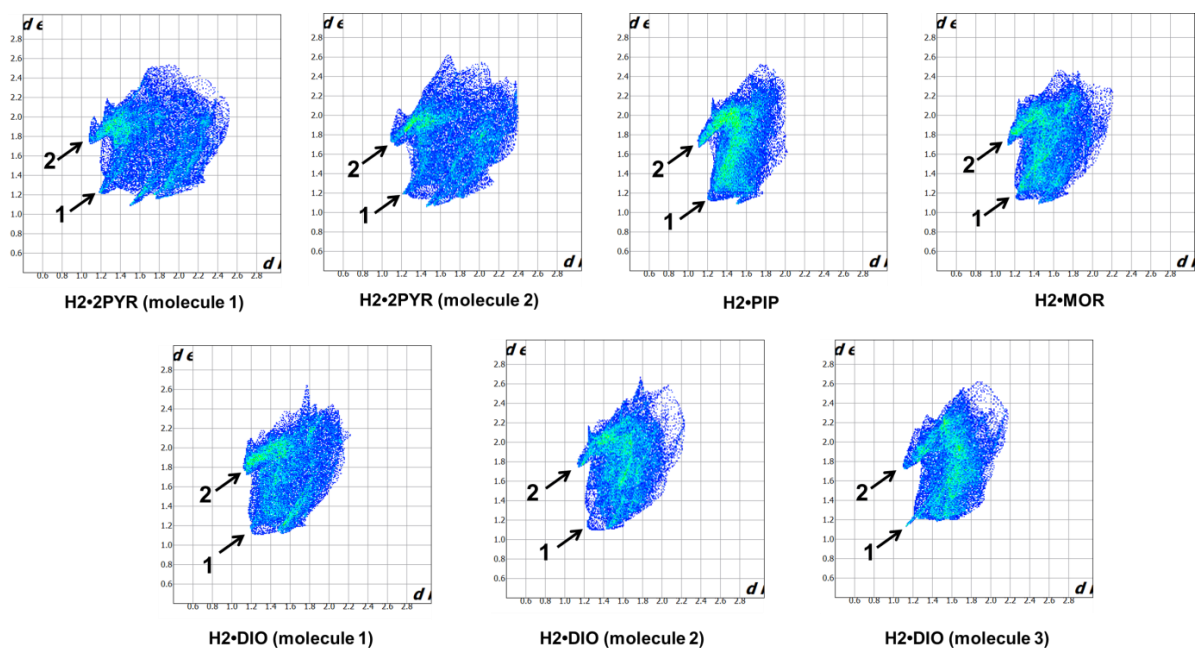


**Figure 3.24** Fingerprint plots of Hirshfeld surfaces generated for **H2•PIP**, **H2•MOR**, **H2•2PYR** and **H2•DIO** crystal structures.

**Table 3.13** Intermolecular interactions in inclusion compounds of **H2**

	H2•PIP	H2•MOR	H2•2PYR (Guest 1)	H2•2PYR (Guest 2)	H2•DIO (Guest 1)	H2•DIO (Guest 2)	H2•DIO (Guest 3)
H•••H (%)	74	68	44	50	61	59	64
C•••H (%)	23	20	41	40	19	20	20
O•••H (%)	0	8	0	0	18	20	16
N•••H (%)	3	3	13	12	0	0	0
C•••O (%)	0	1	0	0	1.5	0.3	0

## 3.6 Inclusion compound of H3 with PYR

### 3.6.1 Thermal analysis of H3•PYR

The DSC and TG trace for the **H3•PYR** is presented in **Figure 3.25**. The TG trace shows a mass loss of 16.6% (calculated 16.5%), which confirms the host:guest ratio of 1:1 in the crystal. The corresponding DSC trace portrays two endotherms, the former representing a volatile guest (**PYR**) release at  $T_{on} = 92.9^{\circ}\text{C}$  and the  $T_{peak} = 99.3^{\circ}\text{C}$ . The second endotherm with  $T_{on} = 203.3^{\circ}\text{C}$  and  $T_{peak} = 204.1^{\circ}\text{C}$  represents the melting of **H3**.

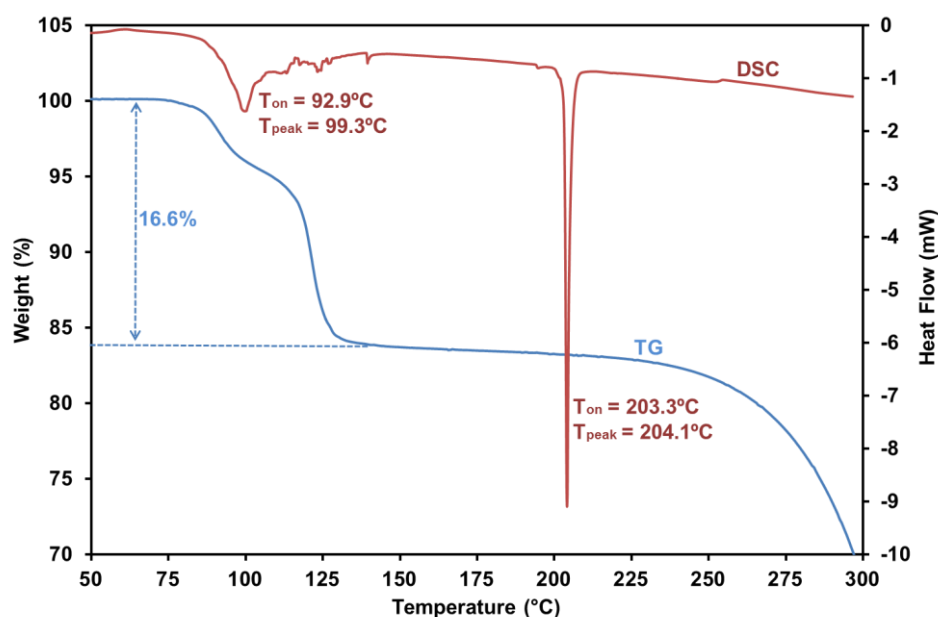


Figure 3.25 TG and DSC traces for **H3•PYR** (endo down).

### 3.6.2 Crystal structure analysis of **H3•PYR**

A colourless **H3•PYR** crystal was selected for single crystal X-ray diffraction analysis. The data collection and refinement parameters are listed in **Table 3.14**. The **H3•PYR** structure was solved in the orthorhombic *Pbca* (No. 61) space group with the molecular formula  $C_{34}H_{25}NO_2$ . The structure refined to  $R_1 = 0.0470$  and  $wR_2 = 0.1215$ . The asymmetric unit consists of one **PYR** molecule and one **H3** host molecule giving the host to guest ratio of 1:1. The interactions that stabilize **H3•PYR** is displayed in **Figure 3.26**. The C-H $\cdots\pi$  interaction (A) occurs between neighbouring hosts (C27-H27 $\cdots$ c<sub>g</sub>(C10-C15), 2.70 Å) in the perpendicular y-shaped position. The contact distances are shown in **Table 3.15**. The close contact B (C11-H11 $\cdots$ C3) takes place between a host molecule and a guest with the distance of 2.79 Å. The O $\cdots$ H contact C (host-guest, C33-H33 $\cdots$ O1, 2.66 Å) and D (host-host, C12-H12 $\cdots$ O2, 2.65 Å) are shorter than the sum of the van der Waals radii of oxygen and hydrogen. The packing of **H3•PYR** is presented in **Figure 3.27** with the guest positioned in channels running along the *a*-axis [100] and the host molecules are positioned in a wave like arrangement.

Table 3.14 Crystal data for H3•PYR

Compounds	H3•PYR
Molecular formula	C <sub>24</sub> H <sub>25</sub> NO <sub>2</sub>
Formula weight (g. mol <sup>-1</sup> )	479.55
Crystal system	orthorhombic
Space group	<i>Pbca</i> (No. 61)
a (Å)	15.858(3)
b (Å)	17.481(4)
c (Å)	18.142(4)
α (°)	90
β (°)	90
γ (°)	90
V (Å <sup>3</sup> )	5029.2(19)
Z	8
ρ calc (g.cm <sup>-3</sup> )	1.267
μ (MoKα) (mm <sup>-1</sup> )	0.078
F (000)	2016
Crystal size (mm)	0.05 x 0.20 x 0.28
Temperature (K)	173 (2)
Radiation (Å)	0.71073
Theta min-max (°)	2.8, 27.5
Dataset (±h, ±k, ±l)	-20:20; -22:22; -23:23
Final R indices [I>2.0 (I)]	R1=0.0470, wR2=0.1029
R indices (all data)	R1=0.1045, wR2=0.1215
Tot., uniq. data, R(int)	10932, 5746, 0.054
N <sub>ref</sub> , N <sub>par</sub>	5746, 335
S	1.01
Max. and Av. Shift/Error	0.00, 0.00
Min. and Max. Resd. Electron Dens. (e/Å <sup>3</sup> )	-0.47, 0.43

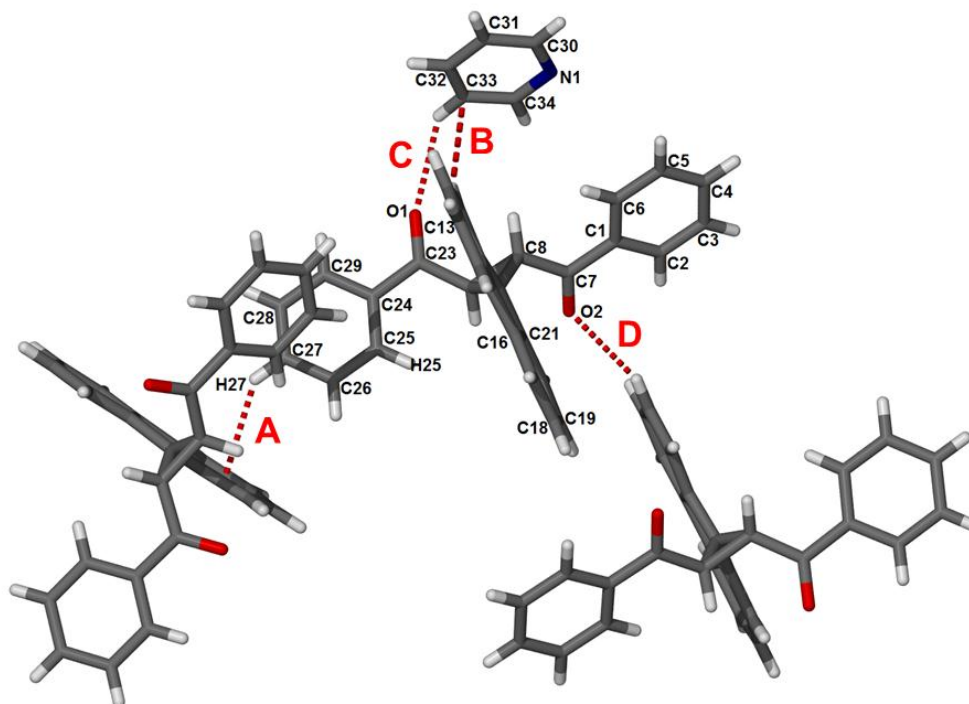


Figure 3.26 Intermolecular interactions in **H3•PYR** structure.

Table 3.15 Intermolecular interactions in **H3•PYR**

	D-H...A	d(D-H) (Å)	d(D-H...A) (Å)	(H...A) (Å)	∠ DHA (°)
A	C27-H27...C <sub>q</sub> (C10-C15)	0.95	3.50	2.70	142
B	C11-H11...C3	0.95	3.64	2.79	150
C	C33-H33...O1	0.95	3.82	2.66	138
D	C12-H12...O2 <sup>a</sup>	0.95	3.29	2.65	149

Symmetry operator: <sup>a</sup>1/2-x,y-1/2,z

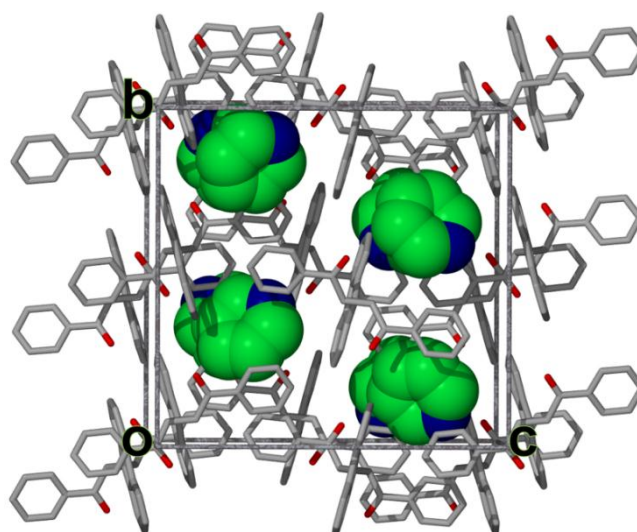


Figure 3.27 Packing diagram for **H3•PYR** viewed along [100]. Guests are presented with space filling and coloured green.

## References

---

- <sup>1</sup> Báthori, N.B. & Nassimbeni, L.R. *Cryst. Growth. Des.*, 2010, 10: 1783.
- <sup>2</sup> Felix-Navarro, R.A., Wai Lin, S., Zizumbo-López, A., Pérez-Sicairos, S., Reynoso-Soto, E. A. & Espinoza-Gómez, J.H. *J. Mex. Chem. Soc.*, 2013, 51: 2.
- <sup>3</sup> Martínez, C.R. & Iversion, B.L. *Chem. Sci.*, 2012, 3: 2191.
- <sup>4</sup> Taylor, R. *Cryst. Eng. Comm.*, 2014, DOI: 10.1039/C4DE00452C.
- <sup>5</sup> Flack, H. D. & Bernardinelli, G. *J. Appl. Crystallogr.*, 2000, 33: 1143.
- <sup>6</sup> Pang, L., Brisse, F. & Lucken, E.A.C. *Can. J. Chem.*, 1995, 73: 351.
- <sup>7</sup> Wolff, S. K., Grimwood, D. J., McKinnon, J. J., Jayatilaka, D. & Spackman, M. A., *Crystalexplorer 3.1.*, University of Western Australia, Perth, 2007. (hirshfeldsurface.net).
- <sup>8</sup> Spackman, M. A. & McKinnon, J. J. *CrystEngComm.*, 2002, 4(66): 378.
- <sup>9</sup> McKinnon, J. J., Spackman, M. A. & Jayatilaka, D. *Chem. Comm.*, 2007, 3814.
- <sup>10</sup> Spackman, M. A. *Phys. Scr.*, 2013, 87, 048103.

# Chapter 4: Selectivity experiments of cyclohexanone derivative guest compounds

## 4.1 Introduction

This study investigates the selectivity of cyclohexanone (**CYHA**), 2-methylcyclohexanone (**2-MCYHA**), 3-methylcyclohexanone (**3-MCYHA**) and 4-methylcyclohexanone (**4-MCYHA**) by employing host-guest chemistry (**Figure 4.1**). **CYHA** is used in the manufacturing of nylon and fabric<sup>1</sup> and the **MCYHA** isomers are used as flavour and fragrant agents. The enclathration experiments of 9,9'-bianthryl (**H1**), 9,9'-spirobifluorene (**H2**) and *trans*-2,3-dibenzoylspro(cyclopropane-1,9'-fluorene) (**H3**) with the cyclic ketone guests were investigated in relation to their crystal structures, thermal analysis and powder X-ray analysis.

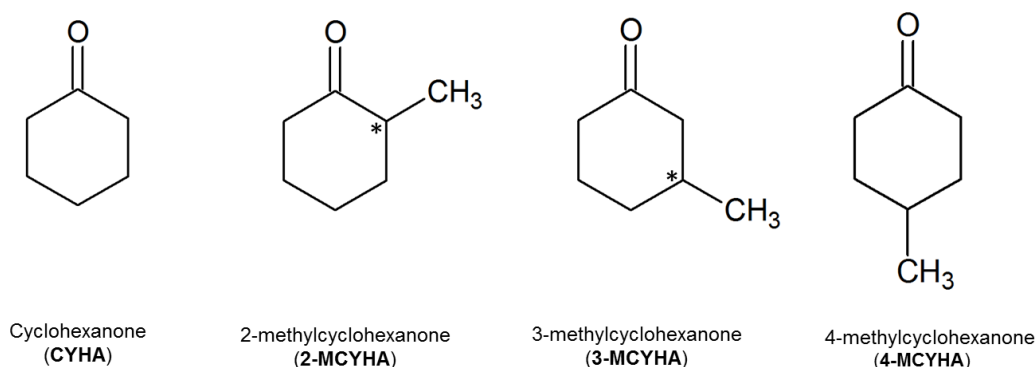


**Figure 4.1** Schematic diagrams of cyclic ketone guest compounds.

## 4.2 Inclusion complex preparation

The inclusion compounds were prepared by the slow evaporation method. Approximately 60-70 mg of each host compound (**H1**, **H2** or **H3**) was dissolved in about 2 ml of pure **CYHA** and then left at room temperature to crystallise. The procedure was then repeated with the binary equimolar mixtures of the three **MCYHA** isomers. Crystalline material appeared after a few days of slow evaporation of the solvents.



### 4.3 Inclusion complex analysis

The crystalline products that formed from the hosts, **H1**, **H2** and **H3** and guest compounds, **CYHA**, **2-MCYHA**, **3-MCYHA** and **4-MCYHA** were subjected to single crystal X-ray diffraction, powder X-ray diffraction and thermal gravimetry and the results are shown in **Table 4.1**. The host compound, **H1**, formed inclusion compounds with **CYHA** and **2-MYCHA** with host-guest ratios of 1:2 and 2:1 respectively. The competition experiments between the host **H1** and **MYCHA** isomers were compromised, due to the unexpected decomposition of **H1**. The host compound **H1** is light sensitive and decomposed into anthracene (**ANT**). This observation is discussed in more detail in this chapter. The host compound **H2** did not form any inclusion compounds with the **CYHA** and **MCYHA** guest molecules. The host compound **H3** only formed a clathrate with **CYHA** with a host-guest ratio of 1:1.

**Table 4.1** Enclathration results of **H1**, **H2** and **H3** with **CYHA** and binary equimolar mixtures of **2-MCYHA**, **3-MCYHA** and **4-MCYHA**

Host	Solvent	Resulting Crystal	TG % mass loss found (calc)
<b>H1</b>	CYHA	H1•2CYHA	34.0 (35.6)
	2-MCYHA/3-MCYHA	H1•ANT	-
	2-MCYHA/4-MCYHA	H1•0.5(2-MCYHA)	H1 decomposed
	3-MCYHA/4-MCYHA	Decomposition	-
<b>H2</b>	CYHA	H2 apohost	-
	2-MCYHA/3-MCYHA	H2 apohost	-
	2-MCYHA/4-MCYHA	H2 apohost	-
	3-MCYHA/4-MCYHA	H2 apohost	-
<b>H3</b>	CYHA	H3•CYHA	≈18.0 (19.7)*
	2-MCYHA/3-MCYHA	H3 apohost	-
	2-MCYHA/4-MCYHA	H3 apohost	-
	3-MCYHA/4-MCYHA	H3 apohost	-

\*See explanation on page 77

## 4.4 Inclusion compounds of H1 with CYHA and 2-MCYHA

### 4.4.1 Crystal structure analysis of H1•2CYHA

A small suitable single crystal was selected for X-ray diffraction and was found to crystallise in the monoclinic  $Pn$  (No.7) space group. The **H1•2CYHA** structure refined to  $R_1 = 0.0450$  and  $wR_2 = 0.1199$  and the crystallographic data is summarised in **Table 4.2**. The asymmetric unit contains one **H1** host molecule and two **CYHA** guest molecules, where one of the latter is ordered and the other is disordered (**Figure 4.2**). The disordered **CYHA** molecule (2) possesses two energetically similar conformations, with site occupancy factors of 80% and 20%. This is known as positional disorder.<sup>2</sup> The **H1•2CYHA** inclusion compound is held together by C-H $\cdots\pi$  interactions and C-H $\cdots$ O contacts. The C-H $\cdots\pi$  interactions, A (C5-H5 $\cdots$ c<sub>g</sub>(C23-C28), 2.75 Å) and B (C19-H19 $\cdots$ c<sub>g</sub>(C9-C14), 2.95 Å) are positioned in the perpendicular y-shaped geometry and result from host to host close contacts. The C-H $\cdots\pi$  interaction C (C29-H29A $\cdots$ c<sub>g</sub>(C16-C21), 2.90 Å) arises between a host and a guest in parallel offset geometry. The C-H $\cdots\pi$  interaction D (C39-H39A $\cdots$ c<sub>g</sub>(C16-C21), 2.89 Å) occurs between a guest and a host in the perpendicular y-shaped geometry. The C-H $\cdots$ O contact, E (C24-H24 $\cdots$ O1B, 2.57 Å) results from the proximity of a host and disordered guest (molecule 2) with an 80% site occupancy factor. The C-H $\cdots$ O contact (F) arises from a close contact between a neighbouring host and a guest (C26-H26 $\cdots$ O1) with the distance of 2.40 Å. The interactions are shown in **Figure 4.3** and summarised in **Table 4.3**. The host compounds are held together by several C-H $\cdots\pi$  interactions in a framework, where the guest molecules are located in channels running along [100] (**Figure 4.4**).

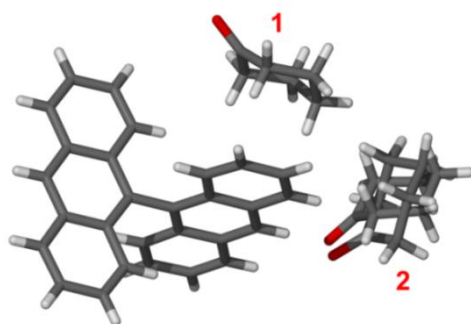


**Figure 4.2** Asymmetric unit of **H1•2CYHA**. Guest molecules 1 is ordered and 2 is disordered.

Table 4.2 Crystal data for H1•2CYHA and H1•0.5(2-MCYHA)

Compounds	H1•2CYHA	H1•0.5(2-MCYHA)
Molecular formula	C <sub>40</sub> H <sub>38</sub> O <sub>2</sub>	C <sub>63</sub> H <sub>48</sub> O
Formula weight (g. mol <sup>-1</sup> )	550.70	821.01
Crystal system	monoclinic	monoclinic
Space group	<i>Pn</i> (No.7)	<i>P2</i> <sub>1</sub> (No.4)
a (Å)	9.3503(19)	9.1061(18)
b (Å)	9.2158(18)	16.846(3)
c (Å)	18.170(4)	14.614(3)
α (°)	90	90
β (°)	104.05(3)	100.38(3)
γ (°)	90	90
V (Å <sup>3</sup> )	1518.9(6)	2205.1(8)
Z	2	2
ρ calc (g.cm <sup>-3</sup> )	1.204	1.237
μ (MoKα) (mm <sup>-1</sup> )	0.072	0.071
F (000)	588	868
Crystal size (mm)	0.10 x 0.10 x 0.10	0.10 x 0.10 x 0.10
Temperature (K)	173(2)	173(2)
Radiation (Å)	0.71073	0.71073
Theta min-max (°)	3.2, 27.5	2.5, 27.8
Dataset (±h, ±k, ±l)	-12:12; -11:11; -23:23	-11:11; -22:22; -19:19
Final R indices [I>2.0 (I)]	R = 0.0450, wR <sub>2</sub> = 0.1123	R = 0.0437, wR <sub>2</sub> = 0.1169
R indices (all data)	R = 0.0557, wR <sub>2</sub> = 0.1199	R = 0.0487, wR <sub>2</sub> = 0.1214
Tot., uniq. data, R(int)	6645, 6636, 0.012	10417, 10417, 0.075
N <sub>ref</sub> , N <sub>par</sub>	6636, 444	10417, 635
S	1.04	1.03
Max. and Av. Shift/Error	0.00, 0.00	1.50, 0.00
Min. and Max. Resd. Electron Dens. (e/Å <sup>3</sup> )	-0.16, 0.28	-0.29, 0.24

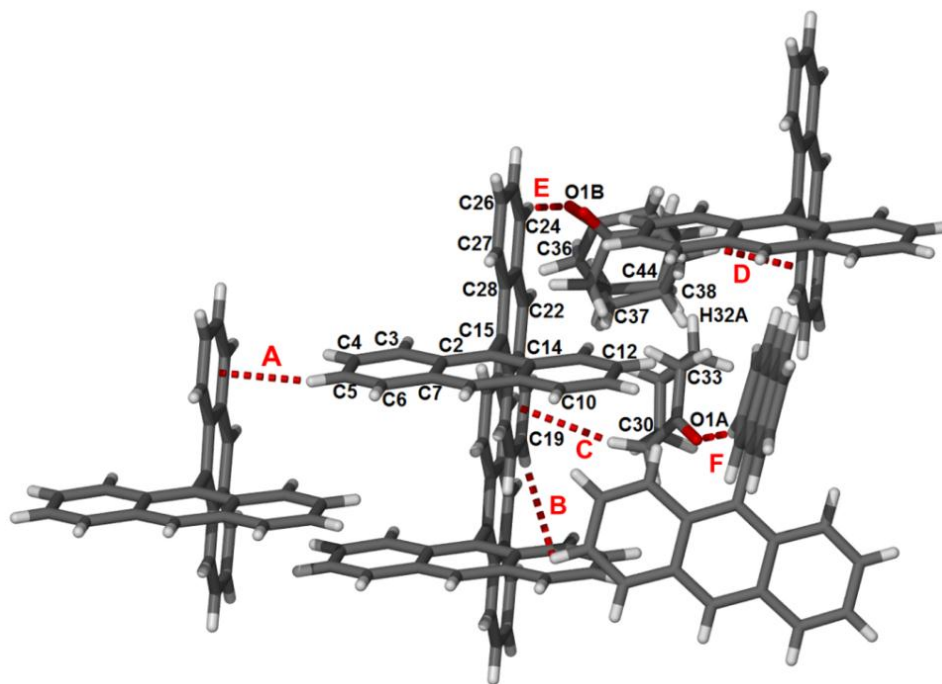


Figure 4.3 Intermolecular interactions in  $H1 \cdot 2CYHA$ .

Table 4.3 Intermolecular interactions in  $H1 \cdot 2CYHA$

	D-H...A	d(D-H) (Å)	d(D-H...A) (Å)	(H...A) (Å)	$\angle$ DHA ( $^\circ$ )
A	C5-H5... $c_g$ (C23-C28)	0.95	3.60	2.75	149
B	C19-H19... $c_g$ (C9-C14)	0.95	3.75	2.95	142
C	C29-H29A... $c_g$ (C16-C21)	0.95	3.83	2.90	157
D	C39-H39A... $c_g$ (C16-C21) <sup>a</sup>	0.99	3.67	2.89	138
E	C24-H24...O1B	0.95	3.47	2.57	158
F	C26-H26...O1 <sup>b</sup>	0.95	3.30	2.40	157

**Symmetry operator:** <sup>a</sup>1+x,y,z <sup>b</sup>1/2+x,z-y,1/2+z

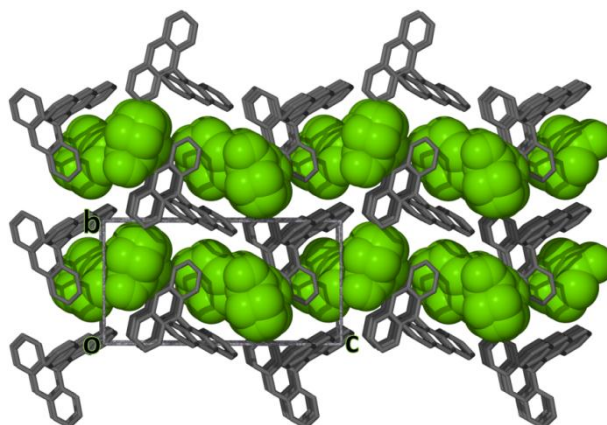
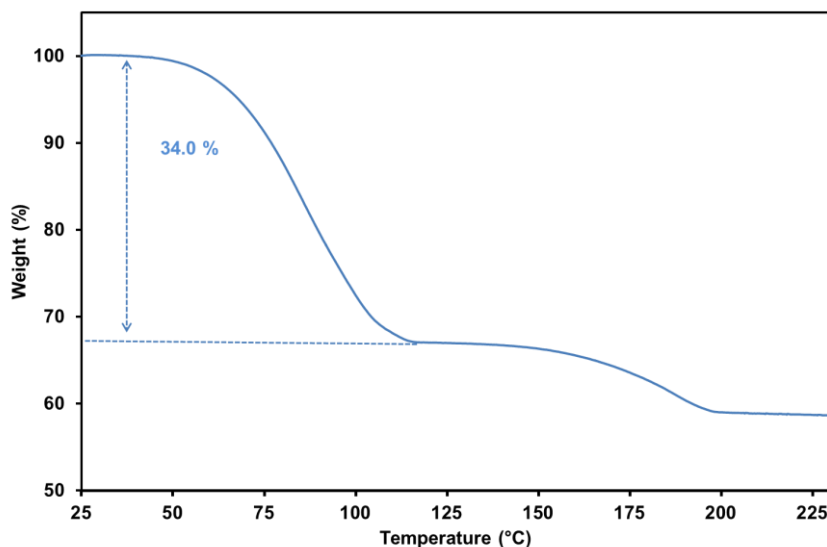


Figure 4.4 Packing diagram of  $H1 \cdot 2CYHA$  viewed along [100]. Guests are presented with space filling and coloured green.

#### 4.4.2 Thermal analysis of H1•2CHYA

The TG trace for **H1•2CYHA** is displayed in **Figure 4.5**. The TG graph shows a 34% mass loss within the temperature range of 69°C to 104°C due to volatile guest loss. The mass loss correlates to a 1:2 host-guest ratio of **H1•2CYHA**.

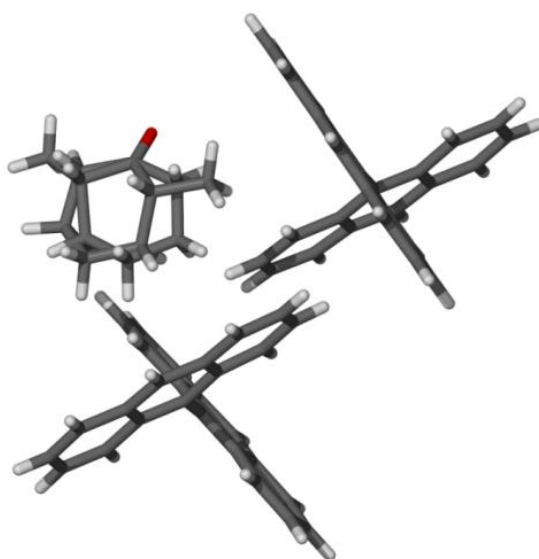


**Figure 4.5** TG trace for **H1•2CYHA**

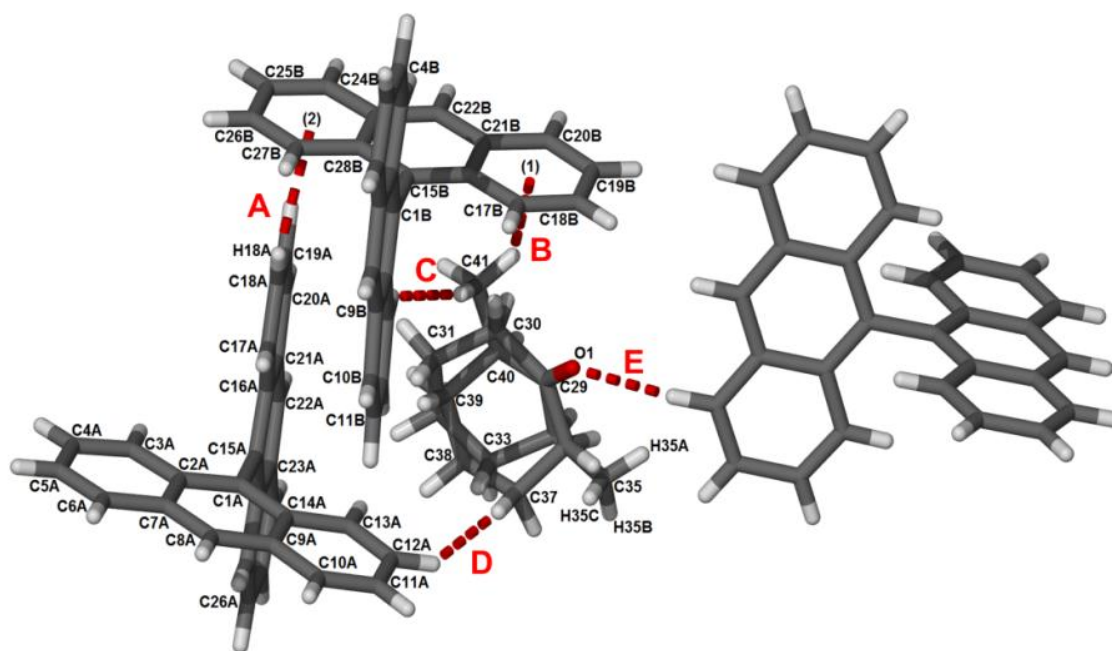
#### 4.4.3 Crystal structure analysis of H1•0.5(2-MCYHA)

A suitable crystal of **H1•0.5(2-MCYHA)** with the dimensions 0.10 x 0.10 x 0.10 mm was subjected to X-ray analysis. The structure crystallises in the monoclinic  $P2_1$  (No.4) space group with the molecular formula of  $C_{63}H_{48}O$ . The asymmetric unit contains two **H1** host compounds and one disordered **2-MCYHA** guest molecule. The nature of the disorder is positional, whereby both molecules have a 50% site occupancy factor<sup>2</sup> (**Figure 4.6**). The structure refined to  $R = 0.0437$  and  $wR_2 = 0.1214$ . The crystallographic data is summarised in **Table 4.2**. The **H1•0.5(2-MCHYA)** structure is stabilised by C-H... $\pi$  interactions, H...H contacts and C-H...O contacts. The C-H... $\pi$  interactions (A) in the perpendicular y-shaped position holds two adjacent host compounds together (C18A-H18A... $c_g$ (C9A-C14A), 3.21 Å). The C-H... $\pi$  interactions (B) occur between a guest molecule (C41-H41C) and a neighbouring centroid ( $c_g$ (C16B-C21B), 3.03 Å) of a host in the perpendicular t-shaped orientation. The H...H contact (C) arises from the close contact between the methyl group of a guest and hydrogen of a host (C41-H41A...H13B-C13B, 2.37 Å).

The H...H contact (D) also occurs between the guest and host (C37A-H37A...H12A-C21A) with the distance of 2.30 Å. The C-H...O contact (E) occurs between the guest and host with the distance of 2.59 Å. The intermolecular interactions are displayed in **Figure 4.7** and their parameters are summarised in **Table 4.4**. The C-H... $\pi$  interactions (B) hold the host framework together and the guest molecules are positioned in channels running along the crystallographic direction [100] as illustrated in **Figure 4.8**.



**Figure 4.6** Asymmetric unit of **H1·0.5(2-MCYHA)**. Guest molecule is disordered.

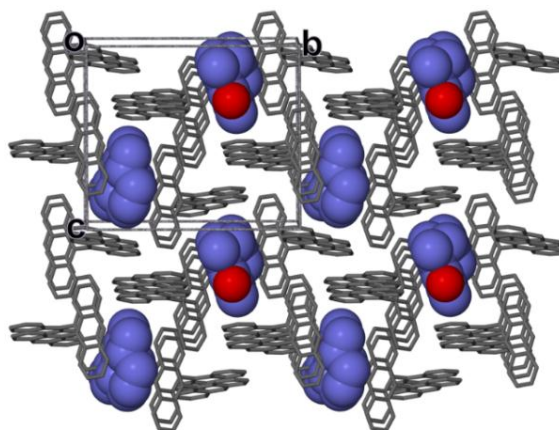


**Figure 4.7** Intermolecular interactions in **H1·0.5(2-MCYHA)**.

**Table 4.4** Intermolecular interactions in **H1•0.5(2-MCYHA)**

	D-H...A	d(D-H) (Å)	d(D-H...A) (Å)	(H...A) (Å)	∠ DHA (°)
<b>A</b>	C18A-H18A...c <sub>g</sub> (C9A-C14A)	0.95	3.83	3.21	125
<b>B</b>	C41-H41C...c <sub>g</sub> (C16B-C21B)	0.98	3.63	3.03	121
<b>C</b>	C41-H41A...H13B-C13B <sup>a</sup>	0.98	3.31	2.37	160
<b>D</b>	C37A-H37A...H12A-C12A	0.99	3.26	2.30	161
<b>E</b>	C6B-H6B...O1 <sup>a</sup>	0.95	3.41	2.59	145

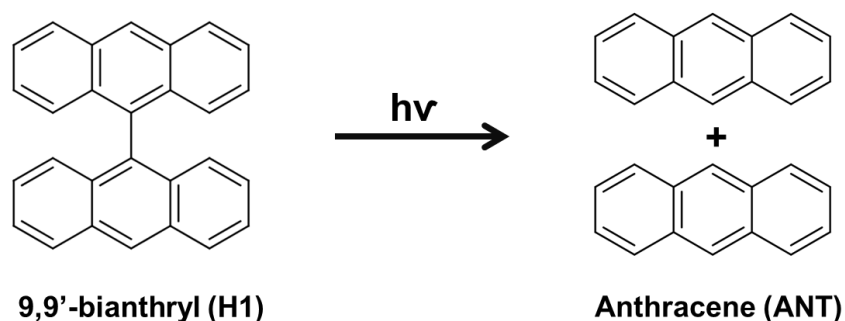
**Symmetry operator:** <sup>a</sup>2-x,y-1/2,1-z

**Figure 4.8** Packing diagram of **H1•0.5(2-MCYHA)** viewed along [100]. Guests are presented with space filling and coloured red and blue.

#### 4.4.4 Decomposition of H1 host compound

##### 4.4.4.1 Photo-decomposition of H1 host

The host compound **H1** is light sensitive and unfortunately this was learnt only during experimentation when the **H1** host transformed into anthracene (**ANT**) (**Figure 4.9**). The competition experiments with the **MCYHA** isomers were compromised and the X-ray diffraction data collection for **H1** and the equimolar mixture of **2-MCYHA/3-MCYHA** gave a structure with **H1** and **ANT** with a 1:1 host-guest ratio.

**Figure 4.9** Decomposition of **H1** host.



#### 4.4.4.2 Crystal structure analysis of H1•ANT

A suitable crystal with the dimensions of 0.10 x 0.21 x 0.38 mm was chosen for single crystal X-ray diffraction. The structure was solved in the monoclinic space group  $P2_1/n$  (No.14). The structure successfully refined to  $R = 0.0484$  and  $wR_2 = 0.1465$ . The asymmetric unit consist of one molecule of **H1** and one molecule of **ANT** with the molecular formula  $C_{42}H_{28}$  ( $Z=4$ ). The crystallographic parameters are summarised in **Table 4.5**. The structure is stabilised by several C-H $\cdots\pi$  interactions in the perpendicular y-shaped position and H $\cdots$ H contacts. The C-H $\cdots\pi$  interaction, A (C5-H5 $\cdots$ c<sub>g</sub>(C9-C14), 3.20 Å) occurs between two neighbouring **H1** compounds. The C-H $\cdots\pi$  interactions, B (C29-H29 $\cdots$ c<sub>g</sub>(C2-C7), 2.98 Å) and C (C37-H37 $\cdots$ c<sub>g</sub>(C23-C28), 3.14 Å) occurs between the **ANT** and the host molecules in close proximity. The H $\cdots$ H interaction (D, C38-H38 $\cdots$ H11-C11, 2.26 Å) also arises from a close contact between an **ANT** molecule and a **H1**. Interactions are presented in **Figure 4.10** and summarised in **Table 4.6**. The packing diagram of the **H1•ANT** is presented in **Figure 4.11**, where the host compounds are held together by C-H $\cdots\pi$  interactions (A) in a chain wave-like framework. The **ANT** molecules are positioned in channels along the crystallographic *a*-axis within the host framework.



Table 4.5 Crystal data for H1•ANT

Compounds	H1•ANT
Molecular formula	C <sub>42</sub> H <sub>28</sub>
Formula weight (g. mol <sup>-1</sup> )	532.64
Crystal system	monoclinic
Space group	<i>P</i> 2 <sub>1</sub> / <i>n</i> (No. 14)
a (Å)	11.5286(10)
b (Å)	19.5609(18)
c (Å)	12.7234(11)
α (°)	90
β (°)	102.846(2)
γ (°)	90
V (Å <sup>3</sup> )	2797.4(4)
Z	4
ρ calc (g.cm <sup>-3</sup> )	1.265
μ (MoKα) (mm <sup>-1</sup> )	0.072
F (000)	1120
Crystal size (mm)	0.10 x 0.21 x 0.38
Temperature (K)	173(2)
Radiation (Å)	0.71073
Theta min-max (°)	1.9, 28.3
Dataset (±h, ±k, ±l)	-15:8; -26:25; -16:16
Final R indices [I>2.0 (I)]	R = 0.0484, wR <sub>2</sub> = 0.1142
R indices (all data)	R = 0.1124, wR <sub>2</sub> = 0.1465
Tot., uniq. data, R(int)	21180, 6945, 0.038
N <sub>ref</sub> , N <sub>par</sub>	6945, 380
S	0.99
Max. and Av. Shift/Error	0.00, 0.00
Min. and Max. Resd. Electron Dens. (e/Å <sup>3</sup> )	-0.21, 0.29

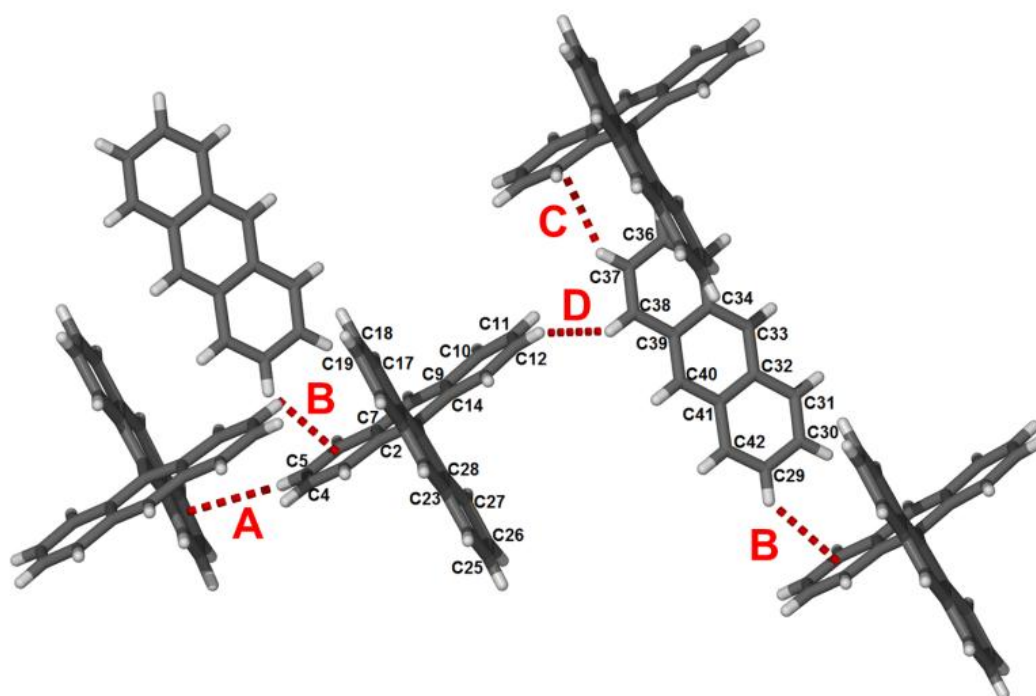


Figure 4.10 Intermolecular interactions in H1•ANT.

Table 4.6 Intermolecular interactions in H1•ANT

	D-H...A	d(D-H) (Å)	d(D-H...A) (Å)	(H...A) (Å)	∠ DHA (°)
A	C5-H5...c <sub>g</sub> (C9-C14)	0.95	3.91	3.20	133
B	C29-H29...c <sub>g</sub> (C2-C7) <sup>a</sup>	0.95	3.72	2.98	136
C	C37-H37...c <sub>g</sub> (C23-C28)	0.95	3.90	3.14	139
D	C38-H38...H11-C11	0.95	3.10	2.26	147
Symmetry operator: <sup>a</sup> x-1,y,z-1					

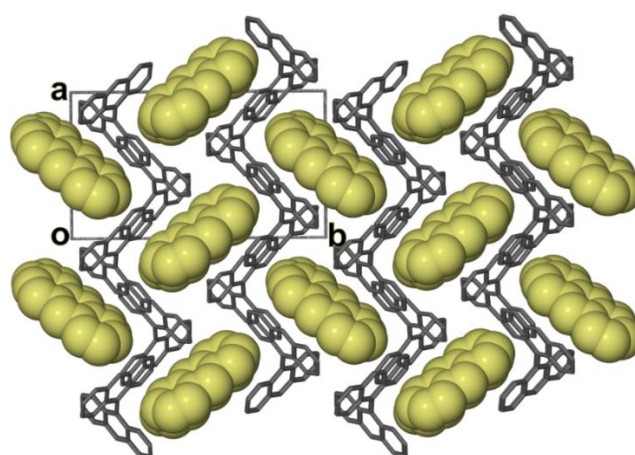


Figure 4.11 Packing diagram of H1•ANT viewed along [100]. ANT molecules are presented with space filling and coloured yellow.

#### 4.4.4.3 Thermal analysis of H1•ANT

Hot-stage microscopy (HSM) was carried out on the pure host **H1**. The **H1** compound melted between the temperature range of 281-301°C. This temperature range corresponds to the previous DSC results obtained from **H1** inclusion compounds. The traces gave a sharp peak at  $\pm 300^\circ\text{C}$  (endotherm) related to the melting point of **H1**. TG and DSC analysis was conducted on the **H1** comprising the pure host **H1** and **ANT** (Figure 4.12). The TG curve shows a mass loss of 12.9% within the temperature range 181°C and 207°C before decomposition of **H1**, associated to the release of **ANT** (melting point of **ANT** is 216°C) with a 1:0.3 **H1**-**ANT** ratio. The corresponding DSC curve has two prominent endotherms; the first relating to the melting point of **ANT** at  $T_{\text{on}} = 189.0^\circ\text{C}$  and  $T_{\text{peak}} = 234.0^\circ\text{C}$  followed by the **H1** at  $T_{\text{on}} = 283.9^\circ\text{C}$  and  $T_{\text{peak}} = 298.7^\circ\text{C}$ .

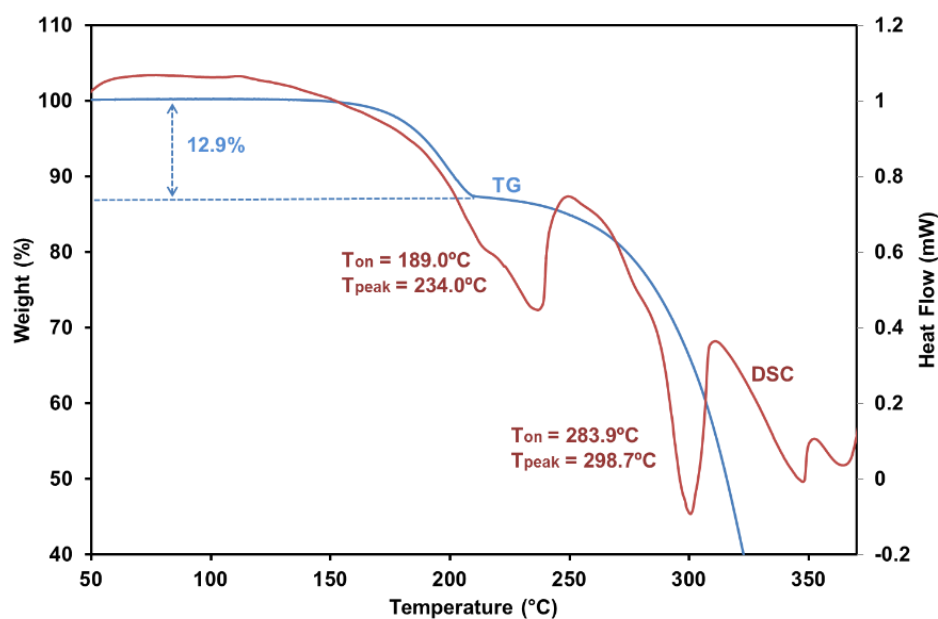
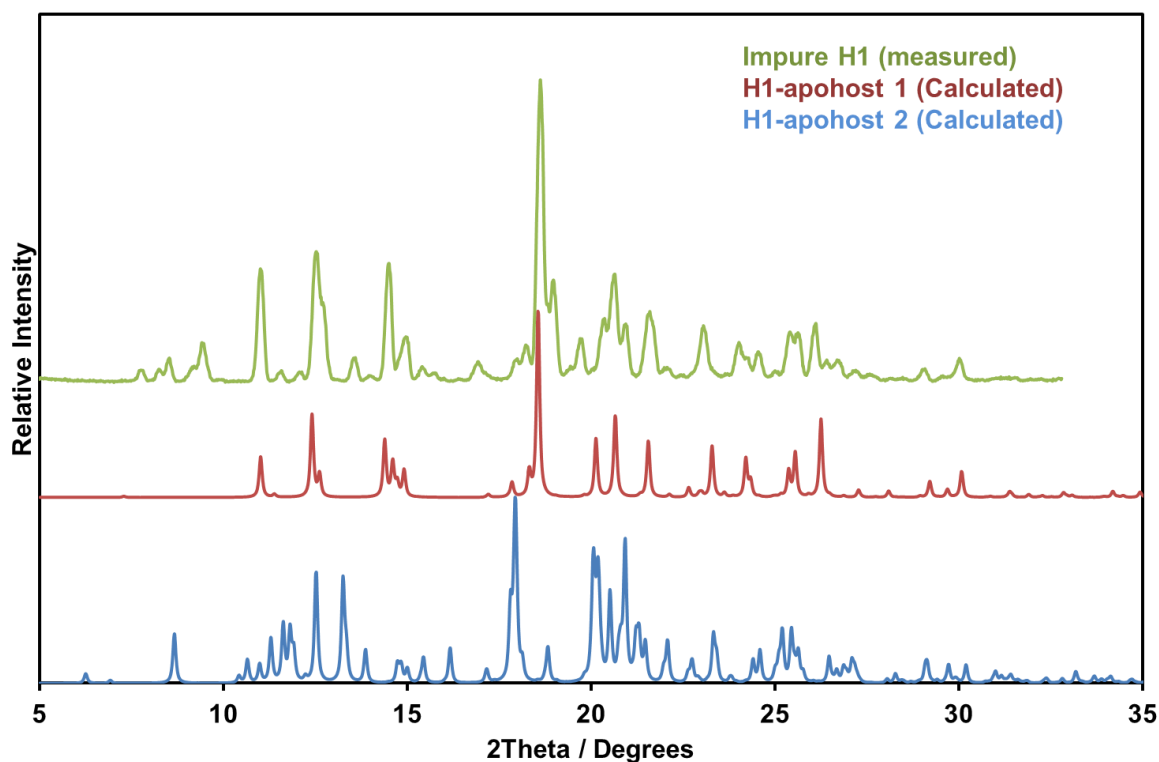


Figure 4.12 TG and DSC traces for **H1** (endo down).

#### 4.4.4.4 Powder X-ray analysis of H1•ANT

Powder X-ray analysis was conducted on the impure **H1** compound (**Figure 4.13**) and compared to the calculated pattern of the existing **H1** structures in the CSD<sup>3</sup>. There are two polymorphs of the apohost **H1**. The measured pattern of **H1** (green) is significantly different from the calculated **H1** patterns suggesting that it is a different compound. It was concluded that the remaining **H1** host is impure. No further experimentation was carried out with the **H1** host compound due to the lack of sufficient material.



**Figure 4.13** PXRD patterns: impure **H1** (measured-green), **H1** apohost 1 (calculated-red) and **H1** apohost 2 (calculated-blue).

## 4.5 Inclusion compound of H3 with CYHA

### 4.5.1 Crystal structure analysis of H3•CYHA

A single crystal with the dimensions 0.07 x 0.09 x 0.18 mm was sent for data collection. The crystal structure was solved in the monoclinic  $P2_1/n$  space group (No.14) and its crystallographic asymmetric unit contains one host and one guest molecule with the molecular formula of  $C_{45}H_{30}O_3$  ( $Z=4$ ). The structure refined to  $R = 0.0545$  and  $wR_2 = 0.1435$ . The data collection and refinement details are summarised in **Table 4.7**. The **H3•CYHA** structure is held together by C-H... $\pi$  interactions and C-H...O close contacts. The C-H... $\pi$  interaction (A) takes place between the C14-H18A of a host to the centroid of another host  $c_g(C16-C21)$  with the interatomic distance of 2.61 Å (perpendicular t-shaped orientation). The C-H... $\pi$  interaction (B) arises from the interaction between a guest and a neighbouring host in the perpendicular t-shaped geometry (C35-H35B... $c_g(C10-C15)$ , 2.77 Å). The C-H...O contact (C) occurs between a host and guest via C41-H41A...O3 with the distance 2.56 Å. The C-H...O contacts D, (C37A-H37A...O1, 2.56 Å) and E, (C27A-H27A...O1, 2.65 Å) arises from close contact of neighbouring hosts (see **Figure 4.14** and **Table 4.8**). The **H3•CYHA** structure **H3** compounds are attached to each other in layers by C-H...O close contacts (**Figure 4.15**). The **CYHA** guests are situated in cavities within the surface of each layer (**Figure 4.16**).

Table 4.7 Crystal data for H3•CYHA

Compounds	H3•CYHA
Molecular formula	C <sub>45</sub> H <sub>30</sub> O <sub>3</sub>
Formula weight (g. mol <sup>-1</sup> )	498.59
Crystal system	monoclinic
Space group	<i>P</i> 2 <sub>1</sub> / <i>n</i> (No.14)
a (Å)	10.222(2)
b (Å)	17.364(4)
c (Å)	15.836(3)
α (°)	90
β (°)	104.65(3)
γ (°)	90
V (Å <sup>3</sup> )	2719.4(10)
Z	4
ρ calc (g.cm <sup>-3</sup> )	1.218
μ (MoKα) (mm <sup>-1</sup> )	0.076
F (000)	1056
Crystal size (mm)	0.07 x 0.09 x 0.18
Temperature (K)	173(2)
Radiation (Å)	0.71073
Theta min-max (°)	1.8, 27.9
Dataset (±h, ±k, ±l)	-13:13; -22:22; -20:20
Final R indices [I>2.0 (I)]	R = 0.0545, wR <sub>2</sub> = 0.1203
R indices (all data)	R = 0.1065, wR <sub>2</sub> = 0.1435
Tot., uniq. data, R(int)	30410, 6504, 0.076
N <sub>ref</sub> , N <sub>par</sub>	6504, 344
S	1.02
Max. and Av. Shift/Error	0.00, 0.00
Min. and Max. Resd. Electron Dens. (e/Å <sup>3</sup> )	-0.20, 0.38

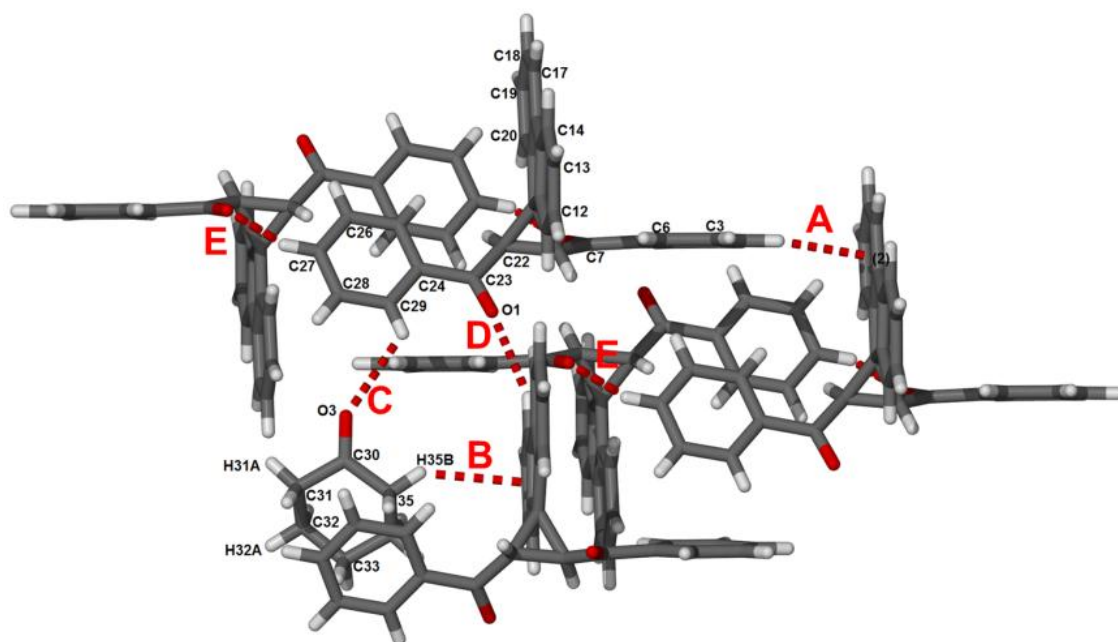


Figure 4.14 Intermolecular interactions in H1•ANT.

Table 4.8 Intermolecular interactions in H3•CYHA

	D-H...A	d(D-H) (Å)	d(D-H...A) (Å)	(H...A) (Å)	∠ DHA (°)
A	C14-H18A...c <sub>q</sub> (C16-C21)	0.95	3.53	2.61	163
B	C35-H35B...c <sub>q</sub> (C10-C15) <sup>a</sup>	0.99	3.84	3.03	140
C	C41-H41A...O3	0.95	3.28	2.77	114
D	C37A-H37A...O1 <sup>b</sup>	0.95	3.43	2.56	152
E	C27A-H27A...O1 <sup>b</sup>	0.95	3.28	2.65	124

Symmetry operator: <sup>a</sup>x-1/2, 1/2-y, z-1/2 <sup>b</sup>2-x, y, 2-z

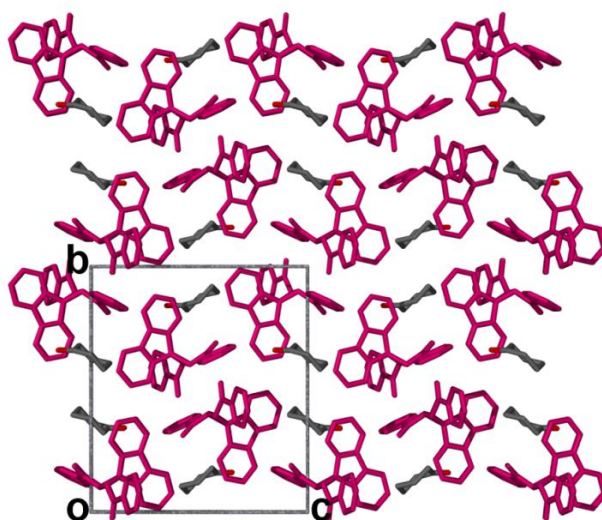
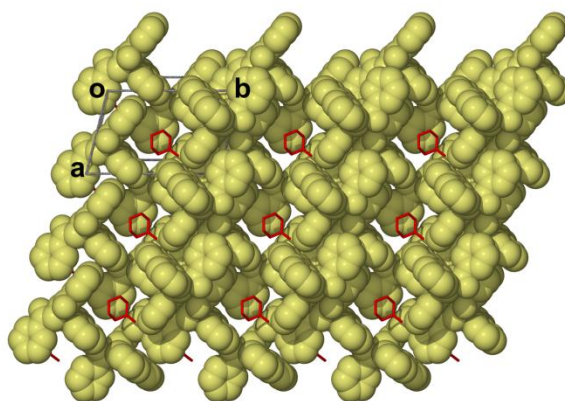


Figure 4.15 Packing diagram of H3•CYHA viewed along [100]. Host are coloured pink and guests are coloured grey.





**Figure 4.16** Packing diagram of **H3•CYHA** viewed along [010]. Host are coloured yellow and guests are coloured red.

### 4.5.2 Thermal analysis of H3•CYHA

The TG curve for **H3•CYHA** is presented in **Figure 4.17**. The **H3•CYHA** inclusion compound loses its guest in a two-step process in the temperature range of 98–200°C. In the first step there is a 6.30% mass loss, while the second step is not well-defined on the TG trace. There is continuous decrease in mass until the host starts to decompose at  $\pm 200^\circ\text{C}$  (**H3** melting point is  $204^\circ\text{C}$ ). Due to this reason it was difficult to get an exact percentage loss of the guest. The total mass loss of the guest is approximately 18%. Several attempts were made to get better experimental values but were unsuccessful. The crystallisation yielded a few reasonably good crystals on the side of the vial, while the bulk of the crystals in the bottom part of the vial were clumps of star-like aggregates. Thus it may be concluded that the single crystal structure may not be representative of the bulk material.

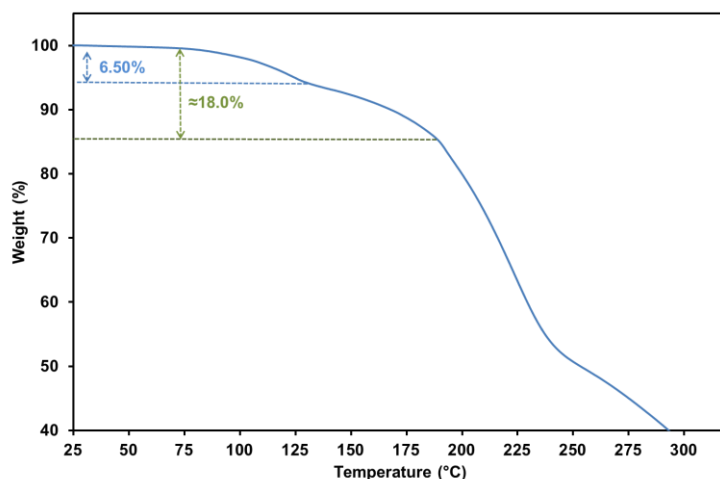


**Figure 4.17** TG trace for **H3•CYHA**.



## References

- 
- <sup>1</sup> Aucejo, A., Burguet, M.C., Muiioz, R. & Vazquez, M.I. *J. Chem. Eng. Data.*, 1993, 38: 379.
  - <sup>2</sup> Pang, L., Brisse, F. & Lucken, E.A.C. *J. Chem.*, 1995, 73: 351. Canada.
  - <sup>3</sup> Groom, C.R. & Allen, F.H. *Angew. Chem. Int. Ed.*, 2014, 53: 662.

## Chapter 5: Separation of xylenes

---

### 5.1 Introduction

Xylenes occur in the three isomeric forms: *ortho*-xylene (**ox**), *meta*-xylene (**mx**) and *para*-xylene (**px**) and are obtained by the naptha reforming catalytic process.<sup>1,2</sup> Due to the similarities in their physicochemical properties, it is extremely difficult to separate them into their pure forms. Their isomers are important raw materials for the manufacture of a variety of products. Their relevant industrial application has led to the study and development of numerous separation techniques. Host-guest chemistry has recently been successful in the separation of xylenes using metal-organic frameworks.<sup>3</sup> In the present study host-guest chemistry is once again employed as a tool of separation and was proved successful.

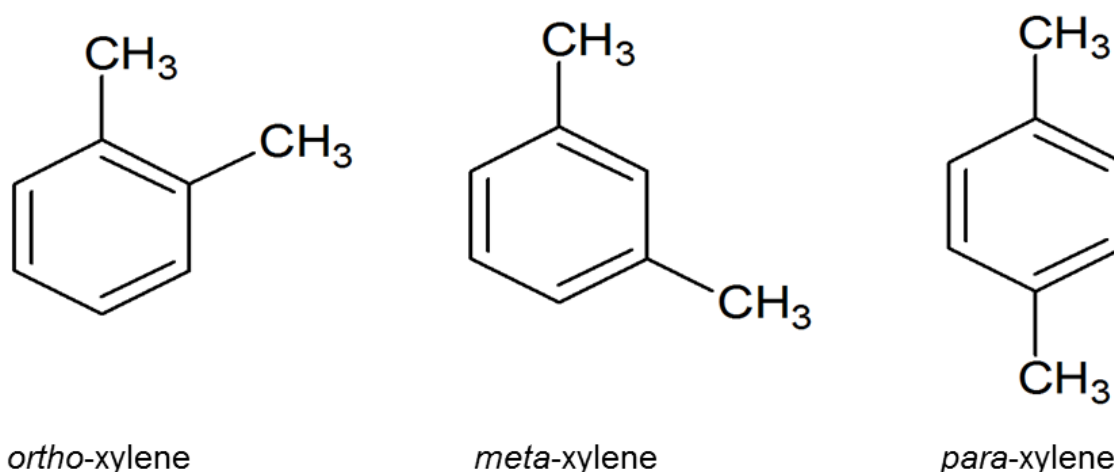


**Figure 5.1** Schematic diagram of xylene isomers.

The results of the enclathration experiments of the three different host compounds, 9,9'-bianthryl (**H1**), 9,9'-spirobifluorene (**H2**) and *trans*-2,3-dibenzoylspro(cyclopropane-1,9'-fluorene) (**H3**) with the xylene isomers will be discussed in terms of their crystal structures, thermal analysis, <sup>1</sup>H-NMR spectroscopy, Hirshfeld surface analysis and lattice energies.

## 5.2 Inclusion complex preparation

The preparation procedure of the complexes entailed dissolving about 60-70 mg of each individual host (**H1**, **H2** or **H3**) into the pure xylene isomer (typically 2 ml) the binary equimolar mixture of two isomers and tertiary equimolar mixture of all three isomers. From all crystallisation experiments chunky crystalline products were obtained after a few days of slow evaporation of the solvent.

## 5.3 Inclusion complex analysis

The resultant crystalline products from each mixture were subjected to single crystal X-ray diffraction,  $^1\text{H-NMR}$  spectroscopy, thermal gravimetry (TG) and differential scanning calorimetry (DSC). The enclathration results are summarised in **Table 5.1**, which gives the resultant crystals obtained from the pure xylenes as well as the competition experiments and their related thermoanalytical results. It may be concluded that the host compounds **H1**, **H2** and **H3** can efficiently discriminate between the isomers of xylene by forming inclusion compounds. **H1** enclathrates both **ox** and **px**, preferring **ox** over **px**, and does not enclathrate **mx**. **H2** and **H3** only enclathrate **px** and **ox** respectively so it is safe to assume **H2** is selective towards **px** and **H3** is selective towards **ox**. The TG results obtained are in good agreement with the calculated values of the stoichiometry derived from the determined crystal structures. The results of the competition experiments were analysed qualitatively by  $^1\text{H-NMR}$  that confirmed which particular xylene isomer had been enclathrated. This was followed by thermal gravimetry which yielded the host: guest ratio. The latter was confirmed by successful single crystal structure analysis.

**Table 5.1** Enclathration results of **H1**, **H2** and **H3** with xylene isomers

Host	Starting solvent	Resulting Crystal	TG % mass loss found (calc)
<b>H1</b>	ox	H1•0.5ox	13.1 (13.0)
	mx	H1 apohost	-
	px	H1•0.5px	12.6 (13.0)
<b>Equimolar</b>	ox/mx	H1•0.5ox	12.5 (13.0)
	ox/px	H1•0.5ox	12.8 (13.0)
	mx/px	H1•0.5px	12.8 (13.0)
	ox/mx/px	H1•0.5ox	12.7 (13.0)
<b>H2</b>	ox	H2 apohost	-
	mx	H2 apohost	-
	px	H2•0.5px	14.9 (14.4)
<b>Equimolar</b>	ox/mx	H2 apohost	-
	ox/px	H2•0.5px	13.6 (14.4)
	mx/px	H2•0.5px	12.8 (14.4)
	ox/mx/px	H2•0.5px	14.0(14.4)
<b>H3</b>	ox	H3•ox	21.0 (20.9)
	mx	H3 apohost	-
	px	H3 apohost	-
<b>Equimolar</b>	ox/mx	H3•ox	21.2 (20.9)
	ox/px	H3•ox	20.8 (20.9)
	mx/px	H3 apohost	-
	ox/mx/px	H3•ox	20.9 (20.9)

## 5.4 <sup>1</sup>H-NMR of H1, H2 and H3 inclusion compounds

The <sup>1</sup>H-NMR spectroscopy was employed in a qualitative manner to identify the guest captured in the crystals obtained from the competition experiments. The procedure was as follows:

1. The <sup>1</sup>H-NMR spectrum of host compounds (**H1**, **H2** and **H3**) was recorded in deuterated chloroform (CDCl<sub>3</sub>) individually.
2. The <sup>1</sup>H-NMR spectrum of each pure xylene isomer (**ox**, **mx** and **px**) in CDCl<sub>3</sub> was recorded and the differences were noted.
3. The <sup>1</sup>H-NMR spectra of crystals obtained from the combination of each host compound with the tertiary equimolar mixture of all three isomers was recorded and comparisons with the <sup>1</sup>H NMR spectra of the pure compounds were made.

**Table 5.2** gives a summary of the spectra of the pure xylene isomers. The **ox** and **px** spectra (**Figures 5.2 and 5.3**) give two non-overlapping sets of peaks. The first singlet peak due to the protons of the two methyl groups on the structures of the isomers and the second set of peaks due to the protons on the aromatic ring of the isomers. Comparisons of the spectral data for the **ox** and **px** show a significant difference in the chemical shifts between the protons on the methyl groups and the protons on the aromatic rings of each isomer. The difference between the **ox** and **px** spectra allows qualitative determination of the inclusion compounds formed.

**Table 5.2**  $^1\text{H-NMR}$  data for **ox**, **mx** and **px**

<b>ox</b>		<b>mx</b>		<b>px</b>	
<b>Assignment</b>	<b><math>\delta</math> (ppm)</b>	<b>Assignment</b>	<b><math>\delta</math> (ppm)</b>	<b>Assignment</b>	<b><math>\delta</math> (ppm)</b>
(A) Methyl	2.42	(A) Methyl	2.52	(A) Methyl	2.58
(B) H	7.26	(B) H	7.18	(B) H	7.33
		(C) H	7.20		
		(D) H	7.35		

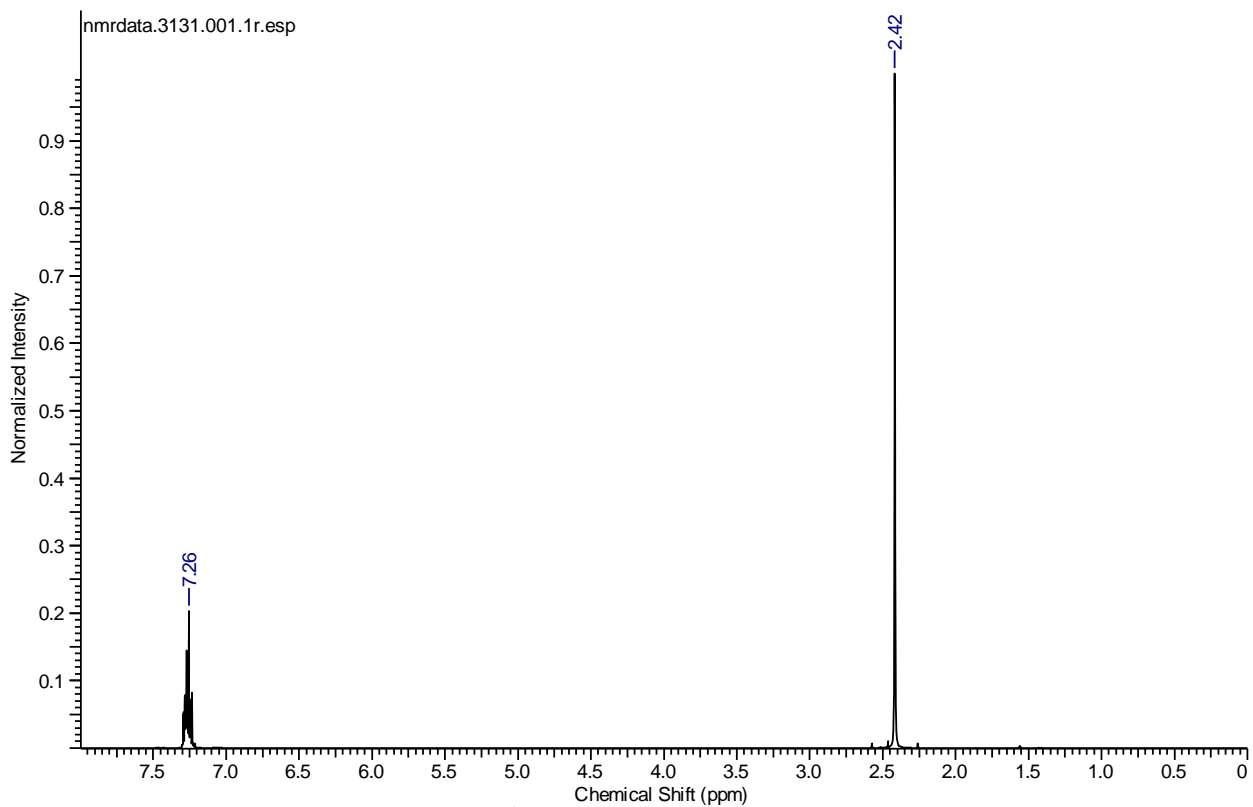


Figure 5.2  $^1\text{H-NMR}$  spectrum for **ox**.

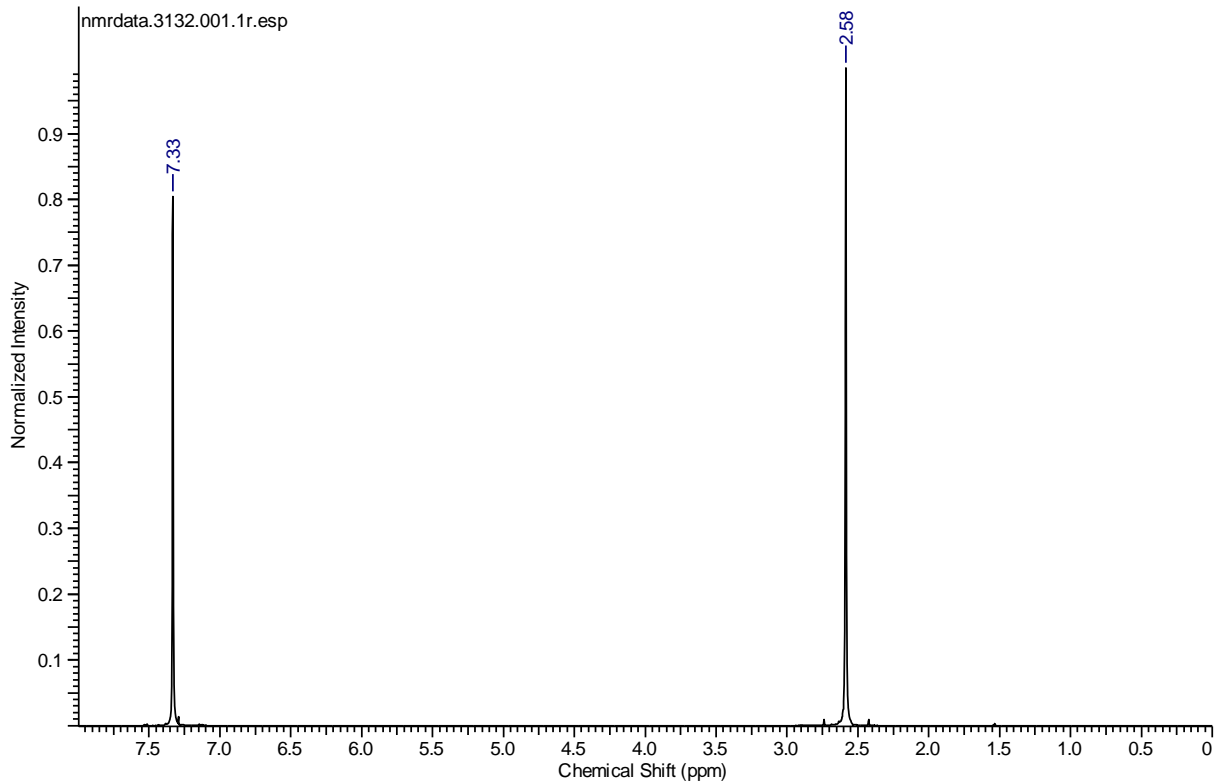
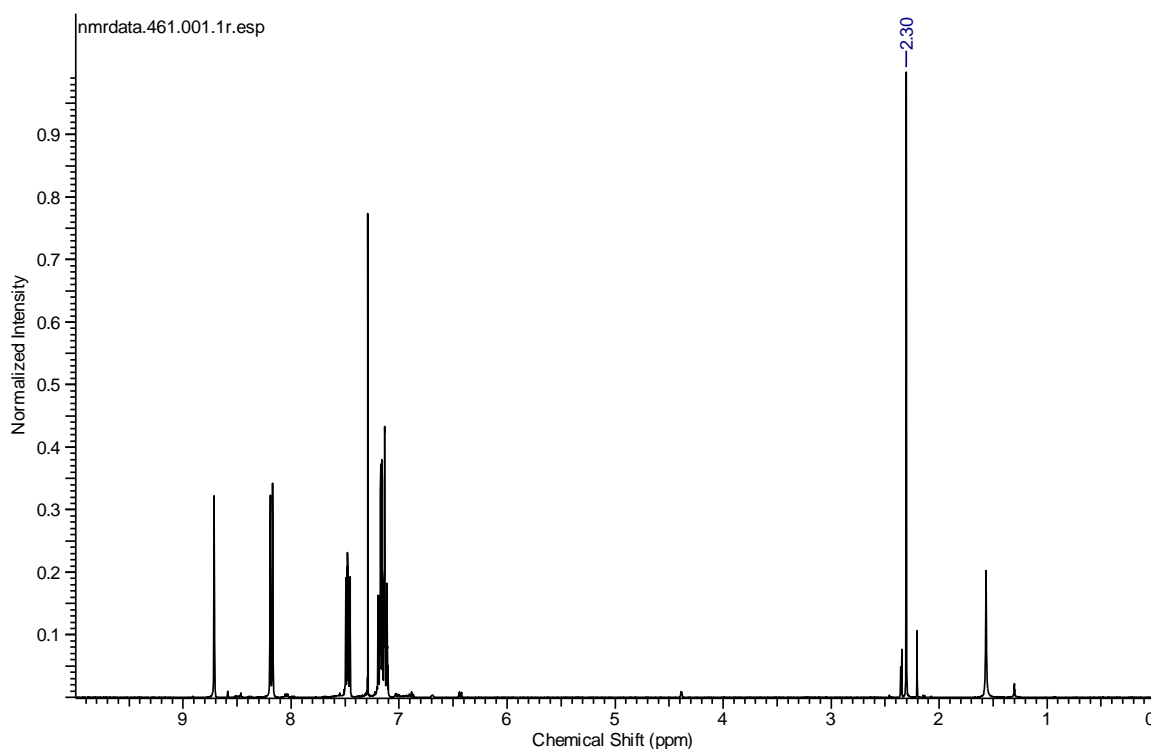


Figure 5.3  $^1\text{H-NMR}$  spectrum for **px**.

The  $^1\text{H-NMR}$  spectrum of **H1** with **ox/mx/px** is shown in **Figure 5.4**. It is reasonable to assign the singlet at 2.30 ppm to the methyl protons of the guest and the cluster of peaks in the range 6.75 ppm to 8.90 ppm to a combination of the host compound protons and the protons on the aromatic ring of the guest. The observed singlet at 2.30 ppm on the **H1** with **ox/mx/px** spectrum was used to determine which host to guest compound formed. The chemical shift of the peak is very close to that of the **ox** methyl protons' peak at 2.42 ppm, so we can conclude that the **H1** host compound forms the inclusion compound with the **ox** guest, agreeing with the results obtained from the single crystal experiments. The **H2** and **H3** with **ox/mx/px** gave similar  $^1\text{H-NMR}$  spectra and the same comparisons were made and the relevant spectral data summarized in **Table 5.3**. The results show **H2** forms an inclusion compound with **px** and **H3** forms an inclusion compound with **ox**, also agreeing with the single crystal results.



**Figure 5.4**  $^1\text{H-NMR}$  spectrum for **H1** with **ox/mx/px**.

**Table 5.3**  $^1\text{H-NMR}$  spectral data for **H1**, **H2** and **H3** with **ox/mx/px**

Host + solvent	Assignment	$\delta$ (ppm)
<b>H1</b> + <b>ox/mx/px</b>	Methyl groups	2.30 (ox 2.42)
<b>H2</b> + <b>ox/mx/px</b>	Methyl groups	2.50 (px 2.58)
<b>H3</b> + <b>ox/mx/px</b>	Methyl groups	2.31 (ox 2.42)

## 5.5 Inclusion compounds of H1 with ox and px

### 5.5.1 Thermal analysis of H1•0.5ox and H1•0.5px

The **H1•0.5ox** TG curve in **Figure 5.5** shows a mass loss in the range of 90°C to 148°C. The 13.1% mass loss is in good agreement with the 13.0% calculated value for a host to guest ratio of 1:0.5. The corresponding DSC curve has two endotherms; the first endotherm depicting a volatile guest loss with the  $T_{on} = 129.0^{\circ}\text{C}$  and  $T_{peak} = 136.8^{\circ}\text{C}$ . The second endotherm relating to the melt of host **H1** ( $T_{on} = 307.3^{\circ}\text{C}$  and  $T_{peak} = 310.5^{\circ}\text{C}$ ).

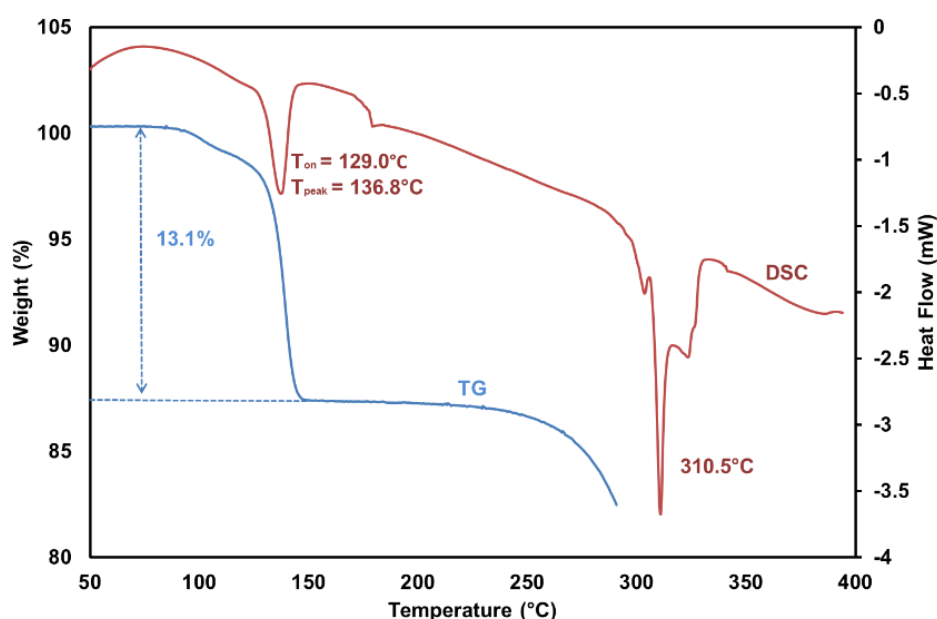


**Figure 5.5** TG and DSC traces for **H1•0.5ox** (endo down).

The TG curve of **H1•0.5px** in **Figure 5.6** shows the mass loss between 111°C and 143°C. The observed % mass loss corresponds to a host to guest ratio of 1:0.5 (found 12.6% and calculated 13.0%). The corresponding DSC shows the first endotherm, due to the loss of guest with the  $T_{on} = 128.4^{\circ}\text{C}$  and  $T_{peak} = 136.7^{\circ}\text{C}$ . The second endotherm is related to the melting of **H1** ( $T_{on} = 311.7^{\circ}\text{C}$  and  $T_{peak} = 313.5^{\circ}\text{C}$ ).



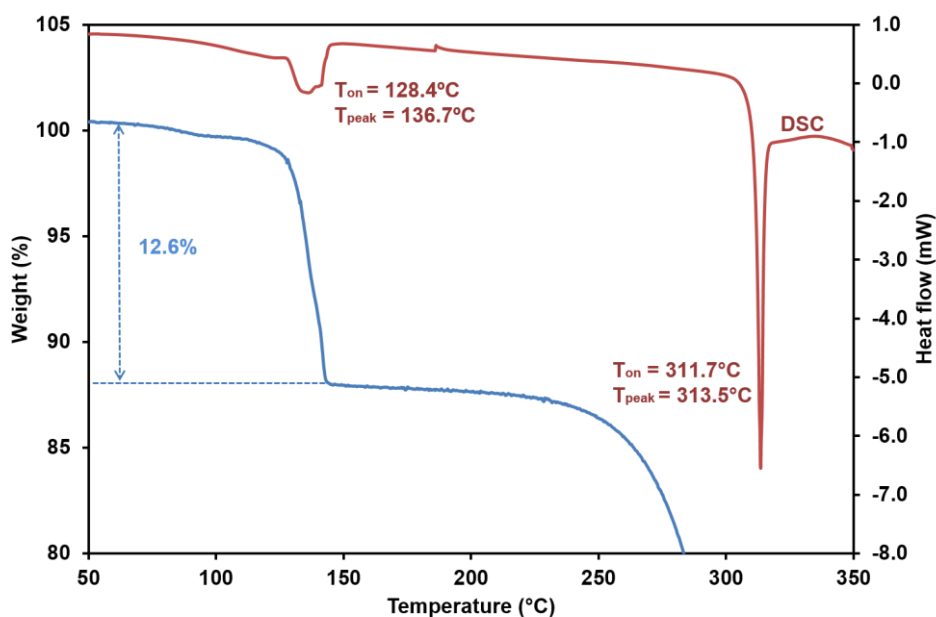


Figure 5.6 TG and DSC traces for **H1•0.5px** (endo down).

## 5.5.2 Crystal structure analysis of **H1•0.5ox** and **H1•0.5px**

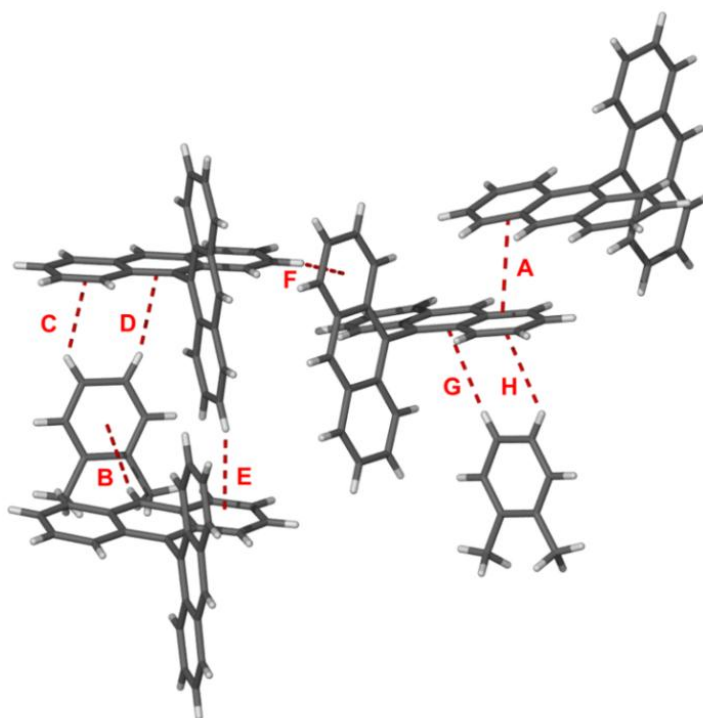
### 5.5.2.1 Structure analysis of **H1•0.5ox**

A crystal of suitable quality with the dimensions of  $0.11 \times 0.18 \times 0.3$  mm was selected for single crystal X-ray analysis. The structure was successfully solved in the triclinic  $P-1$  (No. 2) space group, with the formula  $C_{32}H_{23}$  and low residual values of  $R_1 = 0.0534$  and  $wR_2 = 0.1339$  were achieved after refinement. The crystallographic asymmetric unit contains four **H1** host molecules and two **ox** guest molecules. The crystallographic data and refinement details are summarised in **Table 5.4**.

**Table 5.4** Crystal data for **H1•0.5ox** and **H1•0.5px**

Compounds	H1•0.5ox	H1•0.5px
Molecular formula	C <sub>32</sub> H <sub>23</sub>	C <sub>32</sub> H <sub>23</sub>
Formula weight (g. mol <sup>-1</sup> )	407.50	407.50
Crystal system	triclinic	monoclinic
Space group	<i>P</i> -1 (No.2)	<i>P</i> <sub>2</sub> / <i>c</i> (No.14)
a (Å)	11.346(4)	14.154(3)
b (Å)	14.634(5)	9.1925(18)
c (Å)	27.361(9)	17.307(4)
α (°)	101.652(2)	90
β (°)	99.918(2)	100.42(3)
γ (°)	92.534(2)	90
V (Å <sup>3</sup> )	4368.2(3)	2214.7(8)
Z	4	4
ρ calc (g.cm <sup>-3</sup> )	1.239	1.222
μ (MoKα) (mm <sup>-1</sup> )	0.070	0.069
F (000)	1720	860
Crystal size (mm)	0.11 × 0.18 × 0.30	0.24 × 0.28 × 0.28
Temperature (K)	173(2)	173(2)
Radiation (Å)	0.71073	0.71073
Theta min-max (°)	1.4, 27.5	1.5, 27.9
Dataset (±h, ±k, ±l)	0:14; -18:18; -35:34	-16:18; -8:12; -21:22
Final R indices [I>2.0 (I)]	R <sub>1</sub> =0.0534, wR <sub>2</sub> =0.1212	R <sub>1</sub> =0.0497, wR <sub>2</sub> =0.1120
R indices (all data)	R <sub>1</sub> = 0.0921, wR <sub>2</sub> =0.1393	R <sub>1</sub> =0.0896, wR <sub>2</sub> =0.1304
Tot., uniq. data, R(int)	19956, 19956, 0.012	10258, 5254, 0.028
N <sub>ref</sub> , N <sub>par</sub>	19956, 1157	5254, 290
S	1.026	1.014
Max. and Av. Shift/Error	0.00, 0.00	0.00, 0.00
Min. and Max. Resd.	-0.26, 0.40	-0.20, 0.21
Electron Dens. (e/Å <sup>3</sup> )		

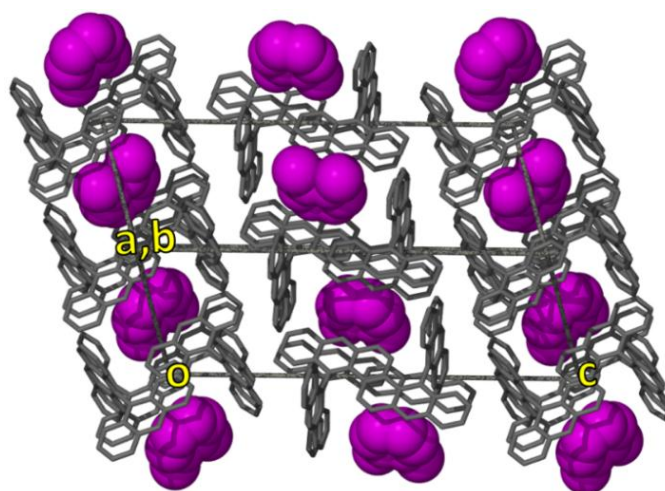
The **H1•0.5ox** inclusion compound is stabilised by the interactions between the  $\pi$ -systems shown in **Figure 5.7**. The  $\pi$ - $\pi$  interaction A ( $c_g(\text{C23E-C28E}) \cdots c_g(\text{C2F-C7F})$ ) falls in the parallel offset geometric orientation with a 3.92 Å interplanar separation between two hosts (**Table 5.5**). The perpendicular t-shaped  $\pi$ -stacking interaction B has the intermolecular distance 3.69 Å between the C22C-H22C of the host and the centroid of the guest  $c_g(\text{C1B-C6B})$ . The C-H $\cdots\pi$  interaction labelled C ( $\text{C3B-H3B} \cdots c_g(\text{C16D-C21D})$ , 3.03 Å) and D ( $\text{C4B-H4B} \cdots c_g(\text{C15D-C28D})$ , 3.12 Å) occurs between a host and a guest in the perpendicular y-shape geometry. The C-H $\cdots\pi$  interaction, E ( $\text{C5D-H5D} \cdots c_g(\text{C23C-C28C})$ , 2.95 Å) and F ( $\text{C5D-H5D} \cdots c_g(\text{C23C-C28C})$ , 3.09 Å) arise from close a contact between guest and host molecules in the perpendicular y-shape geometry. The C-H $\cdots\pi$  interactions between the host and the guest, G ( $\text{C3A-H3A} \cdots c_g(\text{C15E-C28E})$ , 3.35 Å) and H ( $\text{C4A-H4A} \cdots c_g(\text{C23E-C28E})$ , 3.23 Å) are positioned in the perpendicular y-shaped orientation. The packing diagram of **H1•0.5ox** is shown in **Figure 5.8**. The **ox** guest molecules are located in the channels running along [1-10].



**Figure 5.7**  $\pi$ -stacking in **H1•0.5ox**.

**Table 5.5** C-H... $\pi$  interactions in **H1•0.5ox** structure

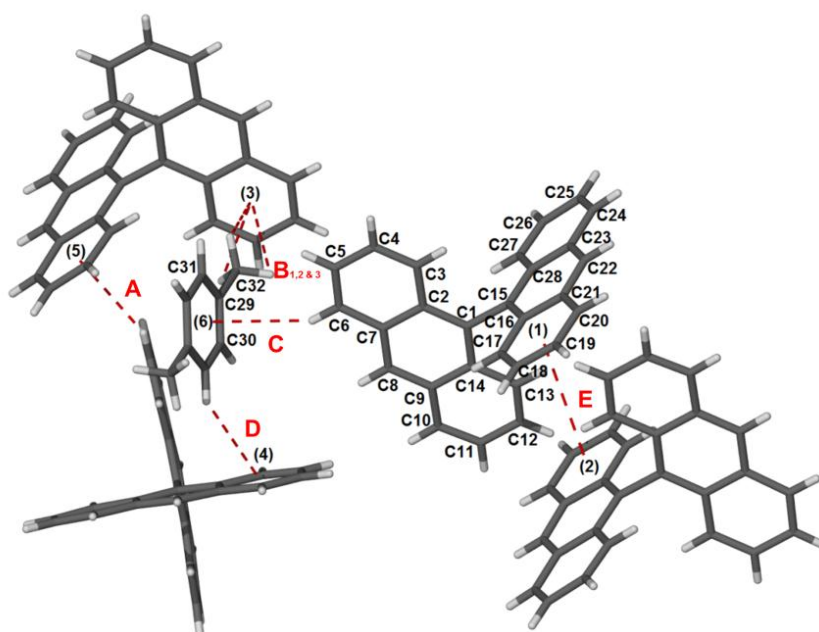
	D-H...A/ $c_g$ ... $c_g$	d(D-H) (Å)	d(D-H...A) (Å)	(H...A)/ ( $c_g$ ... $c_g$ ) (Å)	$\angle$ DHA/ $\angle$ $c_g$ ... $c_g$ (°)
<b>A</b>	$c_g$ (C23E-C28E)... $c_g$ (C2F-C7F)	-	-	3.92	180
<b>B</b>	C22C-H22C... $c_g$ (C1B-C6B)	0.95	4.62	3.69	165
<b>C</b>	C3B-H3B... $c_g$ (C16D-C21D)	0.95	3.81	3.03	140
<b>D</b>	C4B-H4B... $c_g$ (C15D-C28D)	0.95	4.00	3.12	155
<b>E</b>	C5D-H5D... $c_g$ (C23C-C28C)	0.95	3.77	2.95	145
<b>F</b>	C26D-H26D... $c_g$ (C2E-C7E)	0.95	3.75	3.09	128
<b>G</b>	C3A-H3A... $c_g$ (C15E-C28E)	0.95	4.26	3.35	161
<b>H</b>	C4A-H4A... $c_g$ (C23E-C28E)	0.95	3.94	3.23	132

**Figure 5.8** Packing diagram for **H1•0.5ox** viewed along [1-10]. Guests are presented with space filling and coloured purple.

### 5.5.2.2 Structure analysis of H1•0.5px

A suitable crystal with the dimensions  $0.24 \times 0.28 \times 0.28$  mm was selected for single crystal data collection and was found to crystallise in the monoclinic  $P2_1/c$  (No. 14) space group. The structure was successfully refined with the satisfactory  $R_1 = 0.0497$  and  $wR_2 = 0.1304$  values. **Table 5.4** lists the crystal data and refinement parameters. The asymmetric unit comprises one **H1** molecules and a half **px** molecule. The **H1•0.5px** structure, similarly to the **H1•0.5ox**, is characterised by several  $\pi$ -contacts shown in **Figure 5.9** (red dotted lines). The C-H... $\pi$  interactions A ( $C4-H4$ ... $c_g$ (C23-C28), 3.07 Å) occur between two host molecules positioned in the perpendicular y-shaped stacking arrangement (**Table 5.6**). There are three C-H... $\pi$  interactions placed in the perpendicular t-shaped geometry  $B_{1,2\&3}$ , which occur

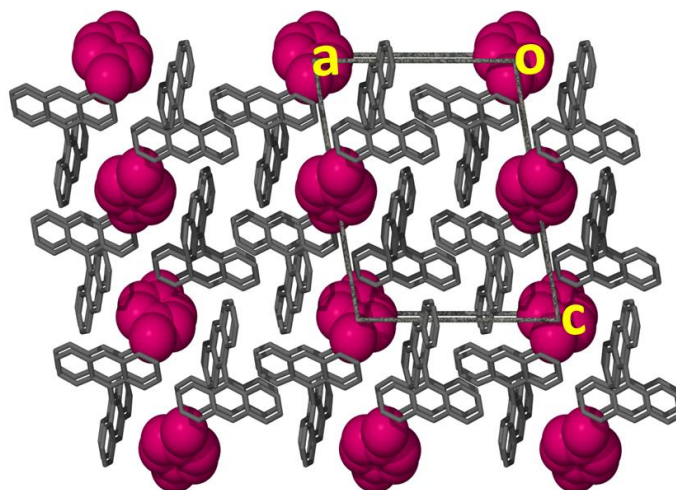
between the methyl group hydrogens (C32-H32A, C32-H32B and C32-H32C) on the guest to the centroid,  $c_g$ (C2-C7) of the neighbouring host molecule with the distances 3.57, 3.24 and 3.24 Å, respectively. The C-H $\cdots\pi$  interactions C (C6-H6 $\cdots c_g$ (C30-C31), 3.19 Å) and D (C31-H31 $\cdots c_g$ (C16-C21), 3.10 Å) take place between a host and guest molecule in the perpendicular y-shaped geometry. The  $\pi\cdots\pi$  interaction E ( $c_g$ (C16-C21) and  $c_g$ (C16-C21), 4.17 Å) is a very weak one and occurs between the two planar **H1** rings in parallel offset position. The packing diagram of **H1**•0.5px structure is represented in **Figure 5.10**, with the **px** guest molecules which are located in the channels running along [010] at the centre of inversion at Wyckoff position c.



**Figure 5.9**  $\pi$ -stacking in **H1**•0.5px.

**Table 5.6** C-H $\cdots\pi$  interactions in **H1**•0.5px structure

	D-H $\cdots$ A/ $c_g\cdots c_g$	d(D-H) (Å)	d(D-H $\cdots$ A) (Å)	(H $\cdots$ A)/ ( $c_g\cdots c_g$ ) (Å)	$\angle$ DHA/ $\angle$ $c_g\cdots c_g$ ( $^\circ$ )
<b>A</b>	C4-H4 $\cdots c_g$ (C23-C28)	0.95	3.79	3.07	133
<b>B<sub>1</sub></b>	C32-H32A $\cdots c_g$ (C2-C7)	0.98	3.54	3.57	81
<b>B<sub>2</sub></b>	C32-H32B $\cdots c_g$ (C2-C7)	0.98	3.54	3.24	100
<b>B<sub>3</sub></b>	C32-H32C $\cdots c_g$ (C2-C7)	0.98	3.54	3.24	100
<b>C</b>	C6-H6 $\cdots c_g$ (C30-C31)	0.95	3.96	3.19	139
<b>D</b>	C31-H31 $\cdots c_g$ (C16-C21)	0.95	3.88	3.10	140
<b>E</b>	$c_g$ (C16-C21) $\cdots c_g$ (C16-C21)	-	-	4.17	180

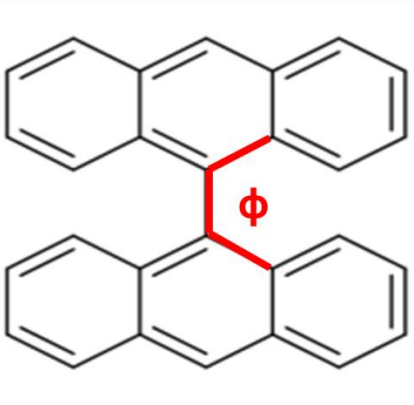


**Figure 5.10** Packing diagram for **H1•0.5px** viewed along [010]. Guests are presented with space filling and coloured pink.

### 5.5.3 Torsion angles in H1 inclusion compounds

The enclathration capabilities of the 9,9'-bianthryl (**H1**) host molecule with a variety of organic and simple heterocyclic guests have been studied. The host **H1** exhibits two polymorphic structures<sup>4,5</sup> and its inclusion compounds with other guests have been elucidated. **Table 5.7** gives the torsion angle values of the **H1** host molecule from the previously studied structures and the currently determined ones. Comparisons of these values shows the torsion angles of **H1** in the **H1•0.5ox** and **H1•0.5px** structures are similar and are within the same range as the previously studied **H1** structures. Therefore the **H1** molecule retains the same conformation during inclusion complex formation and there was no significant distortion of the molecule in order to accommodate the xylene guests.

**Table 5.7** Torsion angles for **H1**

CDCC Reference code	Torsion angle $\phi$ (°)	Measured torsion angle ( $\phi$ )
KUBWAF (molecule 1)	74.0	
KUBWAF (molecule 2)	81.5	
KUBWAF01	79.1	
NIRXAN	76.9	
TABYAW	87.8	
TARWEP (molecule 1)	84.0	
TARWEP (molecule 2)	88.8	
WIMCIE	87.0	
<b>Inclusion compounds</b>	<b>Torsion angle <math>\phi</math> (°)</b>	
H1•0.5ox (molecule 1)	85.4	
H1•0.5ox (molecule 2)	86.2	
H1•0.5ox (molecule 3)	87.5	
H1•0.5ox (molecule 4)	82.0	
H1•0.5px	88.8	

### 5.5.4 Hirshfeld surface analysis of H1•0.5ox and H1•0.5px

The Hirshfeld surfaces provide a unique way of analysis of close contacts for a particular molecule in a crystal structure. This enables the exploration of polymorphs and structures with more than one molecule in the asymmetric unit.<sup>6,7</sup> The program Crystal Explorer<sup>8</sup> was employed to further map the non-bonding interactions that occur between the host and guest molecules in the **H1•0.5ox** structure and the related structure with **px**. The program calculates the Hirshfeld surfaces of the target molecule and depicts all the interactions with its neighbours into a fingerprint plot as illustrated in **Figure 5.11**. The distance pairs ( $d_e$ ,  $d_i$ ) on the plot are relative frequencies for different external and internal points on the Hirshfeld surface. In the **H1•0.5ox** structure there are two crystallographically independent **ox** molecules with the corresponding fingerprints shown in **Figure 5.11 (a)** and **(b)**. The peaks labelled 1 correspond to H•••H interactions and give the shortest internal difference to the selected guest molecule versus the external distances to the surrounding atoms. The sum of these is 2.20 Å (**Figure 5.11 (a)**, **ox** guest A) and 2.33 Å (**Figure 5.11 (b)**, **ox** guest B). Both of these are shorter than the corresponding H•••H contacts in the **H1•0.5px** structure, which shows peak 1 at 2.60 Å. (**Figure 5.11 (c)**). This is the most abundant interaction between the selected molecule and the surroundings which makes it very important. The peaks labelled 2 in all the three figures are associated with (Guest)H•••C(Host) interactions, and their interatomic distances are



similar at approximately 2.65 Å. We surmise that the dominant H•••H interactions, being shorter in the **H1•0.5ox** structure drive the selectivity of **H1** to *ortho*-xylene.

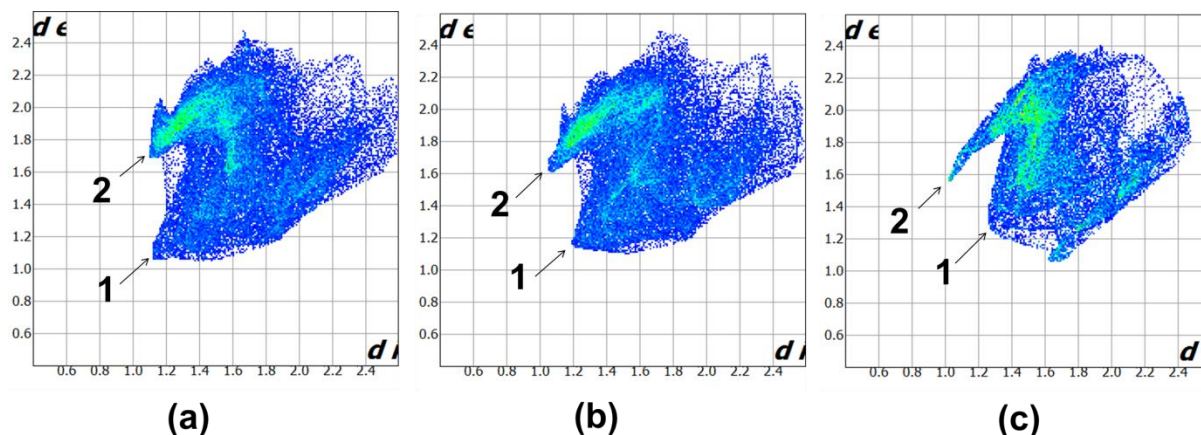


**Figure 5.11** Hirshfeld plots for **H1•0.5ox** (a - molecule A, b - molecule B) and for **H1•0.5px** (c).

The fingerprint plots can be divided into fractions due to the individual atom-type, and numerical comparison can be performed. The relevant intermolecular interactions of **H1•0.5ox** and **H1•0.5px** are summed in **Table 5.8**. In **H1•0.5ox** structure we find  $\pm$  57% of the surface contact between the guests and surrounding molecules involves H•••H contacts and the remaining  $\pm$  43% involve C•••H contacts. The **H1•05px** structure contains 63.1% H•••H contacts and the left over 36.9% comprises of C•••H contacts. The C•••H percentages represent the C-H••• $\pi$  interactions in the crystal structure and the measured values of these particular interaction is about 6% higher in **H1•0.5ox** than **H1•0.5px**. This is important because the C•••H are naturally attractive interactions while the H•••H contacts are repulsive, and in this sense we can assume that **H1•0.5ox** is a more stable structure than **H1•0.5px**. This is relative to **H1**'s superior selectivity towards **ox** in the competition experiments.

**Table 5.8** The intermolecular interactions in the **H1** crystal structures

	<b>H1•05ox molecule A</b>	<b>H1•05ox molecule B</b>	<b>H1•05px</b>
<b>H•••H (%)</b>	56.8	57.1	63.1
<b>C•••H (%)</b>	43.1	42.8	36.9



### 5.5.5 Comparisons of stabilities of H1•05ox and H1•05px

Lattice energy calculations were performed with the program OPIX.<sup>9</sup> The functional form for the i-j atom-atom potential used is  $E_{ij} = A \exp(BR_{ij}) - C/R_{ij}^6$ , where  $R_{ij}$  is the interatomic distance and the coefficients A, B and C have been normalised against the known sublimation energies of organic compounds. The result yielded lattice energies of  $-186.3 \text{ kJ.mol}^{-1}$  and  $-184.9 \text{ kJ.mol}^{-1}$  for the **H1•0.5ox** and **H1•0.5px** compounds respectively (**Table 5.9**), which confirms the results found in the competition experiment. The small difference of  $1.4 \text{ kJ.mol}^{-1}$  is in keeping with the trend in the lattice energies of organic polymorphs, where the values are often in a small range of a few  $\text{kJ.mol}^{-1}$ .<sup>10</sup> The density of the **H1•0.5ox** crystal is also higher than that of the **H1•0.5px** crystals; again corresponding to the results of the competition experiments (**Table 5.9**).

**Table 5.9** Lattice energies and density values for **H1•05ox** and **H1•05px**

Inclusion compound	Lattice energy ( $\text{kJ.mol}^{-1}$ )	Density ( $\text{g.cm}^{-3}$ )
<b>H1•05ox</b>	-186.3	1.239
<b>H1•05px</b>	-184.9	1.222

## 5.6 Inclusion compounds of H2 with px and H3 with ox

### 5.6.1 Thermal analysis of H2•0.5px and H3•ox

The **H2•0.5px** TG curve illustrated in **Figure 5.12** shows a mass loss of 14.9% in the range of  $97^\circ\text{C}$  to  $103^\circ\text{C}$ . The measured mass loss value corresponds to the calculated mass loss value (14.4%) confirming the 1:0.5 host to guest ratio in the crystal structure. The related DSC trace depicts one endotherm due to a volatile guest ( $T_{\text{on}} = 96.7^\circ\text{C}$  and the  $T_{\text{peak}} = 102.1^\circ\text{C}$ ) and the other due to the melting of host **H2** ( $T_{\text{on}} = 201.5^\circ\text{C}$  and  $T_{\text{peak}} = 202.1^\circ\text{C}$ ).

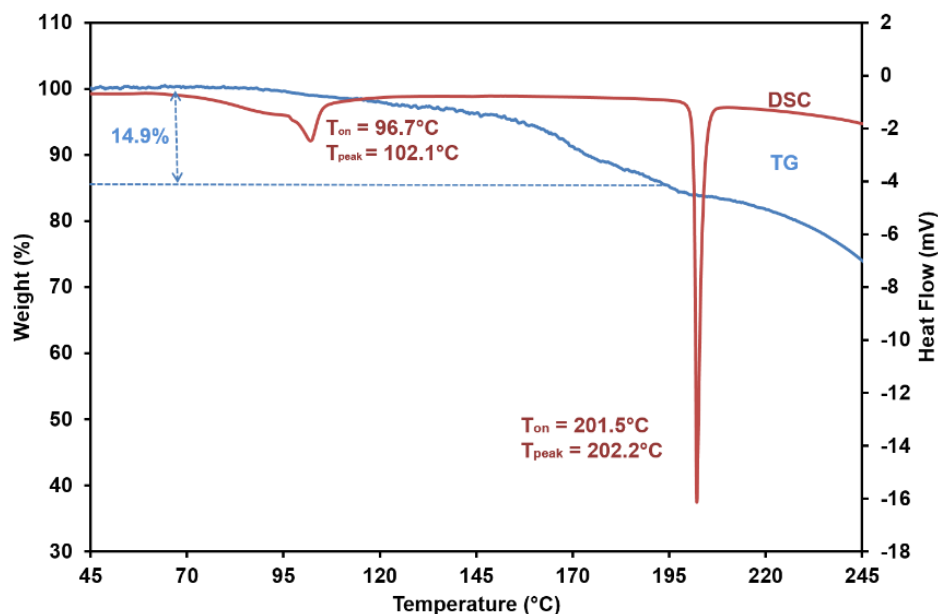


**Figure 5.12** TG and DSC traces for **H2•0.5px** (endo down).

The TG trace of **H3•ox** (**Figure 5.13**) shows a 21.0% mass loss corresponding to the host to guest ratio of 1:1 (calculated 20.9%). The **H3•ox** DSC trace contains two endotherms, the first endotherm depicts the guest loss ( $T_{on} = 81.9^{\circ}\text{C}$  and the  $T_{peak} = 103.5^{\circ}\text{C}$ ) and the second endotherm relates to the melt of **H3** with  $T_{on} = 201.3^{\circ}\text{C}$  and  $T_{peak} = 202.2^{\circ}\text{C}$ .

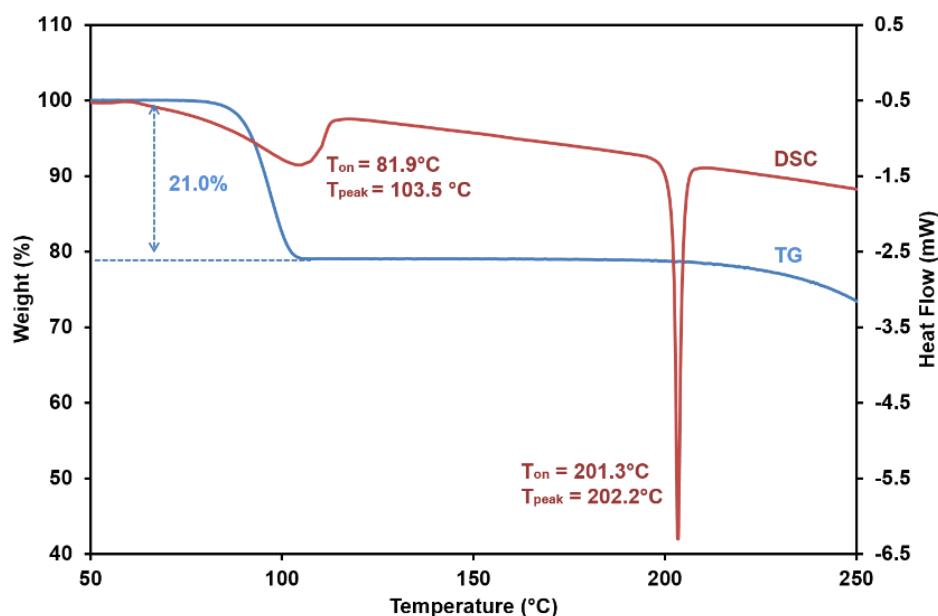


**Figure 5.13** TGA and DSC traces for **H3•ox** (endo down).

## 5.6.2 Crystal structure analysis of H2•0.5px and H3•ox

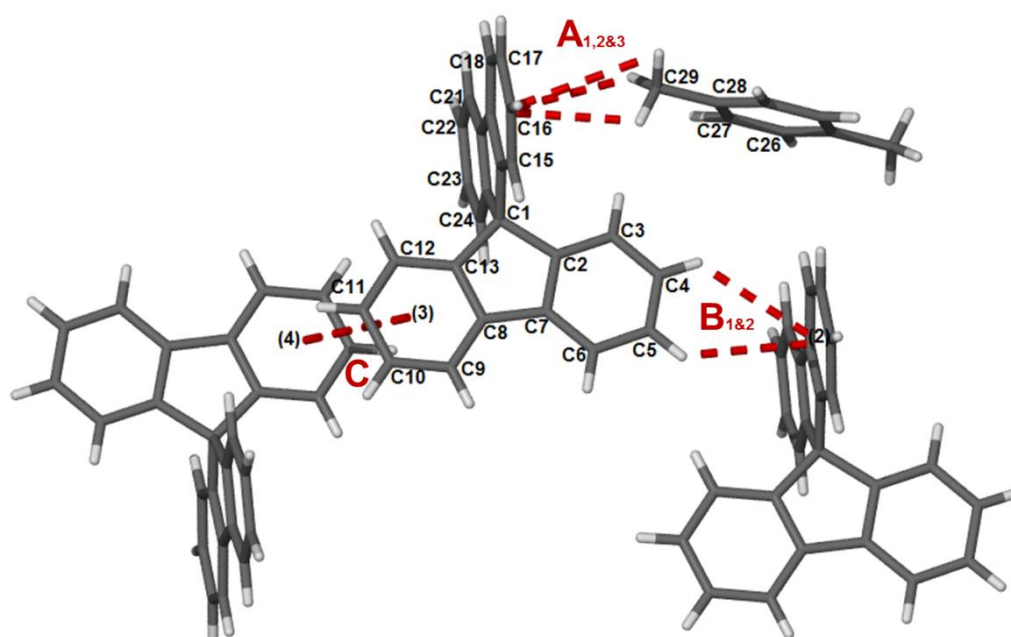
### 5.6.2.1 Structure analysis of H2•0.5px

A 0.15 × 0.40 × 0.44 mm crystal of suitable quality was subjected to single crystal X-ray diffraction. The compound crystallised in the monoclinic crystal system in the space group  $P2_1/c$  (No.14). The crystallographic asymmetric unit consists of one **H2** host and half a **px** guest molecule with the molecular formula of  $C_{26}H_{21}$ . The structure successfully refined to  $R_1 = 0.0451$  and  $wR_2 = 0.1539$ . The related crystal data is summarized in **Table 5.10**.

**Table 5.10** Crystal data for **H2•0.5px** and **H3•ox**

Compounds	H2•0.5px	H3•ox
Molecular formula	$C_{29}H_{21}$	$C_{36.94}H_{29.93}O_2$
Formula weight (g. mol <sup>-1</sup> )	369.46	506.61
Crystal system	Monoclinic	Monoclinic
Space group	$P2_1/c$ (No.14)	$C2/c$ (No.15)
a (Å)	13.911(3)	18.733(4)
b (Å)	9.1555(18)	8.5251(17)
c (Å)	16.101(3)	17.406(4)
α (°)	90	90
β (°)	99.76(3)	95.92(3)
γ (°)	90	90
V (Å <sup>3</sup> )	2021.0(7)	2764.9(10)
Z	4	4
ρ calc (g.cm <sup>-3</sup> )	1.214	1.217
μ (MoKα) (mm <sup>-1</sup> )	0.069	0.074
F (000)	780	1072
Crystal size (mm)	0.15 x 0.40 x 0.44	0.20 x 0.33 x 0.46
Temperature (K)	173(2)	173(2)
Radiation (Å)	0.71073	0.71073
Theta min-max (°)	2.6, 28.4	2.2, 28.3
Dataset (±h, ±k, ±l)	-18:17; -12:12; -21:21	-24:24; -11:11; -23:23
Final R indices [I>2.0 (I)]	$R_1 = 0.0451$ , $wR_2 = 0.1369$	$R_1 = 0.0450$ , $wR_2 = 0.1104$
R indices (all data)	$R_1 = 0.0643$ , $wR_2 = 0.1539$	$R_1 = 0.0614$ , $wR_2 = 0.1199$
Tot., uniq. data, R(int)	21399, 5057, 0.035	16302, 3448, 0.033
N <sub>ref</sub> , N <sub>par</sub>	5057, 272	3448, 210
S	1.050	1.036
Max. and Av. Shift/Error	0.00, 0.00	0.00, 0.00
Min. and Max. Resd.	-0.18, 0.22	-0.22, 0.31
Electron Dens. (e/Å <sup>3</sup> )		

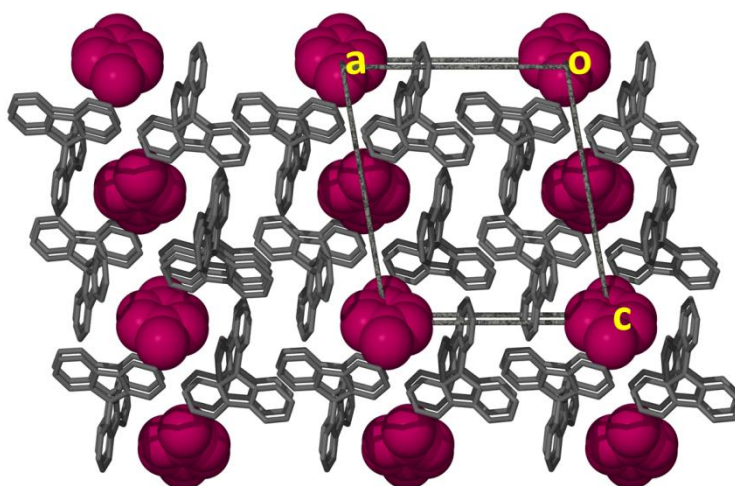
The stability of the **H2•0.5px** structure relies on the  $\pi$ -stacking interactions between the host and guest molecules. **Figure 5.14** demonstrates these interactions labelled A, B and C. The C-H $\cdots\pi$  interactions  $A_{1,2\&3}$  occur between the methyl group (C29-H29A, C29-H29B, C29-H29C) of a guest and the centroid of a host  $c_g$ (C14-C20) in the perpendicular t-shaped geometry with intermolecular distances of 3.19 Å, 3.22 Å and 3.86 Å, respectively (see **Table 5.11**). The C-H $\cdots\pi$  interactions  $B_{1\&2}$  occurs in the perpendicular y-shaped geometry and have distances of 3.34 Å and 3.27 Å between the hydrogen atoms of C4-H4 and C5-H5 to the centroid  $c_g$ (C14-C18), respectively. The parallel offset  $\pi\cdots\pi$  stacking interaction C is relatively weak and takes place between the centroids of two hosts  $c_g$ (C8-C13) and  $c_g$ (C8-C13) with the distance of 4.13 Å. The packing diagram of **H2•0.5px** is shown in **Figure 5.15**. The **px** guest molecules are located on centres of inversion at Wyckoff position *c*.



**Figure 5.14**  $\pi$ -stacking in **H2•0.5px**.

**Table 5.11** intermolecular interactions in **H2•0.5px** structure

	D-H...A/ $c_g$ ... $c_g$	d(D-H) (Å)	d(D-H...A) (Å)	(H...A)/ ( $c_g$ ... $c_g$ ) (Å)	$\angle$ DHA/ $\angle$ $c_g$ ... $c_g$ (°)
<b>A<sub>1</sub></b>	C29-H29A... $c_g$ (C14-C20)	0.98	3.59	3.19	107
<b>A<sub>2</sub></b>	C29-H29B... $c_g$ (C14-C20)	0.98	3.59	3.22	105
<b>A<sub>3</sub></b>	C29-H29C... $c_g$ (C14-C20)	0.98	3.59	3.86	67
<b>B<sub>1</sub></b>	C4-H4... $c_g$ (C14-C18)	0.98	4.00	3.34	128
<b>B<sub>2</sub></b>	C5-H5... $c_g$ (C14-C18)	0.95	3.97	3.27	131
<b>C</b>	$c_g$ (C8-C13)... $c_g$ (C8-C13)	-		4.31	180

**Figure 5.15** Packing diagram for **H2•0.5px** viewed along [010]. Guests are presented with space filling and coloured maroon.

### 5.6.2.2 Structure analysis of **H3•ox**

A suitable **H3•ox** crystal with the dimensions  $0.20 \times 0.33 \times 0.46$  mm was selected for data collection and the structure was solved in the monoclinic space group  $C2/c$  (No. 15). The crystal structure yielded residual indices of  $R_1 = 0.0438$  and  $wR_2 = 0.1199$  after refinement. The asymmetric unit of **H3•ox** contains half a **H3** molecule and one **ox** molecule disordered over two positions with a 50% site occupancy. The empirical formula is  $C_{37}H_{30}O_2$  (See **Table 5.10** for related crystal data). The **H3•ox** structure is stabilised by several  $\pi$ -stacking interactions in the perpendicular t-shaped and perpendicular y-shaped aromatic orientation (**Figure 5.16**). The C-H... $\pi$  interaction A is in the perpendicular t-shaped orientation with the distance of  $2.56$  Å between C22-H22 and the centroid,  $c_g$ (C10-C15) (**Table 5.12**). The C-H... $\pi$  stacking B (C21-H21... $c_g$ (C19-C24),  $3.34$  Å) is between two hosts with perpendicular y-

y-shaped orientation. The last C-H $\cdots\pi$  interaction C also falls in the perpendicular y-shaped orientation and it occurs between the **H3** host and the disordered **ox** guest (C23-H23 $\cdots$ c<sub>g</sub>(C2-C8), 3.01 Å). The host **H3** is located on a diad at Wyckoff position *e* and the disordered **ox** guest lies on the centre of inversion at Wyckoff position *c*. The packing is shown in **Figure 5.17**.

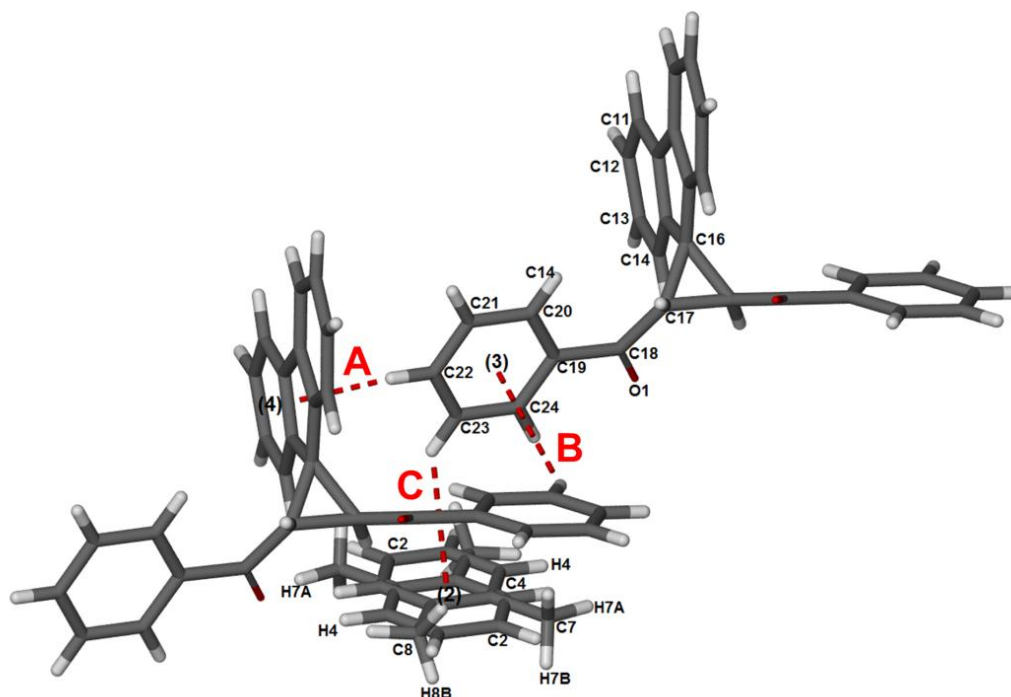


**Figure 5.16**  $\pi$ -stacking in **H3•ox**.

**Table 5.12** C-H $\cdots\pi$  interactions in **H3•ox** structure

	D-H $\cdots$ A	d(D-H) (Å)	d(D-H $\cdots$ A) (Å)	(H $\cdots$ A) (Å)	$\angle$ DHA ( $^\circ$ )
<b>A</b>	C22-H22 $\cdots$ c <sub>g</sub> (C10-C15)	0.95	3.49	2.56	166
<b>B</b>	C21-H21 $\cdots$ c <sub>g</sub> (C19-C24)	0.95	3.97	3.34	126
<b>C</b>	C23-H23 $\cdots$ c <sub>g</sub> (C2-C8)	0.95	3.82	3.04	140

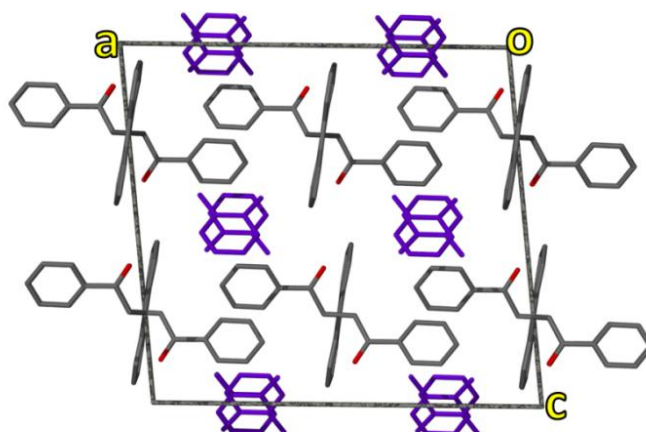


**Figure 5.17** Packing diagram for **H3•ox** viewed along [010]. Guests coloured are blue.

## References

---

- <sup>1</sup> Turaga, U.T., Ramanathan, R. *J. Sci. Ind. Res.*, 2003, 62: 963.
- <sup>2</sup> Rahimpour, M.R., Jafari, M. & Iranshahi, D. *Appl. Energy.*, 2013, 109: 79.
- <sup>3</sup> Lusi, M. & Barbour, L.J. *Angew. Chem. Int. Ed.*, 2012, 51: 3931.
- <sup>4</sup> Langer, V., Sieler, J. & Becker, H.D.Z. *Kristallogr.*, 1992, 199: 300.
- <sup>5</sup> Kyziol, J.B. & Zaleski, J. *Acta Crystallogr. Sect. E*, 2007, 63: 1235.
- <sup>6</sup> Spackman, M.A., *Phys. Scr.*, 2013, 87.
- <sup>7</sup> Spackman, M.A., McKinnon, J.J. & Jayatilaka, D. *CrysEngComm*, 2008, 10, 377.
- <sup>8</sup> McKinnon, J.J., Spackman, M.A. & Mitchell, A.S. *Acta Crystallogr. Sect. B*, 2004, 60: 627.
- <sup>9</sup> Gavezzotti, A., OPIX, University of Milan, Italy, 2003.
- <sup>10</sup> Ismail, S.Z., Anderton, S.C.L., Copley, R.C.B., Price, L.S. & Prize, S.L. *Cryst. Growth Des.*, 2013, 13: 2396.



## Chapter 6: Summary and Conclusion

---

### Summary and conclusion

One of the most difficult procedures in the chemical industry is the separation of isomers with similar chemical structures. This is because their physical and chemical properties are generally so similar that most of the common techniques are not successful. A typical example is that of the three xylenes (dimethylbenzenes) which have boiling points differing by only 6 °C, have almost identical densities and dielectric constants. These three compounds have similar chemical reactivity and cannot easily be separated by distillation or density columns. In such situations one can employ host-guest chemistry, a useful tool in separation technology. This study addresses the problem of separating the xylene isomers (*ortho*-xylene, **ox**; *meta*-xylene, **mx** and *para*-xylene, **px**), and investigates the selectivity for heterocyclic compounds (pyridine, **PYR**; piperidine, **PIP**; morpholine, **MOR** and 1,4-dioxane, **DIO**) and cyclohexanone derivative compounds (cyclohexanone, **CYHA**; 2-methylcyclohexanone, **2-MCYHA**; 3-methylcyclohexanone, **3-MCYHA** and 4-methylcyclohexanone, **4-MCYHA**) with applying three host compounds namely 9,9'-bianthryl (**H1**), 9,9'-spirobifluorene (**H2**) and *trans*-2,3-dibenzoylspiro(cyclopropane-1,9'-fluorene) (**H3**). These aromatic host compounds were chosen because of their ability to form  $\pi$ - $\pi$  interactions with selected guests.

The main aim of the research is to understand the mechanism which renders a particular host selective towards a given guest and to understand the properties which are concomitant with the resulting host-guest compound. In that way we hope to set up the 'rules' for the design of efficient separations.

In the first part the selectivity of three different host compounds, 9,9'-bianthryl (**H1**), 9,9'-spirobifluorene (**H2**) and *trans*-2,3-dibenzoylspiro(cyclopropane-1,9'-fluorene) (**H3**) for the structurally similar heterocyclic compounds pyridine (**PYR**), piperidine (**PIP**), morpholine (**MOR**) and dioxane (**DIO**) were investigated. Overall six inclusion compounds were obtained: **H1•MOR**, **H2•2PYR**, **H2•PIP**, **H2•MOR** and **H2•DIO**. The single crystal structures, thermal behaviour, <sup>1</sup>H-NMR spectra, powder diffraction patterns and Hirshfeld surface analysis of these crystals were discussed.

Competition experiments carried out with **H2** inclusion compounds revealed that **H2** discriminates between the four heterocyclic compounds as follows: **PIP** > **MOR**  $\approx$  **DIO**  $\approx$  **PYR**. It was concluded that the close packing and large number of H...H contacts in the **H2•PIP** structure corresponded to the superior selectivity of **H2** towards **PIP**.

In the second part, the selectivity of **H1**, **H2** and **H3** for cyclohexanone (**CYHA**), 2-methylcyclohexanone (**2-MCYHA**), 3-methylcyclohexanone (**3-MCYHA**) and 4-methylcyclohexanone (**4-MCYHA**) was investigated. Four inclusion compounds were prepared with the host compounds 9,9'-bianthryl (**H1**) and *trans*-2,3-dibenzoylspiro(cyclopropane-1,9'-fluorene) (**H3**): **H1•2CYHA**, **H1•ANT**, **H1•0.5(2-MCYHA)** and **H3•CYHA**. The single crystal structures, powder diffraction patterns and thermal behaviour of these crystals were discussed. The **H1•ANT** inclusion compound is a product of the unpredicted photodecomposition of **H1**.

Part three of this study considered the separation of the xylene isomers: *ortho*-xylene (**ox**), *meta*-xylene (**mx**) and *para*-xylene (**px**) using the three host compounds: **H1**, **H2** and **H3**. The following four structures were obtained: **H1•0.5ox**, **H1•0.5px**, **H2•0.5px** and **H3•ox** were obtained. The crystal structures and thermal behaviour of each host with a single xylene isomer have been elucidated. Competition experiments with **H1**, **H2** and **H3** and the binary equimolar mixture of two isomers and tertiary equimolar mixture of all three isomers were analysed qualitatively by <sup>1</sup>H-NMR and confirmed which particular xylene isomer had been enclathrated. This was followed by thermal gravimetry and single crystal structure analysis. The analysis revealed that **H1** selects **ox** over **px**. **H2** is selective towards **px** and **H3** is selective towards **ox**. The Hirshfeld surfaces, density and relative lattice energies were analysed for the inclusion compounds of **H1** with **ox** and **px**. It was found that the packing of the structures, the densities and lattice energies corresponded to **H1** selectively preferring **ox** over **px**. The overall conclusion was that **H1**, **H2** and **H3** efficiently discriminate between the isomers of xylene by forming inclusion compounds. **H1** enclathrates both **ox** and **px** but prefers the former. **H2** and **H3** only enclathrate **px** and **ox** respectively. Host compounds with small conformational movements are potentially good in selective inclusion.

Overall it was found that large, bulky, relatively rigid scissor-like host compounds whereby the apohost alone is difficult to crystallise are efficient host for separations experiments discussed in the thesis.

The thesis makes a contribution to supramolecular chemistry, host-guest chemistry, selectivity of structurally similar heterocyclic compounds, cyclohexanone derivatives and xylene isomers and it is hoped that this study will encourage new research directions in the field of crystal engineering.